Interfacial activity and membrane-binding properties of α-synuclein and its Parkinson's disease variants

A thesis submitted in partial fulfilment of the requirements

for the award of the degree of

Doctor of Philosophy

BY

ANSHUMAN MOHAPATRA

Department of Biosciences and Bioengineering

Indian Institute of Technology Guwahati

Guwahati, Assam -781 039, India

March 2022

Interfacial activity and membrane-binding properties of α-synuclein and its Parkinson's disease variants

A thesis submitted in partial fulfilment of the requirements

for the award of the degree of

Doctor of Philosophy

BY

ANSHUMAN MOHAPATRA

Department of Biosciences and Bioengineering

Indian Institute of Technology Guwahati

Guwahati, Assam -781 039, India

March 2022

Dedicated to my family

INDIAN INSTITUTE OF TECHNOLOGY GUWAHATI

DEPARTMENT OF BIOSCIENCES AND BIOENGINEERING

DECLARATION

The research work presented in this thesis is an original work carried out by me in the Department of Biosciences and Bioengineering, Indian Institute of Technology Guwahati, India, for the degree of the Doctor of Philosophy. The research work was carried out under the guidance of my supervisors Prof. Nitin Chaudhary and Prof. Sachin Kumar, and no work has been submitted, in part or whole, for any other degree to any other University/Institute. As per the standards of reporting research findings, due acknowledgements have been made wherever the work described is based on the findings of other researchers.

Anshuman Mohapatra

(Anshuman Mohapatra)

Date: 15-03-2022

INDIAN INSTITUTE OF TECHNOLOGY GUWAHATI

DEPARTMENT OF BIOSCIENCES AND BIOENGINEERING

CERTIFICATE

This is to certify that the work incorporated in the thesis titled "**Interfacial activity and membrane-binding properties of α-synuclein and its Parkinson's disease variants**" submitted by Mr Anshuman Mohapatra for the award of the degree of Doctor of Philosophy is an authentic record of the research work carried out under my guidance in the Department of Biosciences and Bioengineering, Indian Institute of Technology Guwahati, India. The work is original and has not been submitted in part or full for any other degree of any other University/Institute.

Prof. Nitin Chaudhary

(Supervisor)

Date: 21/03/2022

Prof. Sachin Kumar

(Co-supervisor)

Date: 21/3/2022

Acknowledgements

Completing this thesis would not have been possible without the fantastic people around me who helped me along this journey. I want to take a moment to thank them and express my sincere gratitude to all of them.

Firstly, I would like to convey my sincere gratitude to my supervisor Prof. Nitin Chaudhary for the patient guidance, encouragement and advice he has endowed during my research tenure. He believed in my potential and my ability to learn new skills. His valuable comments and encouragement have enhanced my research and academic writing skills. My co-supervisor Prof. Sachin Kumar, always blessed me with his insightful suggestion and thoughtful comments. I would always be grateful for the kindness that he has bestowed on me.

I want to thank the chairperson of my doctoral committee, Prof. Vibin Ramakrishnan, for his valuable suggestions related to my academic progress. Furthermore, I am grateful to my doctoral committee members Prof. Senthilkumar Sivaprakasam and Dr. Gagan Kumar, for their guidance and encouragement during my research seminars. Further, I thank Dr. Gagan Kumar for lending me optical parts used to record linear dichroism experiments.

I want to thank Dr.Sowmya Bekshe Lokappa for collaborating with us on the Cavin project, resulting in a publication in the BBRC journal. I sincerely acknowledge Dr. Jobin Varkey, who has kindly proofread our work on the Cavin peptides.

I acknowledge the Department of Biosciences and Bioengineering and the Departmental Central Instrument Facility (DCIF), and the institute's Central Instrument Facility (CIF) to access state-of-the-art instrumentation and resources for executing my research experiments. I acknowledge the Department of Chemistry, IIT Guwahati, for providing the instrumentation support in some of my experiments.

I admire the department's technical staff, Mr. Nurul Islam, Mr. Niranjan Barah, Ms. Prarthana Swargari and Mr Dipankar Barman, for their timely support to solve instrumentation problems. In addition, I would like to express gratitude to the non-teaching staff of the department to make our stay in the department more pleasant every day.

I acknowledge the Ministry of Education, Government of India, for providing me with the financial assistance to carry out my research work with peace of mind. Further, it was my

privilege to work on a project funded by the Department of Biotechnology, Government of India.

I extend my sincere gratitude to the present and former lab members Karabi, Sravani, Vinay, Debika, Feba, Aishwarya, Shubhangini, Prakash, Sajitha, Gaurav J, Gaurav P, Anirban, Vivek, Kalpana, Anjali S, Shubhra, Pranav, Naveen, Franklin, Nethi, Saumya, Ganesh, Subbi, Rakesh, Sudhir, Barnali, Manisha, Yoya, Anjali G, Kamal, Karam, Vishnu, and Vijay from NC, VR, SK, and BioPat lab for their invaluable support, motivation, and blessings throughout this journey. I shared beautiful memories with my friends Ritiritao, Jon, Abhijit, Aman, Anurag, Minati, Ila, Swapna, Gopal, Prajna, Dina, Alphul, Charu and Darshana, who made my life a lot easier and were an integral part of my journey. My friends Smita, Uzwal, Saroj, Ankur, Sushant, Prasim, and Mehak, were the backbone of support. I received motivation from them each day. I will always cherish the wonderful time spent with them.

Above all, I thank my parents for their love, affection, blessings, and belief in me. It was always a tough decision to be away from them in their old age. However, they have always allowed and supported me to seek my journey and interests despite of the limited resources. I want to express my sincere gratitude to my elder brother and my sister-in-law. My brother has inculcated the scientific temperament inside me from my early childhood days (he allowed me to work on his pet projects!). My close family members, especially my uncle and aunts, have always supported me. My best friend Pritismita stood by me in all my ups and downs, and her love and support were unfathomable in my journey. I extend remembrance to my dearest friend Purnendu, who always believed in my ability to succeed in the academic arena. You are gone, but your belief in me has made this journey possible. I cherish our friendship every day.

Lastly, thank you God for giving me the strength to keep going.

Anshuman Mohapatra

Table of Contents

DECLARATION i

CERTIFICATE iii

Acknowledgements iv

Table of Contents vi

Abbreviations x

Synopsis xii

List of Publications xvi

CHAPTER 1 Introduction and Literature Review 1

1.1 Introduction 2

1.2 The historical perspective of neurodegenerative diseases 2

1.3 The amyloid state of protein 5

1.4 Parkinson's disease 7

1.4.1 The aetiology of inheritance 7

1.4.2 αS sequence features 10

1.4.3 Structural polymorphism of αS 12

1.4.4 αS's physiological function 14

1.4.5 Membrane interaction of αS 15

1.4.6 αS gets stabilized as an α-helix 16

1.4.7 Lipid rafts and αS 16

1.4.8 Electrostatics of αS membrane interaction 16

1.4.9 αS lipid-binding specifics 18

1.4.10 Regulation of membrane interaction 18

1.4.11 Curvature sensing by αS 19

1.4.12 Curvature induction by αS 19

1.4.13 αS at the air-aqueous interface 21

1.4.14 In vitro aggregation of αS 24
1.4.15 Pathological structure of αS 26
1.5 Research design and objectives 28
CHAPTER 2 Materials and Methods 31
2.1 Materials 32
2.2 Methods 32
2.2.1 Protein expression 32
2.2.2 Anion exchange chromatography 33
2.2.3 Size exclusion chromatography (SEC) 33
2.2.4 Dynamic light scattering (DLS) 34
2.2.5 Surface activity 34
2.2.6 Protein-lipid interaction 36
2.2.7 Circular dichroism (CD) spectroscopy of the LB film 37
2.2.8 Linear dichroism (LD) spectroscopy of the LB films 37
2.2.9 Atomic force microscopy (AFM) 38
2.2.10 Thioflavin T (ThT) fluorescence assay 38
2.2.11 Transmission electron microscopy (TEM) 38
2.2.12 Neuronal cell viability assay 38
CHAPTER 3 The Effect of N-terminal Acetylation on the αS's Interfacial Properties 41
3.1 Summary 42
3.2 Introduction 43
3.3 Results and discussion 45
3.3.1 Characterization of the purified protein 45
3.3.2 Surface activity 46
3.3.3 Compression/expansion isotherms 47
3.3.4 Blodgett deposition and CD spectroscopy 49
3.3.5 LD spectroscopy of the LB films 50

3.3.6 AFM of the LB film....51
3.4 Conclusion....52
CHAPTER 4 Interfacial Properties of αS's Parkinsonian Variants....55
4.1 Summary....56
4.2 Introduction....57
4.3 Results and discussion....58
4.3.1 Surface activity....58
4.3.2 Compression/expansion isotherms....59
4.3.3 The compressibility modulus....61
4.3.4 CD spectroscopy....64
4.3.5 LD spectroscopy....65
4.3.6 AFM of the LB films....66
4.4 Conclusion....67
CHAPTER 5 Polymyxin B-catalysed αS Aggregation....69
5.1 Summary....70
5.2 Introduction....71
5.3 Results....73
5.3.1 Characterisation of the purified protein....73
5.3.2 Aggregation kinetics of αS in the presence of PMB....74
5.3.3 CD spectroscopy....75
5.3.4 TEM imaging....76
5.3.5 Cell viability assay....76
5.3.6 Surface activity of PMB and PMB-αS interaction....77
5.3.7 Compression/expansion isotherms....78
5.3.8 Circular dichroism (CD) of the LB film....80
5.4 Discussion....81
CHAPTER 6 Conclusions and Future Prospects....83

Appendix.....87

References.....99

Abbreviations

αS	α-synuclein
PD	Parkinson's disease
LB	Langmuir-Blodgett
AFM	Atomic force microscopy
CD	Circular dichroism
LD	Linear dichroism
FE-TEM	Field emission-transmission electron microscope
UHPLC	Ultra high performance liquid chromatography
MALDI-TOF	Matrix-assisted laser desorption ionization time-of-flight
DLS	Dynamic light scattering
ThT	Thioflavin T
PB	Phosphate buffer
GM1	Monosialotetrahexosylganglioside
POPC	1-palmitoyl-2-oleoyl-sn-glycero-3-phosphocholine
POPE	1-Palmitoyl-2-oleoyl-sn-glycero-3-phosphoethanolamine
SM	Sphingomyelin
POPS	1-palmitoyl-2-oleoyl-sn-glycero-3-phospho-L-serine
PI	Phosphatidylinositol
PA	Phosphatidic acid
SUV	Small unilamellar vesicles
GUV	Giant unilamellar vesicles
LUV	Large unilamellar vesicles

GnRH	Gonadotropin-releasing hormone
SNARE	Soluble N-ethylmaleimide-Sensitive Factor Attachment Protein Receptor
PMB	Polymyxin B

Synopsis

Parkinson's disease is a movement disorder that happens due to the loss of neurons in the brain's nigral dopaminergic pathway (Garrett E. Alexander, 2004). The accumulation of the protein α-synuclein (αS) in the nigrostriatal pathway has been held responsible for the loss of neurons in the substantia nigra pars compacta (SNpc) (Vila et al., 2000). The disease's familial form is associated with gene duplication and six missense mutations in the αS gene that translate to the mutant proteins (Pozo Devoto & Falzone, 2017). In the disease's sporadic form, various environmental factors are linked to the development of neuronal inclusions and the formation of Lewy bodies (Modi et al., 2016; Rhinn et al., 2012).

In the current thesis, we compared the interfacial properties of the N-terminal acetylated αS (Ac-αS) with non-acetylated αS (NH_2-αS) at the air-water interface. Both these protein forms display very high surface activity with the surface pressure reaching up to ~30 mN/m upon monolayer compression. The interfacial activity for both the protein forms was very similar. Compression/expansion cycles display large hysteresis, suggesting self-assembly upon compression. The Blodgett-deposited protein were investigated using CD and LD spectroscopy, and the AFM. The protein displayed a random coil to α-helical transition as the air-water interface, and the protein films get anisotropically deposited.

The study was further extended to explore the interfacial behaviour of the Parkinsonian variants of the αS protein (A30P-αS, E46K-αS, H50Q-αS, G51D-αS, A53E-αS, and A53T-αS) at the air-aqueous interface. We have demonstrated the structural transition of the unordered conformation in the aqueous solution into the α-helix-rich protein monolayer at the air-aqueous interface. The protein's LB film's anisotropic nature was established using linear dichroism spectroscopy. Binding of the αS's parkinsonian variants to the flat membranes was investigated using lipid monolayers. The αS's Parkinsonian variants have a higher affinity for the negatively charged lipid flat membranes than towards the zwitterionic membranes. The atomic force microscopy of the αS Parkinsonian variants LB films revealed vivid microstructure formation with minimal defects.

We subsequently investigated the role of polymyxin B, a circular lipopeptide that seem to improve the movement disorders in PD patients, on αS amyloid formation. Polymyxin B was found to have a strong effect on the αS aggregation. The lag phase in the presence of equimolar polymyxin B was reduced to ~40%. Using circular dichroism spectroscopy and transmission electron microscopic imaging, we show that the β-sheet rich fibril formation is complete in the

presence of equimolar polymyxin B, whereas it does not even start in the polymyxin B's absence.

Overall, the insights gained from the interfacial assembly of αS and its Parkinsonian variants have led to a better understanding of the unstructured protein's behaviour when it interacts with interfaces. Such insights open opportunities to the design of therapeutics targeting the interfacial assembly of the protein.

The scientific content of this thesis is organized in the six chapters.

Chapter 1 - Introduction

The αS is an exciting protein present only in primates (Burre, 2015). It obtained its name after being identified as a protein localized on synaptic vesicles and nuclear envelopes (Maroteaux, Campanelli, & Scheller, 1988). The protein was also identified as the non-beta-amyloid component of the amyloid plaques in Alzheimer's disease (Ueda et al., 1993). While reports about its nuclear localization have been inconsistent, its presynaptic localization is well established (Burre, 2015). αS has been long known as an intrinsically disordered protein (Fink, 2006; V. N. Uversky, 2003). However, the N-terminal region folds into an amphipathic helix interacting with the membranes (Bussell, Ramlall, & Eliezer, 2005; Eliezer, Kutluay, Bussell, & Browne, 2001). In neurons, αS is reported to exist in a dynamic equilibrium between soluble and membrane-bound state (Bartels, Choi, & Selkoe, 2011). This interaction with the membrane is crucial for αS's cellular functions, which are poorly understood even after three decades of its discovery. Other exciting features of αS are its curvature-sensing and curvature-inducing properties; the protein binds to the relatively flat membranes through an extended α-helix but can bind highly curved membranes (<50 nm diameter) in a broken helical conformation (Chandra, Chen, Rizo, Jahn, & Sudhof, 2003).

An air-aqueous interface is a powerful place that helps phase separation of protein-based on the bulk-to-interface diffusion, protein's structural flexibility and amphipathicity (Macritchie, 1978). It is a well-established fact that proteins lose their tertiary structure when subjected to interfaces. However, for intrinsically disordered proteins like αS, interfaces might help in gaining the secondary structures (C. Wang, Shah, Thakur, Zhou, & Leblanc, 2010).

Chapter 2 - Materials & Methods

The material used in carrying out the experiments and the detailed methodology of protein expression, purification, characterization is presented. We also detail the material

characterization techniques like surface activity, circular dichroism spectroscopy, linear dichroism spectroscopy, atomic force microscopy, and aggregation kinetics assays.

Chapter 3 - The effect of N-terminal acetylation on the αS's interfacial properties

αS is a membrane-binding protein found predominantly in neurons and erythrocytes. The protein remains unordered in aqueous solutions but folds into an α-helical structure when bound to membranes. Besides, it gets deposited as β-sheet rich aggregates in diseases known as synucleinopathies. The native αS has been reported to be acetylated at the N-terminus. Here, we compare the interfacial properties of the N-terminal acetylated αS (Ac-αS) with non-acetylated αS (NH_2-αS) at the air-water interface. Both the protein forms are highly surface-active, with surface pressure reaching up to ~30 mN/m upon compression. The pressure-area isotherms obtained from the repeated compression-expansion cycles display large hysteresis suggesting self-assembly at higher surface pressures. The expansion isotherm is characterized by a rapid decrease in surface pressure followed by a slower transition phase starting around 15–17 mN/m. These data suggest that the compressed monolayer breaks into small clusters upon expansion, followed by these clusters' loosening. The circular dichroism spectroscopic analysis of the Blodgett-deposited films suggests the protein to be in largely α-helical conformation. The linear dichroism investigations suggest the protein to be anisotropically deposited. Therefore, Blodgett deposition of the Langmuir films is a relatively simple method for preparing oriented monolayers of surface-active macromolecules.

Chapter 4 - Interfacial properties αS's parkinsonian variants

In the past decade, six autosomal dominant mutations have been identified in the αS (SNCA) gene that translates into A30P, E46K, H50Q, G51D, A53E, and A53T mutation in the protein. This mutation alters the electrostatics and hydrophobicity of a cardinal region of the protein. A comprehensive comparison of the interfacial properties of these mutations is crucial to understand their membrane dynamics. Here, using the Langmuir-Blodgett technique, we have determined the mutant-type proteins' surface activity, which lies between 20-22 mN/m at the air-aqueous interface. The said mutations alter the net charge and hydrophobicity of the protein, affecting their membrane-binding activity. The A30P and H50Q mutants have a higher binding affinity towards the negatively charged lipid monolayer. The structural constraints conferred by A30P mutation influences the flexibility of the protein monolayer. We observed secondary structure transition into α-helix rich clusters at the air-aqueous interface using circular dichroism spectroscopy of the protein LB film. We could very carefully transfer the

microstructures formed during the compression/expansion cycle into LB film on a silicon substrate with minimal defects. The atomic force microscopy of the protein LB film revealed uniform packing patterns and microstructures.

Chapter 5 - Polymyxin B-catalyzed αS aggregation

Parkinson's disease (PD) is a progressive neurodegenerative disorder caused by the loss of dopaminergic neurons. It is characterised by the deposition of insoluble α-synuclein aggregates in the brain. Constipation is a common PD-associated condition, and the treatment of constipation with certain antibiotics seem to improve the PD symptoms. Polymyxin B, a last resort drug in treating the life-threatening Gram-negative bacterial infections, is one such antibiotic. The administration of polymyxin B in PD patients is known to alleviate the movement disorder symptoms; the mechanism of action, however, remains unclear. We, therefore, wondered if polymyxin B could modulate the aggregation of α-synuclein. We find that the polymyxin B catalyses the aggregation of α-synuclein into amyloid fibrils. At equimolar polymyxin B concentration, the lag phase was reduced to around one-third of that in the absence of polymyxin B.

Chapter 6: Conclusions and future prospects

This chapter discusses the highlights of the findings presented in chapter 2-5 and the future possibilities.

List of Publications

Journal Articles Related to the Thesis Work

1. **Mohapatra, A.**, & Chaudhary, N. (2021). Interfacial properties α-synuclein's parkinsonian variants. (Manuscript under review in *Colloids and Surfaces B: Biointerfaces).*
2. **Mohapatra, A.**, Bohara, V., Kumar, S., & Chaudhary, N. (2021). Polymyxin B accelerates the α-synuclein aggregation. *Biophysical Chemistry*, 277, 106628. DOI: 10.1016/j.bpc.2021.106628
3. **Mohapatra, A.**, & Chaudhary, N. (2021). N-terminal acetylation does not alter α-synuclein's interfacial properties. *International Journal of Biological Macromolecules*, *174*, 69-76. DOI: 10.1016/j.ijbiomac.2021.01.147

Journal Article from Other Collaborative Work (Not in the Thesis)

1. **Mohapatra, A.**, Lokappa, S. B., & Chaudhary, N. (2020). Interaction of cavin-1/PTRF Leucine Zipper Domain 2 and Its Congenital Generalized Lipodystrophy Mutant With Model Membranes. *Biochemical and biophysical research communications*, *521*(3), 732-738. DOI: 10.1016/j.bbrc.2019.10.167

Conference Proceedings

1. **Mohapatra, A.**, Bekshe Lokappa, S., & Chaudhary, N. (2021). Congenital Generalized Lipodystrophy Mutation p. Glu176Argfs Renders Cavin-1 Leucine Zipper Domain 2 to Off-Targets. *Biophysical Journal*, *120*(3), 233a.
2. **Mohapatra, A.**, & Chaudhary, N. (2021). Assembly of N-acetylated α-Synuclein at the air-aqueous interface. The 45th FEBS Congress, 2021.
3. **Mohapatra, A.**, & Chaudhary, N. (2018). Investigations into α-synuclein assembly using p-cyanophenylalanine as an intrinsic fluorescent and infrared probe. FCS 2018.

CHAPTER 1

Introduction and Literature Review

1.1 Introduction

Alpha-synuclein (αS) is a protein found in the neurons of the human brain (Burre, 2015). In the past few decades the αS has been linked to the pathophysiology of Parkinson's disease (PD) (S. He, Zhong, Liu, & Yang, 2020; Polymeropoulos et al., 1997; Spillantini et al., 1997). PD is a progressive neurodegenerative disease that develops slowly over the years in its patient's brain (Fröhlich, 2016). αS protein undergoes a structural transformation during the PD pathogenesis (H. T. Li, Du, Tang, Hu, & Hu, 2002). Hence, it is paramount to understand the physiological ambience associated with the protein in the human brain. The dry brain mass is about 60 % rich in lipids (O'Brien & Sampson, 1965). In living cells, phospholipids are the building blocks of the cellular membrane system (Bohdanowicz & Grinstein, 2013). Lipids play a significant role in the delivery of several cellular cargos across the cell and outside (van Meer, Voelker, & Feigenson, 2008). The lipid membrane composition and dynamics largely influence the structural conformation of the associated membrane proteins (Casares, Escriba, & Rossello, 2019). Understanding the protein-lipid interaction broadens our understanding of the occurrence of several neurodegenerative diseases.

1.2 The historical perspective of neurodegenerative diseases

Human intervention has many a time disturbed the delicate balance of the environment. A classical case is documented in Europe at around 1985 when industrial cattle-farming opted for cheaper meat and bone meal over a regular plant-based diet for their cows (Pattison, 1998). Since then, across Europe, several cases of abnormal behaviour of the animal were reported (Pattison, 1998). Soon over a year, the "mad cow disease" was identified officially as Bovine Spongiform Encephalopathy (BSE), i.e., as a neurodegenerative disease (Wells et al., 1987). These pathological lesions seen in the animal brain were not new. They strongly resembled various earlier reported diseases such as scrapie of sheep and goat, chronic wasting disease of mule deer and spongiform encephalopathy of rocky mountain elk (Williams & Young, 1980, 1982). The development of immunohistochemical methods identified the presence of PrP^{Sc} (scrapie isoform of the prion protein) in the *post-mortem* brain tissue of sick animals (Collinge, 2001). These tiny protein/peptide isoforms are resistant to heat denaturation and harsh treatment. A small amount of PrP^{Sc} can distort the structure/function of normal brain prion protein (PrP) when infected (Collinge, 2001). Eating the contaminated beef has led to a zoonotic transfer of BSE to humans and causes variant Creutzfeldt–Jakob disease (vCJD) in humans (J. Lee, Kim, Hwang, Ju, & Woo, 2013). Funeral cannibalism is a traditional tribal practice wherein people eat the dead remains of their close family members (J. Lee et al., 2013).

The practice has been linked to a rare neurodegenerative disease *Guria,* also known as "Kuru" (Hoskin, Kiloh, & Cawte, 1969). In the early years of the 20th century, the patients undergoing neurosurgery developed post-surgery neurodegeneration (Powell-Jackson et al., 1985). Similar neurodegeneration is observed for those undergoing, corneal grafting, and even with the administration of animal origin hormones (Powell-Jackson et al., 1985).

In recent years, the explosion of amyloid research has led to a paradigm shift in understanding the molecular origin of neurodegeneration (Peng, Trojanowski, & Lee, 2020). Abnormal protein condition dictates several human diseases (Table 1.1). These protein diseases have become the anchor point of the ever-increasing life expectancy amidst healthcare facilities' advancement. Understanding the abnormal protein's structure-function relationship has boosted the drug development platforms. The amyloid drug market is multiplying and would reach hundreds of billion dollars over the years (M. A. Cole & Seabrook, 2020). On a different note, the progressive control over the intrinsic phenomenon of amyloidosis has been instrumental in developing new functional materials (Table 1.2). A growing understanding of the protein aggregation process has made advances in the development of hydrogels. The water-laden soft hydrogels have several applications including, the sustained release of drugs, scaffolds for tissue engineering, cosmetic products and biological pest control, to name a few (Majcher & Hoare, 2019).

Table 1.1. Amyloid protein and associated diseases in humans.

Disease	Protein	Reference
Alzheimer's disease	β-amyloid and tau	(Glenner & Wong, 1984; Kosik, Joachim, & Selkoe, 1986)
Parkinson's disease	α-synuclein	(Spillantini, Crowther, Jakes, Hasegawa, & Goedert, 1998)
Amyotrophic lateral sclerosis (ALS)	TAR DNA-binding protein 43 and superoxide dismutase 1 (SOD1) pathology	(Neumann et al., 2006)
Huntington's disease (HD)	Huntingtin (HTT) protein with long polyQ stretches	(DiFiglia et al., 1997)
Spongiform encephalopathies	Prion protein	(Caughey & Chesebro, 1997)

Familial amyloidotic polyneuropathy	Transthyretin (TTR)	(Coelho, 1996)
AA amyloidosis	Serum amyloid A protein	(Nienhuis, Bijzet, & Hazenberg, 2016)
Senile systemic amyloidosis	Wild-type transthyretin	(Pinney et al., 2013)
Haemodialysis-related amyloidosis	β_2-Microglobulin	(Gejyo, 2001)
Finnish hereditary amyloidosis	Fragments of gelsolin mutants	(Kiuru, 1998)
Lysozyme amyloidosis	Mutants of lysozyme	(Nasr et al., 2017)
ApoAI amyloidosis	Fragments of apolipoprotein AI	(M. Das, Mei, Jayaraman, Atkinson, & Gursky, 2014)
Type II diabetes	Amylin	(Prager, Ludvik, & Hartter, 1991)
Medullary carcinoma of the thyroid	Calcitonin	(Emmertsen, 1985)
Hereditary cerebral haemorrhage with amyloidosis	β-amyloid	(Castano et al., 1996)
Injection-localized amyloidosis	Insulin	(Gupta, Singla, & Singla, 2015)

Table 1.2. Functional materials from amyloid proteins/peptides.

Functional material	Usage	Building block	Reference
Amyloid fibres	capturing carbon dioxide from flue gas	VQIVYK from tau	(D. Li et al., 2014)
Functionalized amyloid fibrils	role in cell adhesion	Modified transthyretin sequence	(Gras et al., 2008)
Short and long-acting sustained-release drugs	long-acting analogs of gonadotropin-releasing hormone (GnRH)	GnRH analogs	(Maji et al., 2008)
Nanostructured films	free-standing films from amyloid protein fibrils	Hen egg white lysozyme	(Knowles, Oppenheim, Buell, Chirgadze, & Welland, 2010)

1.3 The amyloid state of protein

The genetic information in a biological system often follows “the central dogma” (C. He, 2019). The information gets faithfully translated into a protein sequence. While the protein gets synthesized, the cellular machinery orchestrates the folding of the protein into its intended physiological conformation (Fig. 1.1). The weak molecular interactions like hydrogen bonding, hydrophobic interaction, and salt bridges help maintain the protein’s physiological state (Panja, Maiti, & Bandyopadhyay, 2020). Inside the cells, proteins serve their purpose through a particular secondary/tertiary/quaternary structure in their physiological state. However, some proteins stumble upon conformational impediments during their life-cycle and become a liability to their living host (Koonin, 2012). Their disruption of the physiological confirmation leads to a loss of their physiological functions and sometimes gain of function like cytotoxicity (Aguzzi & Heppner, 2000; Westergard, Christensen, & Harris, 2007).

The intrinsically disordered proteins (IDPs) do not maintain a rigid three-dimensional conformation throughout their life cycle (V. N. Uversky, 2013). They would typically be rich in charged and polar residues and therefore remain largely unordered in solution. However, they undergo structural transition upon plausible interactions with other surrounding molecules such as other proteins, lipid membranes or interfaces (V. N. Uversky, 2013). However, growing evidence suggests that the disordered conformation of proteins is thermodynamically driven towards the stable amyloid state (Knowles, Vendruscolo, & Dobson, 2014). The local free energy minima state at physiological condition undergo self-assembly to reach a global minimum free energy state during amyloid formation (Eisenberg & Jucker, 2012). While the disordered proteins don’t adopt any specific tertiary structure, the fibrillar form is enriched with β-sheet conformation. The phenomenon of IDPs crossing the energy barrier to attain the amyloid state has bothered researchers for decades. To study the structure of proteins, scientists rely on the gold standard X-ray crystallography and NMR-spectroscopy methods. Further, the polymorphic nature of IDPs makes them more challenging to be probed via these conventional tools. Several direct and indirect biophysical techniques have been in practice to look into the conformation of the IDPs. The last few decades have gathered overwhelming interest in understanding the molecular biology of neurodegenerative diseases arising from the disordered state of the proteins.

Although IDPs are privileged to undergo a regular structural transformation, any ordinary protein can also experience a similar fate when subjected to appropriate test tube condition. Thus, it is apparent that most of the proteins/peptides have hidden amyloidogenic stretches waiting to get an ideal state to initiate self-assembly. Among the various amyloids analyzed, the data from "x-ray" fiber diffraction experiments indicate a typical amyloid fibril architecture containing 'cross-β' patterns with β-strands oriented perpendicular to the fibrillar axis (Eisenberg & Jucker, 2012).

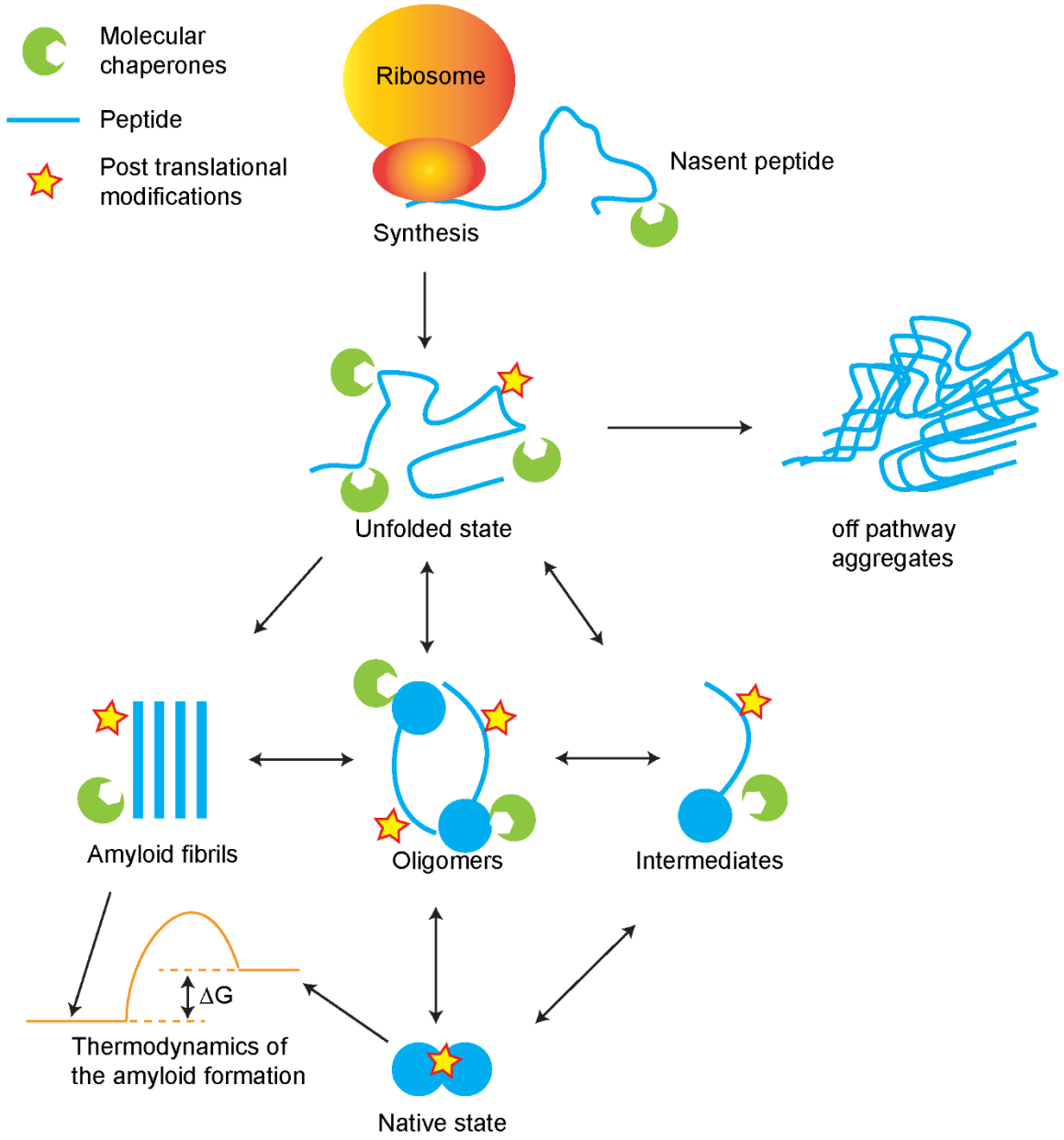

Fig. 1.1. Schematic diagram showing the fate of an IDP. The life-cycle of an IDP starts from a nascent polypeptide synthesized in a ribosome. It passes through post-translational modifications and conformational changes and sample transient metastable states. These

interconversions are thermodynamically coupled to the stabilities of the intermediates and the free energy barriers available to attain the states. The native form of the protein is stabilized by chaperones and undergo constant alterations to cross the energy barrier to form the amyloid state. The amyloid fibres are highly ordered and remain in the energy minimum, a highly stable state. Adapted from (Knowles et al., 2014).

1.4 Parkinson's disease

In the ancient text of Ayurveda, the Indian medical system, we find the mention of neurological diseases (वात प्रकृति, *Sanskrit*). In particular, we find Kampavta (Kampa: Tremor) description of its symptoms and herbal remedies to alleviate the symptoms (Manyam, 1990). James Parkinson, in 1817 first described the clinical symptoms of "shaking palsy" in the modern medical text, which later is known after his name the Parkinson's disease (PD) (Goetz, 2011). PD, a movement disorder, is the second most common neurodegenerative disease in the world (Blaszczyk, 2016). Even after decades of research, the clinical diagnosis of PD relies on the symptomatic identification of elements. The PD symptoms include muscular rigidity, bradykinesia, abnormal posture, and resting tremor (Blaszczyk, 2016). The progressive disease onsets with age as early as 21 years to 50 years (10-20 % of total cases) (Giovannini et al., 1991). The disease is most prevalent post 60 years of age. Few instances of juvenile occurrence below 20 years linger among the PD family tree (Giovannini et al., 1991). The debilitating disease makes physical and mental burden imprints on the patients and their caregivers. Increased awareness has moved impetus on the development of a support group around the patient. Online platforms like ParkinsonNet International (www.parkinsonnet.com) with like-minded individuals help to ease disease management. A thorough research on the neurodegeneration during PD has reflected with better understanding in prognosis and treatment (Llorens et al., 2015).

1.4.1 The aetiology of inheritance

Analysis of the post-mortem brain has deciphered several anomalies about neurodegenerative diseases. Problems in the basal ganglia of the human mid-brain disrupt the neuronal dopamine signalling during movement disorders. In PD patients, a characteristic nigrostriatal pathway impairment condition affects control and motor execution (Marsden, 2006). There is a progressive loss of neuronal synapses connecting the globus pallidus, subthalamic nuclei, and the substantia nigra pars compacta (SNpc) during the PD progression. The subsequent loss of

dopaminergic signalling to the putamen (Pu) results in the loss of a direct signalling pathway hampering the motor control (Fig. 1.2) (Shulman, De Jager, & Feany, 2011). Thus, the loss of circulating striatal dopamine inhibits the brain's feedback loop controlling the muscular movements (Shulman et al., 2011). The loss of motor activity begins with the symptoms of PD (Lima, Andersen, Reksidler, Vital, & Tufik, 2007). Currently, the L-DOPA, a precursor of dopamine, is used to control the symptoms of PD. However, such treatment is temporary and does not cure the underlying pathology. Progressively, the patients develop brain lesions that appear in the histopathological staining in the post-mortem brain tissue. The lesions appear as intraneuronal inclusions in the form of Lewy bodies and Lewy neurites (Nussbaum & Ellis, 2003). Uéda et al. in 1993 identified an unknown peptide in addition to Aβ in the amyloid preparation of the brain (Ueda et al., 1993). They termed this peptide fragment as NAC (non-Aβ component of AD amyloid). They reported 140 amino acid protein, a precursor to the NAC peptide fragment (NACP).

The gene sequence of this newly discovered NACP was not new. Maroteaux et al. in 1988 first identified the αS protein from the electric organ of the Pacific electric ray Torpedo (*Torpedo californica*). The SNCA gene present in the genome 4q22.1 cytogenetic location encodes the αS protein in human (Perandones et al., 2014). Biochemical analysis of the Lewy bodies by Goedert et al. in 1997 first described the accumulation of αS protein in the brain lesions and narrated PD as an αS disease (Spillantini et al., 1997). Henceforth, the NACP is better known as αS, occurrence protein that is largely present at the presynaptic nerve terminal. Besides, the two isoforms of αS, namely the β-synuclein (βS) and the γ-synuclein (γS) are αalso expressed in vertebrates. In the early onset cases, a surge of expression of αS in the blood is seen (Miller et al., 2004; Singleton et al., 2003). Barbour et al. in 2008 pinpointed the peripheral expression of αS to the red blood cells (Barbour et al., 2008). Generally, the PD cases appear sporadically in individuals without any known inheritance pattern; neither can these individuals propagate the disease. A closer look at the familial inheritance pattern suggests a different picture. The SNCA gene multiplication invokes dose-dependent early onset of the familial form of PD. Besides, the scientists have discovered six autosomal dominant missense mutations in the SNCA gene that translate into A30P-αS, E46K-αS, A53T-αS, A53E-αS, G51D-αS, and H50Q-αS variants of αS (Kruger et al., 1998; Lesage et al., 2013; Pasanen et al., 2014; Polymeropoulos et al., 1997; Proukakis et al., 2013; Zarranz et al., 2004). Compared to the idiopathic PD cases, the presence of a missense mutation (A30P, E46K, and A53T) encourages the early onset of PD (de Oliveira & Silva, 2019).

The αS pathology manifests in multiple system atrophy (MSA) as well as in dementia with Lewy bodies (DLB). A genome-wide association study (GWAS) of PD suggests the role of multiple genes in pathogenesis (Goldman & Fahn, 2020). The most widely studied genes linking PD apart from the SNCA gene include leucine-rich repeat kinase 2 (LRRK2), glucocerebrosidase (GBA), parkin (PARK2), Pten-induced kinase 1 (PINK1), and microtubule-associated protein tau (MAPT) (Rui, Ni, Li, Gao, & Chen, 2018). This thesis focuses on the αS protein from the SNCA gene.

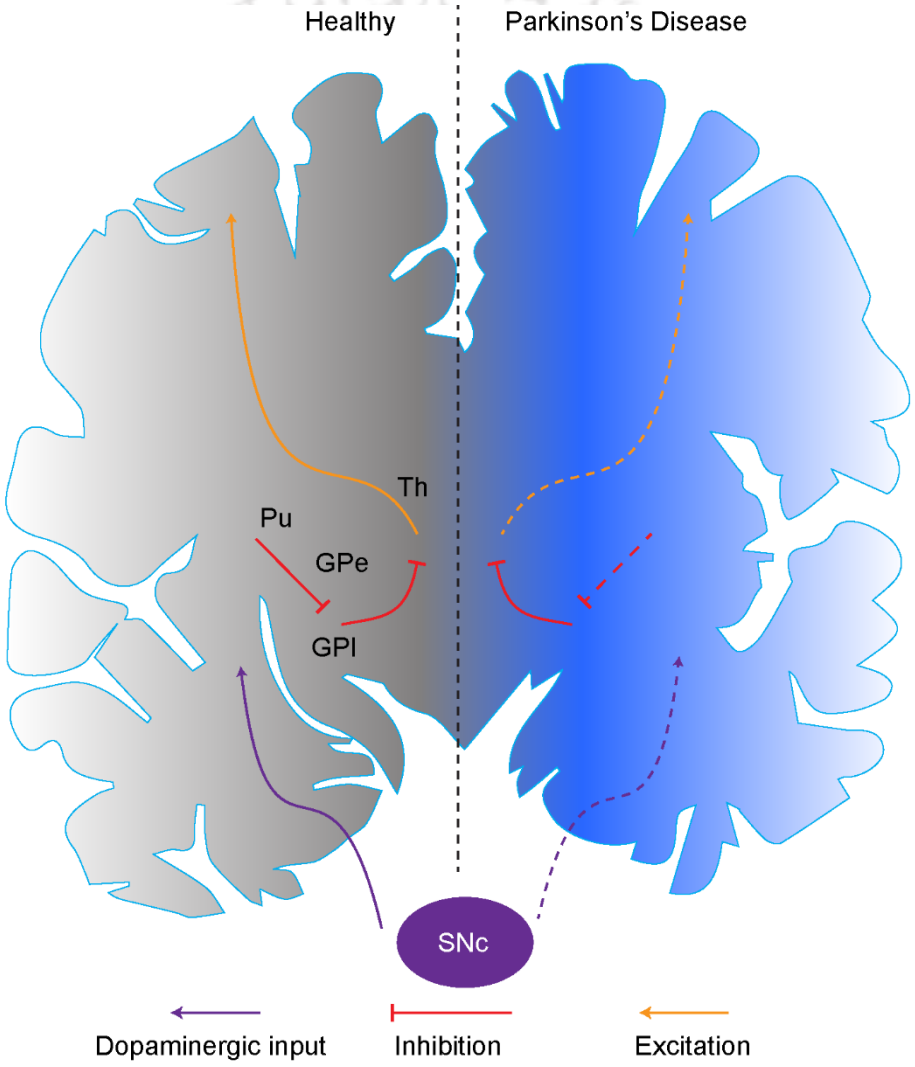

Fig. 1.2. Human dopaminergic system. The human brain cartoons of healthy and PD patients are compared side by side. The human brain physiology is compromised during PD. The substantia nigra pars compacta (SNc) of the midbrain controls the brain's dopaminergic system. The dopamine delivery to putamen (Pu) is hampered during PD, resulting in the subsequent loss of the excitatory pathway. In a cascade of reaction during PD, the globus pallidus interna

(GPI) inhibits the thalamus (Th), and the thalamus inhibits the motor cortex. The globus pallidus externa (GPe) and the subthalamic nucleus, which are inhibitory to the movement, are activated during PD due to loss of SNpc activity. Adapted from (Shulman et al., 2011).

1.4.2 αS sequence features

The αS is a 140 amino acid protein that travels with an apparent molecular weight of around 17 kDa in an SDS-PAGE (Coelho-Cerqueira, Carmo-Goncalves, Pinheiro, Cortines, & Follmer, 2013). The apparent heaviness is attributed to the negatively-charged C-terminal region of the protein that evades the binding of negatively-charged SDS (Giehm, Lorenzen, & Otzen, 2011; Huang, Ren, Zhou, & Wang, 2005). Physiologically, the αS dwells as an N-terminally acetylated protein. αS carries an isoelectric point (pI) of 4.67 (Fernandez & Lucas, 2018b; Mor, Ugras, Daniels, & Ischiropoulos, 2016). The protein can be described broadly with a 1-95 residue N-terminal amphipathic stretch and a 96-140 residue long acidic C-terminal tail (Fig. 1.3). The long N-terminal stretch of the protein has seven 11-mer imperfect repeats with a six residue KTKEGV consensus sequence. The first 60 residues (M1 - K60) house the majority of positive charges. The repeats contain charged residues flanked by paired lysine residues at the polar-apolar interface, making a class A_2 helix (Pfefferkorn, Jiang, & Lee, 2012). The N-terminal region forms a continuous or broken amphipathic helix that binds to membranes (Pfefferkorn et al., 2012). The central portion of the protein E61 - V95, generally termed as non-Aβ component (NAC) region, is rich in hydrophobic amino acids (Sode, Ochiai, Kobayashi, & Usuzaka, 2006). The C-terminal (K96 - A140) of αS is rich in acidic amino acids with a net charge of -12 and remains primarily unstructured even in the membrane-bound protein. The C-terminal region of αS harbours 10 Glu and 5 Asp residues, regularly spaced along the sequence (Pfefferkorn et al., 2012). The stretch 103-140 lacks Lys and Arg residues and harbours proline residues at 8-18 residue interval (Pfefferkorn et al., 2012). Overall the protein carries a negative charge at the physiological pH (isoelectric point of pI 4.67) (Pinheiro & Ventura, 2019). At lower pH, the protein loses charge, followed by compaction due to hydrophobic collapse, which drives the whole protein's aggregation (Pinheiro & Ventura, 2019).

The six known missense mutations in the αS lie upstream to the NAC region, and influence the self-assembly profusely (Mohite et al., 2018). The central NAC region ^{71}VTGVTAVAQKTV^{82} is necessary to drive the self-assembly of the protein. A peptide derived from this NAC region is sufficient to drive the fibrillation of the whole protein (Giasson, Murray, Trojanowski, & Lee, 2001). The aggregation-resistant βS isoform lacks the

NAC stretch (Fig. 1.3), and offers neuroprotection against the αS aggregation (Oeckl et al., 2016). Meanwhile, the γS isoform is associated with widespread neurodegeneration (Ninkina et al., 2009).

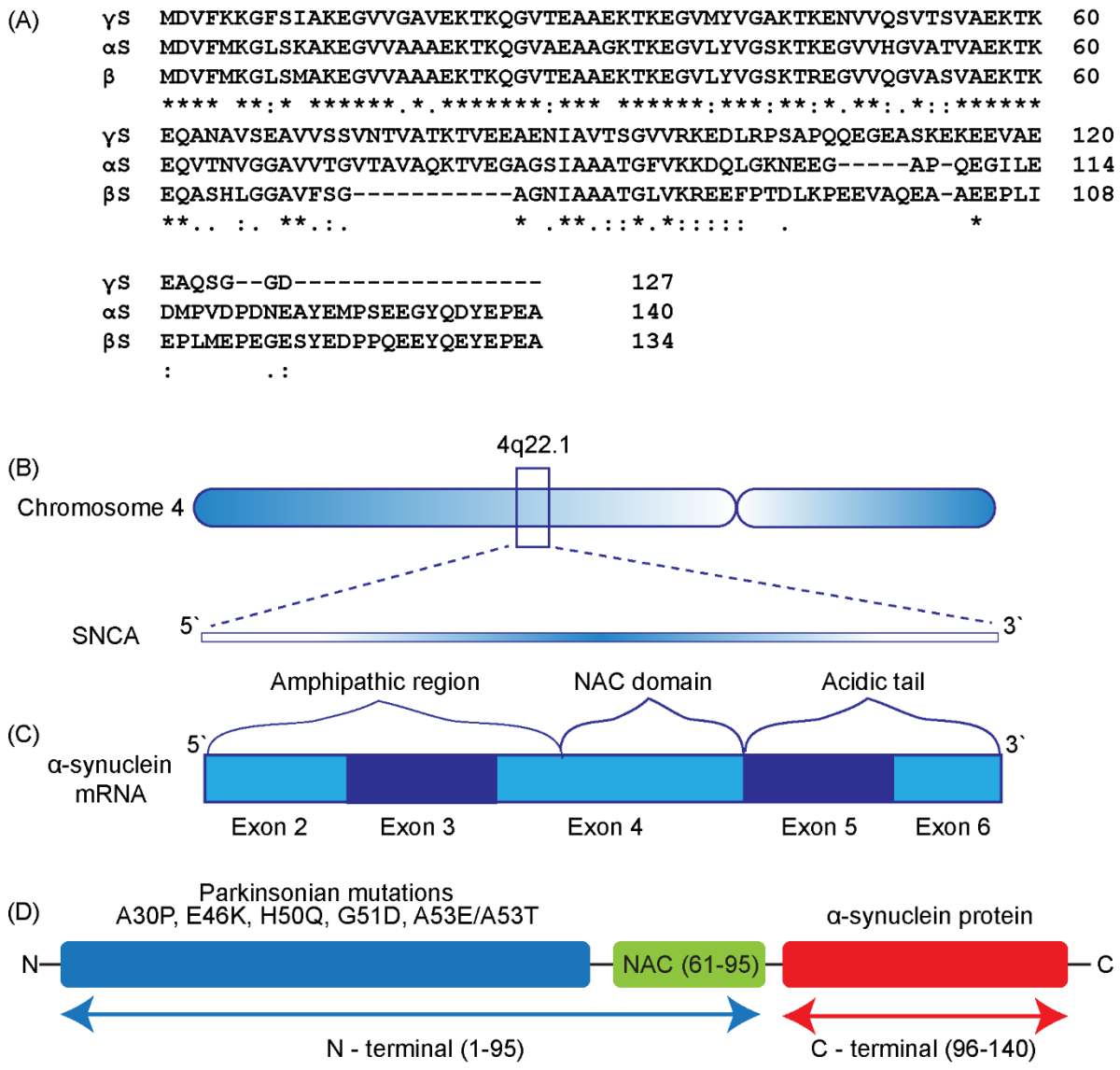

Fig. 1.3. The αS isoforms and Parkinsonian mutations. (A) The sequence comparison of the α, β and γ-synuclein isoforms reveals homology and divergence in the sequence. The asterisks represent the amino acids that are identical among the three isoforms. The dashes represents gaps in the sequence. The dots and colons represent a change of amino acid in one or two of the isoforms. (B) The αS protein is encoded in the SNCA gene in chromosome 4. (C) The last five exons of the SNCA gene encodes for αS protein. (D) A broad classification of the sequence features of αS: N-terminal region (enriched with basic residues), the NAC region (hydrophobic residues), and the C-terminal (acidic residues). The Parkinsonian's mutations reside in the N-terminal region of the αS.

1.4.3 Structural polymorphism of αS

Under physiological condition, αS remains largely unstructured in solution (Fig. 1.4) (Mor et al., 2016). Upon binding to lipid membranes, however, the protein attains an uninterrupted extended helical conformation of about 130 Å length (Jao, Der-Sarkissian, Chen, & Langen, 2004). The helix encompasses the first 90 residues of the protein (Jao et al., 2004). αAs αS contains 11-residue repeats, αit adopts an 11/3 α-helix configuration with 3.67 residues per turn to achieve an unbroken membrane-bound helix (Bussell & Eliezer, 2003). The protein transforms into a broken helix upon binding to SDS micelle, a highly-curved entity (Ferreon, Gambin, Lemke, & Deniz, 2009; Lokappa & Ulmer, 2011). The broken helical stretches span over Val^{3}-Val^{37} and Lys^{45}-Thr^{92} residues and remain connected in an antiparallel arrangement through an extended linker (Bisaglia, Mammi, & Bubacco, 2009). The structural transformation of αS during membrane interaction happens in a sequence of events. During the protein-lipid interaction, the lysine residues found flanking the consensus sequence stabilize the polar head groups (Pfefferkorn et al., 2012). This is followed by the hydrophobic face of the helix diving into the interior of the lipid membrane (Varkey et al., 2010). In a micelle bound broken helical confirmation, the positively charged N-terminal region interacts with the lipid membrane (Ulmer, Bax, Cole, & Nussbaum, 2005). The acidic tail remains away from the micelle (Ulmer et al., 2005).

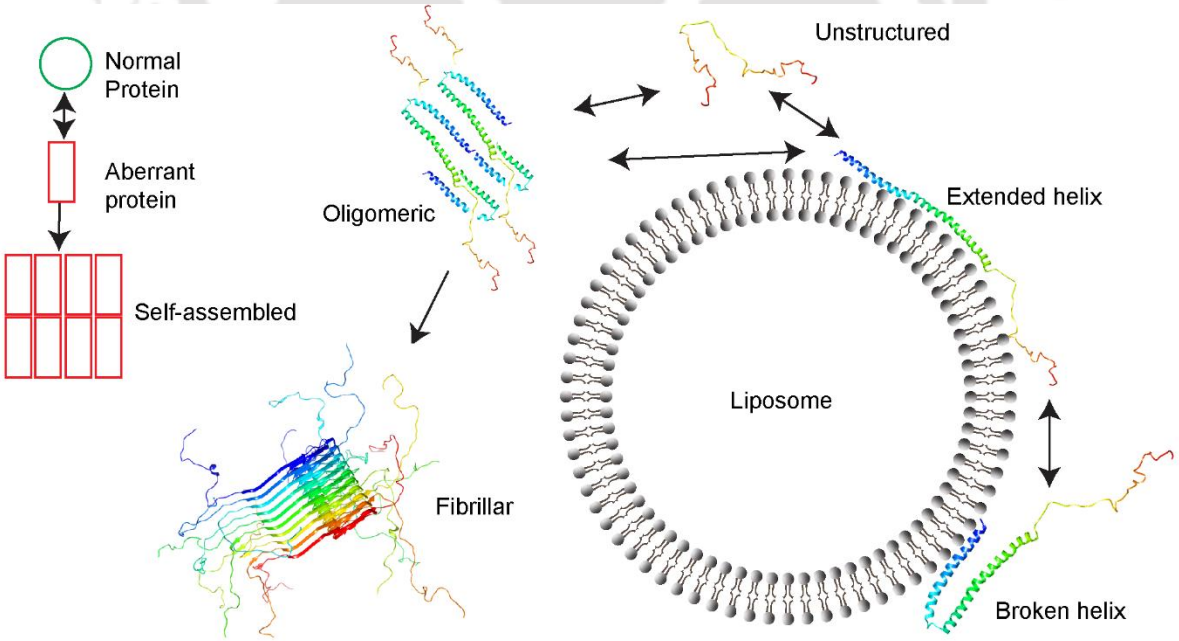

Fig. 1.4. The polymorphic nature of αS. The intrinsically disordered protein αS, undergoes several structural transformations. The unstructured protein attains broken or extended helical conformation while it encounters micelles and lipid vesicles, respectively. The highly

controversial tetrameric form of the protein is regarded as the native form. The metastable forms of the protein cross the energy barrier and form highly stable amyloid fibrils.

The αS is a polymorphic protein. The protein's physiological conformation remains in a delicate balance with various competing assembly and disassembly pathways at work (V. N. Uversky, 2010). The α-helix rich conformation of the protein promotes assembly into dimeric and multimeric forms (Ulmer et al., 2005). Physiologically, αS is known to exist as an α-helical tetrameric state (Lucas & Fernandez, 2020). Bartels et al, in 2011 first isolated this endogenous tetrameric form and described its occurrence in various cells *viz.* neuronal and non-neuronal cell lines, brain tissue and living human cells (Bartels et al., 2011). The reports from Bartels et al also suggested the importance of acetylation in the protein structure-function (Moriarty, Janowska, Kang, & Baum, 2013). However, due to the limited success in isolation of tetrameric form, it is referred to as the most controversial state of the protein (Lucas & Fernandez, 2020). Generally, the tetrameric form is believed to occur as a transient metastable state of the protein (Lucas & Fernandez, 2020; Moriarty et al., 2013). Recently, few groups have isolated both N-acetylated and non-acetylated recombinant protein in tetrameric form with limited success following the non-denaturing native conditions (Lucas & Fernandez, 2020). The α-helical form is believed to be aggregation resistant, and current research focuses on finding this form's biological roles and therapeutic potential (Lucas & Fernandez, 2020).

Lipid membrane can induce multimerization of αS up to at least octamers (Burre, Sharma, & Sudhof, 2014; Tsigelny et al., 2007). Toxic oligomers of αS are known to drive neurodegeneration (V. N. Uversky, 2010). In biophysical experiments, oligomeric αS readily ruptures the vesicles (Stefanovic, Stockl, Claessens, & Subramaniam, 2014). The three-dimensional shape of the Archemedian protein clusters regulates their self-assembly and periodicity (Yeates, 2019). The initial protein concentration, seeding strength, temperature, agitation, pH, buffer, and salt concentration are crucial determinants of self-assembly. (Danzer et al., 2007). Broadly, three types of oligomeric shapes have been described for αS (V. N. Uversky, 2010). The oligomers exist as spherical (2 - 6 nm), spheroidal, and annular (30 - 50 nm) shapes (V. N. Uversky, 2010). The type A oligomers of αS observed by Danzer et al. are seen as annular structures in living cells that facilitate calcium influx (Danzer et al., 2007). The pentameric and hexameric oligomers of αS are ring-shaped (Tsigelny et al., 2007). At times, the protein undergoes a stochastic non-amyloid amorphous aggregation in solution (Fauerbach et al., 2012). Fauerbach et al. (2012) have extensively studied the supramolecular early-stage assembly of αS using atomic force microscopy and transmission electron microscopy

(Fauerbach et al., 2012). The authors describe the formation of sub-micron species characterized by distinctive segmentation and filamentous fuzzy fringes, which nucleate and expands into growing fibres. In disease conditions, the αS protein assembles into the β-sheet rich fibrillar species. The journey to the fibril formation starts with the propagation of the oligomers (Alam, Bousset, Melki, & Otzen, 2019).

1.4.4 αS's physiological function

The physiological role of αS has always been elusive. Researchers have relied on mouse knockout studies to understand the protein's function (Tashkandi, Shameli, Harding, & Maitta, 2018). Interestingly, however, in the absence of αS, its role is taken over by other alternative pathways. The αS knockout mice do not exhibit noticeable phenotypic changes (Pfefferkorn et al., 2012). The membrane-binding ability of the protein has attracted researchers to understand its role in vesicular trafficking. The protein deficiency leads to altered shape and an increase in the size of the secretory particles in leukocytes (Tashkandi et al., 2018). In the absence of αS in knockout mice, ultrastructural changes are seen in blood leukocytes (Tashkandi et al., 2018). The formation of brain inclusions is significantly enhanced in the mice overexpressing human αS (Masliah et al., 2000).

In humans, αS accumulates in the presynaptic terminal of the neurons (Burre, 2015). Overexpression of αS inhibits dopamine release (Bendor, Logan, & Edwards, 2013). A mouse knockout study also suggests that αS is crucial for the vesicular trafficking across the synaptic terminal (Abeliovich et al., 2000). The protein controls the size of the presynaptic vesicles. It helps in vesicular genesis and maintains a reservoir of the vesicles across the synapses (Cabin et al., 2002; Murphy, Rueter, Trojanowski, & Lee, 2000). The negative feedback directed reduction in the reservoir pool of vesicles is seen in mice hippocampus under the surge of αS expression (Nemani et al., 2010). The overexpression of αS influences the exocytosis of neurotransmitters in PC12 cells (Larsen et al., 2006). Mice that modestly overexpress αS show redistribution of vesicles away from the synapses (Mor et al., 2016). The density of vesicles in synaptic buttons is also reduced, suggesting αS inhibits vesicle clustering (Mor et al., 2016). A conflicting result is seen with yeast overexpressing αS, which indicates that αS causes vesicle clustering (Mor et al., 2016). Similarly, αS restricts vesicle diffusion away from synapses in mouse hippocampal neurons (Mor et al., 2016).

Animal studies have shown the harmful implications of the SNCA A30P germline mutation. Induced expression of A30P-αS in Snca−/− mice has been shown to diminish dopamine release

(Zhang et al., 2019). It also depletes proliferation of subventricular zone in mice brain and alters olfactory bulb neurogenesis. The A30P-αS is known to diminish autophagic flux in the midbrain dopaminergic neuron leading to accumulation of intracellular proteinaceous aggregates (Lei, Cao, & Wei, 2019).

During the song production in the zebra finch, differential expression αS mRNA is seen in the motor pathway suggesting a direct cognitive role (George, Jin, Woods, & Clayton, 1995). The homologous sequence to 14-3-3 protein suggests αS has a chaperoning role inside the cells (Park et al., 2002). The amphipathic N-terminus interacts with the target protein, and the acidic tail gives them solubility (Park et al., 2002). The protein participates in the neurotransmitter release by helping cysteine-string, protein-alpha and SNARE proteins (Chandra, Gallardo, Fernandez-Chacon, Schluter, & Sudhof, 2005). The unstructured protein adopts α-helical conformation upon interaction with lipid membranes and protects the unsaturated lipids from oxidative stress (Zhu, Qin, Hu, Munishkina, & Fink, 2006). Intracellular acidification resulting from stress can induce αS translocation from cytosol to the mitochondrial surface (N. B. Cole, Dieuliis, Leo, Mitchell, & Nussbaum, 2008). The αS protein is also seen to protect cells from hydrogen peroxide challenge by a synergetic increase in the JNK-interacting protein (JIP)-1b/islet-brain (IB)1 (Hashimoto et al., 2002). Further, the protein is involved in response to injury and neurodegeneration (Hashimoto et al., 2002). Overall, the physiological functions of αS remain poorly understood despite numerous studies on various aspects of the protein over the last few decades (Bendor et al., 2013). The role of αS in membrane modelling, however, is pretty established (Bendor et al., 2013). The αS is referred to as the minimal machinery for vesicle budding in the recent literature (Varkey et al., 2010). The αS has been referred to have a role in vesicle trafficking and enhancing endocytosis (Varkey et al., 2010). In neurological disorders like PD and Alzheimer's disease, the αS protein misfolds and forms aggregates in the brain. The misfolded αS protein also behaves as a prion and can spread the neurodegeneration through the neuraxis (Bendor et al., 2013).

1.4.5 Membrane interaction of αS

The αS localizes in the presynaptic nerve terminal of the neurons (Maroteaux et al., 1988). The protein surrounds the synaptic vesicles inside the neurons (Davidson, Jonas, Clayton, & George, 1998). In brain homogenates, the αS partitions into soluble and membrane-bound fractions (George et al., 1995). Although the αS does not have any specific transmembrane or lipid anchor domains, the protein smoothly interacts and modify the lipid membranes (Runwal

& Edwards, 2021). The two-thirds stretch of αS is the membrane-binding region (Perrin, Woods, Clayton, & George, 2000).

1.4.6 αS gets stabilized as an α-helix

Upon interaction with SDS micelles, the N-terminal of αS forms two helices in an antiparallel arrangement separated by an extended linker (helix-N, residues 3–37 and helix-C, residues 45-92) (Lorenzen, Lemminger, Pedersen, Nielsen, & Otzen, 2014). The protein attains up to 80 % helical content upon binding with lipid vesicles and resembles the class A_2 family of lipid-binding helices of apolipoproteins (Davidson et al., 1998; Perrin, Woods, Clayton, & George, 2001). The N-terminal acetylation does not cause structural changes in the membrane bound form of the protein (Runfola, De Simone, Vendruscolo, Dobson, & Fusco, 2020). The hydrophobic side chains get engrooved into the lipid-face of the membrane (Davidson et al., 1998). The residue-specific electrostatics are essential in the lipid-membrane interaction. Membrane binding gets hampered while the membrane facing hydrophobic residues are replaced with charged residues (Perrin et al., 2000).

1.4.7 Lipid rafts and αS

Cells have lipid-raft like microdomains in the plasma membrane. These membrane micro-clusters encourage targeted protein interaction (Davidson et al., 1998). Further, the lipid composition asymmetrically varies between inner/outer leaflets of the plasma membrane (Davidson et al., 1998). In Alzheimer's disease, lipid rafts are essential to induce pathogenesis (Rushworth & Hooper, 2010). The lipid rafts are plasma membrane micro-clusters enriched with cholesterol and sphingolipids (Y. Wang et al., 2020). In HeLa cells, αS colocalizes with GM1 and PI(4,5)P_2 suggesting its binding to lipid rafts (Fortin et al., 2004). The protein tends to identify and target raft-like patches in the plasma membrane (Fortin et al., 2004). Furthermore, reducing lipid rafts induces a downstream depopulation of synaptic αS pool (Fortin et al., 2004). The A30P Parkinsonian mutant is known to inhibit the raft-inclination of the protein (Fortin et al., 2004). On the contrary, confocal imaging of GUVs suggests that αS binds to anionic lipids in the liquid-disordered phase instead of rafts (Stockl, Fischer, Wanker, & Herrmann, 2008). The αS enrichment in lipid rafts, therefore, remains controversial.

1.4.8 Electrostatics of αS membrane interaction

The core of the N-terminal amphipathic helices of αS houses the KTKEGV consensus sequence (Fanning, Selkoe, & Dettmer, 2020). These helices resemble lipid-binding domain of the

apolipoproteins. In a helical-wheel model of αS, one-half side of the helix is rich with hydrophobic residues, which are involved in the penetration of the helix into lipid membranes (up to ~ 1-5 Å below the lipid head groups) (Fanning et al., 2020). The lysine residues in the edge of the other half of the α-helix interact with the negatively charged lipid headgroups. Several factors dictate the interaction of αS with the lipid membranes, which includes membrane curvature, charge, lipid-phase state, solution pH, salt concentration, and the lipid-protein ratio (Pirc & Ulrih, 2015). The αS has a strong affinity towards SUVs with at least 30 % acidic phospholipids (Davidson et al., 1998). The protein does not bind to neutral lipid bearing SUVs (Davidson et al., 1998). The synaptic vesicle membranes are rich in phospholipids and cholesterol (Table 1.3). The acidic phospholipid microdomains in the plasma membrane or the bilayer asymmetry dictate differential localization of αS in synaptic vesicles (Davidson et al., 1998). However, substantial binding is observed with up to 500 mM salt, indicating electrostatics may not be the only driving force (Pfefferkorn et al., 2012). Also, the lipids with smaller headgroups may provide more space to accommodate αS, which might drive the protein into the vesicles despite no apparent electrostatics (Pfefferkorn et al., 2012). Moreover, the affinity of αS towards phosphatidylserine is mediated by the internal regions of the protein (Perrin et al., 2000). At the same time, phosphocholine allures the αS mediated by any one of the three exons (Perrin et al., 2000). Quantitatively, αS has the highest affinity towards phosphatidic acid (PA) and a 60-fold less affinity towards POPG or POPS lipids (Middleton & Rhoades, 2010). In contrast, the affinity toward zwitterionic lipid POPC is nominal (Middleton & Rhoades, 2010). Recently it has been shown that altering the N-terminal electrostatics by acetylation increases the αS's membrane binding affinity (Runfola et al., 2020).

Table 1.3. Synaptic vesicle membrane composition. Adapted from (Michaelson, Barkai, & Barenholz, 1983).

Lipids	Content (% of total phospholipids)
PC	40.9 ± 2.5
PE	24.6 ± 6
SM	12.0 ± 2

Plasmenylethanolamine	11.5 ± 1
PS	7.35+ 1.3
PI	3.7 + 0.7
Cholesterol/total phospholipid molar ratio	0.63

1.4.9 αS lipid-binding specifics

While acidic headgroups are preferred, PE enhances αS-membrane interaction (Pfefferkorn et al., 2012). The TLC overlay experiments with isolated lipids showed that αS favours PE and PI over PS for binding (Jo, McLaurin, Yip, St George-Hyslop, & Fraser, 2000). In addition, αS is shown to prefer PA and PI over PS and PG (Middleton & Rhoades, 2010). Moreover, firm binding is reported to PC:PA vesicles (Middleton & Rhoades, 2010). In addition, αS also binds to gangliosides, lipid droplets, and SDS micelles (Pfefferkorn et al., 2012).

The lipid-binding ability and lipid-induced helicity in αS is a property linked strongly to its conserved sequence (Perrin et al., 2000). Deletion of a single N-terminal amino acid drastically affects the binding ability of the protein (Perrin et al., 2000). The A30P mutation is known to hamper regular membrane binding ability and raft association *(Fortin et al., 2004; Perrin et al., 2000)*.

The A53T mutation does not seem to influence the membrane-binding ability neither it disrupts raft association. The affinity of parkinsonian mutants towards negatively charged vesicles is E46K > WT = A53T > A30P (Middleton & Rhoades, 2010).

1.4.10 Regulation of membrane interaction

The regulation of membrane interaction might be an intrinsically controlled feature in αS (Snead & Eliezer, 2014). The phosphorylation of serine, threonine, and tyrosine residues (Y39, S87, Y125, and S129) plays an essential role in regulating the membrane binding of αS (Snead & Eliezer, 2014). Despite the polar side-chain of the threonine residues, the presence of long aliphatic chains helps them accommodate inside the non-polar face of the membrane (Davidson et al., 1998). The membrane interaction is readily lost upon phosphorylation of the threonine residues (Davidson et al., 1998). Another aspect is the absence of proline residue in αS; thereby, the lack of hairpin turns in the secondary structure (Davidson et al., 1998). Proline induced hairpin turns are a common feature of the apolipoprotein helices (Davidson et al., 1998). These

proteins can adjust the degree of turn across various sizes of particles. Thus, the αS have the flexibility toward binding to spherical lipids and the flat membrane, probably with regards to the missing proline residues (Davidson et al., 1998).

1.4.11 Curvature sensing by αS

The αS has a higher partition coefficient with the gel phase vesicles rather than liquid phase vesicles (Kjaer, Giehm, Heimburg, & Otzen, 2009). Further, the protein has a preference towards smaller diameter vesicles with affinity highest towards vesicles with the lowest diameter 46 nm > 77 nm > 93 nm > 116 nm (Middleton & Rhoades, 2010). The membrane curvature guides the structural conformation of αS (Middleton & Rhoades, 2010). The nature of the headgroups and lipid tails dictates the fluidity of the lipid bilayer (Seu, Cambrea, Everly, & Hovis, 2006). DPPG/DPPC have symmetric and saturated tail fragments conferring a gel-like phase to the bilayer at room temperature (Middleton & Rhoades, 2010). The POPC/POPS lipids have asymmetric tail bearing unsaturation, which confers the bilayer fluid-like phase at room temperature (Middleton & Rhoades, 2010). The αS have a three-fold affinity to the gel phase bilayer compared to the fluid phase bilayer (Middleton & Rhoades, 2010). In the absence of anionic lipids, αS has a nominal affinity towards LUVs and GUVs (Middleton & Rhoades, 2010). In contrast, it is not the case with smaller vesicle such as SUVs. The αS protein binds to SUVs independent of lipid composition (Middleton & Rhoades, 2010). Middleton et al. have a unique finding with the gel phase zwitterionic vesicles (Middleton & Rhoades, 2010). The αS has a 10-fold increased affinity towards LUVs prepared with DPPC compared with POPC enriched LUVs (Middleton & Rhoades, 2010). The multi-fold enhancement sheds light on the importance of lateral pressure of bilayer in alluring the αS.

1.4.12 Curvature induction by αS

In a lipid membrane, attractive and repulsive forces act at the level of lipid polar head group and the hydrophobic tail (Fig. 1.5) (M. F. Brown, 2017). The forces acting due to the chemistry of amphipathic lipid molecules along with the surface tension of water constitute the lateral pressure profile, which now acts and shape the lipid membrane (M. F. Brown, 2017). These pressure profiles are invisible and can only be obtained through theoretical simulations. Generally, a mismatch with the area of the lipid head group with that of the cross-sectional area of the tail results in a bending moment in the individual lipid monolayer (M. F. Brown, 2017). This results in a spontaneous curvature generation. There are three kinds of curved membrane viz. zero, positive and negative curvature. If the head group area exceeds the tail area, a tendency to curl dominates, paving the way towards micelle formation (gangliosides,

surfactants). In the case of head group area matches that of the chain, a planar bilayer formation is favoured (POPC). A small less hydrated head group leads to inside out forming a water-in-oil kind of dispersion, forming a negative curvature (M. F. Brown, 2017).

The normal cellular function involves on-demand curvature induction i.e., endocytosis, membrane scaffolding etc (Varkey et al., 2010). Some proteins are well known for artificial curvature induction *viz.* Apolipoprotein, Epsin1 and bin-amphiphysin-Rvs167 (BAR) (Ward, Ropa, Adu-Gyamfi, & Stahelin, 2012). In the case αS, the lipid interaction is mediated by the 11 amino acid repeats forming the amphipathic helices (Varkey et al., 2010). The hydrophobic region of the lipid tail seems amicable for the insertion of αS's hydrophobic side chains into the lipid membranes (Varkey et al., 2010). SUVs have comparatively greater curvature than LUVs. The αS has more affinity towards SUVs with lipids in gel-phase (DPPC) as compared to SUVs with lipids in the liquid-crystalline phase (POPC) (Hogen et al., 2012). The αS interacts with curved membranes and induces lateral expansion of lipids resulting in bilayer remodelling (Ouberai et al., 2013). The αS protein induces membrane thinning and divulges the lipids away from the membrane, resulting in curvature induction (Ouberai et al., 2013). The αS remodels the membrane to an extent, converting large vesicles into highly curved tubules and vesicles (Varkey et al., 2010). The membrane curvature generated with αS are analogous to that of the curvature generated by amphiphysin. However, the curvature induction by αS does not involve additional scaffolding and is robustly carried out by membrane insertion and wedging by the amphipathic helices alone (Varkey et al., 2010). This minimal machinery for vesicle budding comes with a furry of regulatory control. The degree of curvature control is a tightly controlled process in cells. One hypothesis which should be pondered upon is to evaluate the local tubulating protein density along-side the *in-vivo* tubulation requirement.

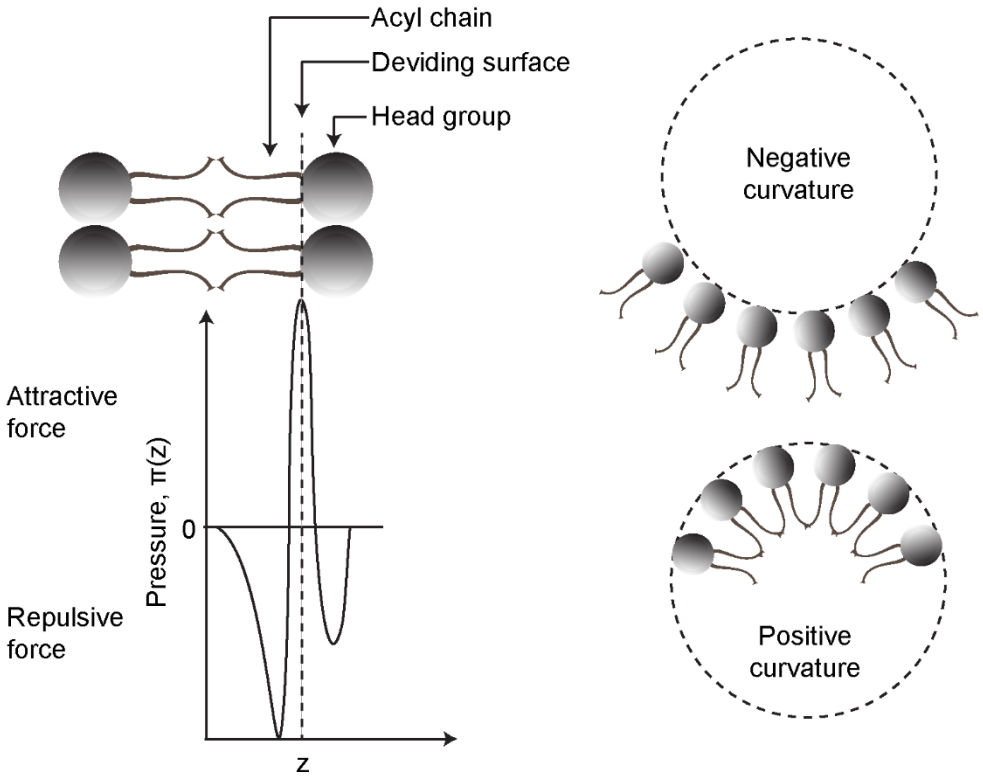

Fig. 1.5. Lateral pressure profile alongside a lipid molecule. The steric hindrance, electrostatic and hydrophobic interactions dictate the shape and size of the vesicle/micelles the lipids will form. Adapted from (Booth & Curnow, 2009).

1.4.13 αS at the air-aqueous interface

A protein's interaction with the surrounding bio-molecules is determined by the physicochemical properties conferred by its amino acid sequence and the conformation. The membrane proteins are well known to interact and slide into the membrane; some stay back in the inner/outer leaflet of a membrane (Yeagle, 2016). This mystical feat is achieved at the interfacial surface.

Dr. Irving Langmuir received a Nobel prize in chemistry in 1932 for his work on interfacial chemistry (Tanford, 1997). He introduced the Langmuir technique of mono-molecular layer preparation at the air-aqueous interface (Tanford, 1997). Rathinakumar et al. described the "Interfacial activity" as "the ability of a molecule to bind to a membrane, partition into the membrane–water interface, and to alter the packing and organization of the lipids" (Rathinakumar, Walkenhorst, & Wimley, 2009). Proteins with rich amphipathic domains are membrane/interface seekers. They readily partition into a membrane and usually undergo structural transformation due to complementary electrostatics and hydrophobic sweet spots available in the membrane.

In an air-aqueous system, water molecules present at the interface experience an imbalance of force (Fig. 1.6). The surface tension is the measure of the cohesive energy at the interface. Molecules having an amphiphilic nature get readily adsorbed into an interface. An incoming amphiphile to an interface lowers the interfacial surface tension (Menger, Galloway, & Chlebowski, 2005). It is possible to monitor the change in the surface tension using a Langmuir instrument (Chaari et al., 2013). The surface pressure π (mN/m) is the change in the surface tension due to the presence of a monolayer. Typically, the amphiphiles are added in the bulk aqueous phase. Their kinetics of adsorption at the interface is determined by monitoring the change in the surface pressure over time. Depending upon the study, the amphiphiles may directly be layered over the aqueous subphase, giving a monomolecular layer (often somewhat loosely called a monolayer). The packing or density of the molecules at the interface can be controlled by compressing/expanding the physical barriers that change the are of the interface (Fig. 1.7) (Chaudhary & Nagaraj, 2011). The compression/expansion of the monolayer, at a constant temperature, gives a surface pressure (π)-area (A) isotherm. The data is often presented as π against molecular area *i.e.* the area per molecule. The π-A isotherm, is a measure of molecular crowding and provides valuable information about the phase changes (Dennison, Harris, & Phoenix, 2014) (Chaudhary & Nagaraj, 2011). Typically, the experiment is carried out by spreading the amphiphiles over the subphase. The barriers are kept fully open, *i.e.* the amphiphiles are spread over a large area (Dennison et al., 2014). The amount of the amphiphile added is such that there is no significant change in the surface pressure. The monolayer, therefore, is said to be in the gaseous phase because there is little interaction between the molecules due to low density. The gas-phase monolayers, therefore, are highly compressible. As the barriers move towards each other, the density increases, thereby causing a decrease in surface tension or an increase in the surface pressure. (Dennison et al., 2014). Beyond a certain pressure, the molecules may display phase transition. Lipids, for example, show a transition from a gas phase to what is known as a liquid-expanded phase. Further compression could lead to more such phase transitions, ultimately leading to the solid or gel phase. Beyond a critical surface pressure, known as collapse pressure, the monolayers break down (Dennison et al., 2014). The phase transition is better visualized in a compressibility modulus (C_s^{-1}) vs π plot (Dennison et al., 2014). The C_s^{-1} is calculated as the negative product of molecular area and the ratio of the first derivative of pressure with respect to the molecular area (Dennison et al., 2014).

$$C_s^{-1} = -A\frac{d\pi}{dA}$$

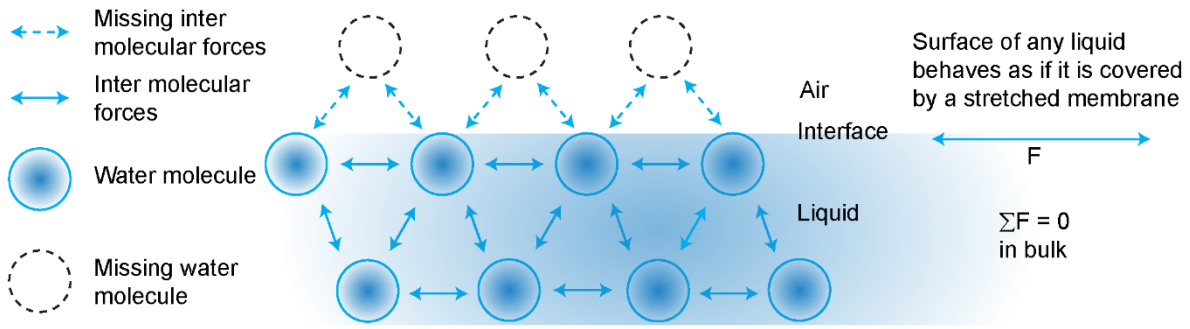

Fig. 1.6. The surface tension of water. The surface tension measures the cohesive energy present on the interface. In bulk, the net force experienced by molecules is zero. The molecule at the interface experience an imbalance of forces, as there are no molecules above them. Thus, there exists a stretching force across the surface of any liquid.

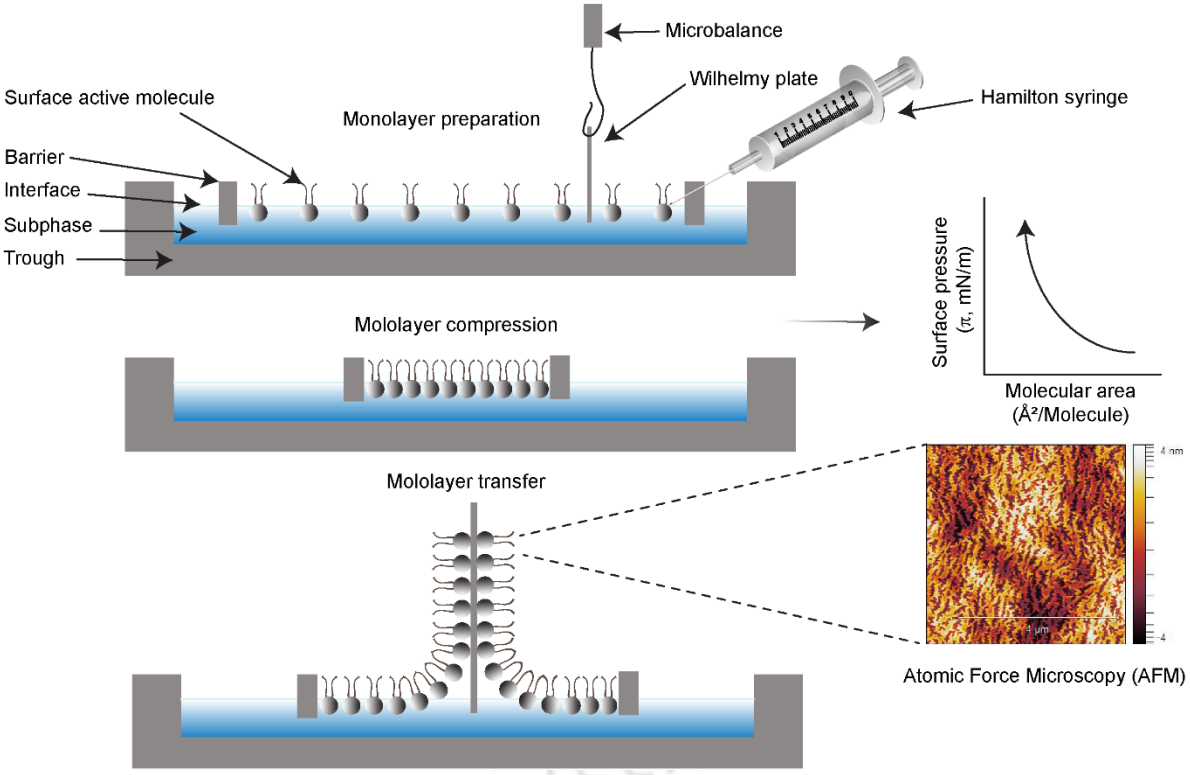

Fig. 1.7. Self-assembly at the interface. The interface plays a vital role in the adsorption of the amphiphiles from the bulk. Using a Langmuir apparatus, it is possible to compress the amphiphiles present on the surface to prepare a Langmuir monolayer. The monolayer can be transferred very carefully into substrates like silicon wafers and glass or quartz using the Langmuir-Blodgett apparatus to create an LB film. The characterisation of the LB film reveals molecular interactions among the amphiphiles.

Over the decade, the membrane interaction of αS has been worked out in detail (C. Liu et al., 2021). The readily available interfaces (micelles, vesicles, and membranes) inside the cells influence the polymorphic form of the αS (Borbat, Ramlall, Freed, & Eliezer, 2006; Zhu & Fink, 2003). The unstructured αS in solution adopts a helical conformation upon adsorption at the interfaces (Lokappa & Ulmer, 2011). Some research mandates the association of membrane towards the existence of the helical form of the protein (Killinger, Melki, Brundin, & Kordower, 2019). The lipid interaction has been shown to promote the oligomerization of the αS protein (Perrin et al., 2001). Killinger et al. argued that soluble tetrameric αS is associated with a lipid cofactor (Killinger et al., 2019). Also, the membrane interface has been suggested to inhibit fibrillation of αS (Zhu & Fink, 2003). It is challenging to study the self-assembly of proteins attached to lipid vesicles. Researchers often have to rely on single-molecule techniques to study self-assembly on supported bilayers. However, a fundamental understanding of the behaviour of αS at the interface is lacking. Recently people are interested in evaluating the interfacial properties of the αS at the air-aqueous interface. The monolayer technique has been instrumental in studying surface-active molecules. Chaari et al. estimated the interfacial activity of the highly surface-active αS protein (Chaari et al., 2013). The authors rightly pointed out that αS's surface activity is comparable to that of the lytic peptide of bee venom melittin (Raghuraman & Chattopadhyay, 2007). The monomeric αS rapidly adsorbs to the air-aqueous interface and attains a surface pressure π of ~20 mN/m. The fibrils of the protein have a lesser surface activity (Chaari et al., 2013). Using the LB technique, it has been shown that αS molecules adopt an α-helical conformation at the air-aqueous interfaces (C. Wang et al., 2010). The protein helices remain parallel to the interface (C. Wang et al., 2010).

Moreover, the flat-monolayer of lipid has been helpful to understand the protein-lipid interaction (Chaari et al., 2013). Under a monolayer of lipid, the monomeric and fibrillar αS both show a little higher surface activity (Chaari et al., 2013). The αS has higher surface activity under an anionic lipid monolayer than under a zwitterionic lipid monolayer (Chaari et al., 2013).

1.4.14 In vitro aggregation of αS

The *in vitro* aggregates of αS in solution resemble PD brain-derived aggregates; both of them are fibrillar structures with cross-β structures (Hoyer et al., 2002). The time scale of *in vitro* αS aggregation depends on various parameters (Hoyer et al., 2002). Some of the parameters that have a strong influence on the aggregation kinetics and the morphology of the aggregates are the protein concentration, pH, ionic strength, temperature, and agitation (Jain, Singh, Roy, &

Bhat, 2018). At lower pH, the aggregation of the αS occurs rapidly, fuelled by the masking of inter-molecular repulsion between the acidic C-terminal tails. Besides, charge neutralization of the C-terminal tail leads to compaction of the NAC region. The compaction of the NAC region diminishes intramolecular diffusion, thereby facilitating self-assembly. (McClendon, Rospigliosi, & Eliezer, 2009). The kinetics of fibrillation is usually monitored using the intercalating fluorescence dye Thioflavin T. Dyes such as 8-anilino-1-naphthalene sulfonic acid (ANS) and Nile red are also often used to probe the exposed hydrophobic stretch during protein misfolding and aggregation (Hoyer et al., 2002). The aggregation proceeds via a long lag phase, a sigmoidal phase with a rapid increase in fluorescence, followed by a plateau phase (see Fig. 1.8). (Kulikova, Makarov, & Kozin, 2015). The microscopic characterization of the fibrils is done using atomic force microscopy and transmission electron microscopy (Ruggeri et al., 2018).

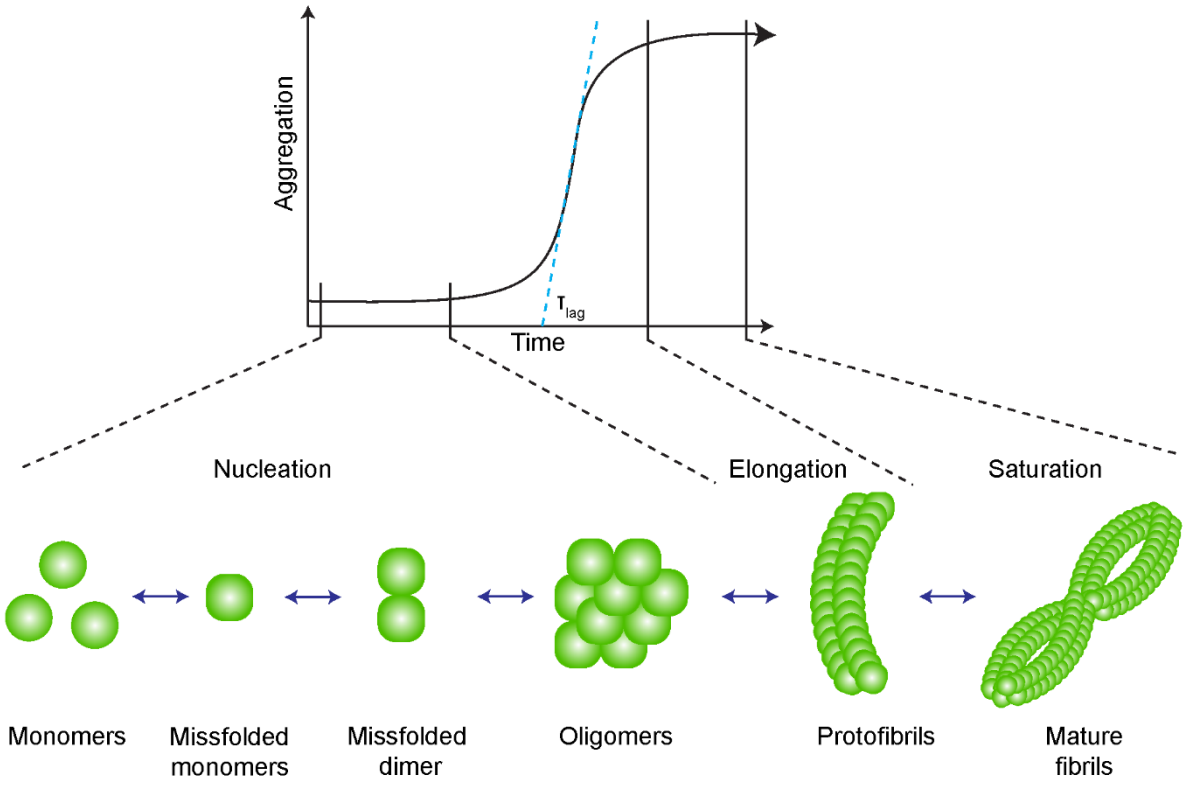

Fig. 1.8. The aggregation kinetics followed by an amyloidogenic protein. During the self-assembly, the monomeric form of an IDP is present in equilibrium with its misfolded counterpart. Protein misfolding is a stochastic process. It takes time for the nucleation of the monomer to form oligomers, which is visualised as a lag phase during the aggregation kinetics. The nucleation of oligomers rapidly destabilises the equilibrium resulting in fibrillation. Once

the fibrils mature, the fibrillation reaches a stationary phase. Adapted from (Kulikova et al., 2015).

1.4.15 Pathological structure of αS

The hallmark of PD pathogenesis is the presence of cytosolic Lewy bodies and Lewy neurites in the post mortem brain (G. E. Alexander, 2004). Lewy bodies are primarily composed of filamentous αS aggregates (Mahul-Mellier et al., 2020). The 12-residue hydrophobic stretch in the middle of NAC (^{71}VTGVTAVAQKTV^{82}) encompasses the core of the αS filaments (Giasson et al., 2001). This mid-NAC stretch is necessary and sufficient to induce fibrillation in an otherwise monomeric αS (Giasson et al., 2001). The secondary structure of the aggregates formed by full protein and various peptide fragments is estimated using CD spectroscopy, nuclear magnetic resonance spectroscopy (NMR) and solid-state NMR spectroscopy (ssNMR) (Atsmon-Raz & Miller, 2015; Comellas et al., 2011; Gath et al., 2012; Heise et al., 2008; Heise et al., 2005; Vilar et al., 2008). In 2016, Tuttle et al. reported the first high-resolution 3D structure of the full-length pathogenic fibril using ssNMR (Tuttle et al., 2016). Since then few high resolution structure have been reported using Cryo-EM (Guerrero-Ferreira et al., 2019; B. Li et al., 2018; Y. Li et al., 2018). It appears that the self-assembly condition and the familial mutations influence the final fibrillar architecture of the polymorphs (B. Li et al., 2018; Tuttle et al., 2016). To date, there are four different types of polymorphs of αS fibrils reported.

In the ssNMR structure of αS deciphered by Tuttle et al., the inner core of the fibril remains in a parallel in-register β-sheet with a Greek key motif topology (PDB ID: 2N0A) (Tuttle et al., 2016). The fibril architecture is further stabilized with an intermolecular salt-bridge (E46-K80), few steric zippers (V49, V77, V82), a glutamine ladder (Q79) and hydrophobic packing arrangements (I88, A91, and F94). The presence of smaller yet flexible residues (serine, alanine, and glycine) at crucial stretches of the protein helps the protein attain the β-sheet rich Greek key architecture. The fibril structure is 4.6 nm wide. The β-sheet rich fibrillar core is largely composed of the 46-96 residue stretch. The stretches flanking this region remain largely solvent-exposed.

Li et al., in 2018, reported the cryo-EM derived amyloid fibril structure of αS (PDB ID: 6A6B) encompassing residues V37 - Q99 (Y. Li et al., 2018). The fibril forms a helix ~10 nm wide, with a helical pitch of 239 nm. The individual fibril structure shows two protofilaments in a side-by-side arrangement. Each of the protofilaments forms a Greek key topology facing opposite to each other in an intertwined manner (Fig. 1.9B). The eight-residue intertwined

steric zipper region covers the stretch ^{50}HGVATVAE^{57}. Four of the six familial PD mutations (H50Q, G51D, A53E, A53T) are restricted to the dimer interface, while the E46K mutation is likely to perturb the E46-K80 salt bridge. The dimer is stabilized by the residues forming hydrophobic interaction (A53 and V55). The E57 and H50 flanking the steric zipper core together with the K45 forms electrostatic interaction and shields the steric zipper from solvent exposure (Fig. 1.9).

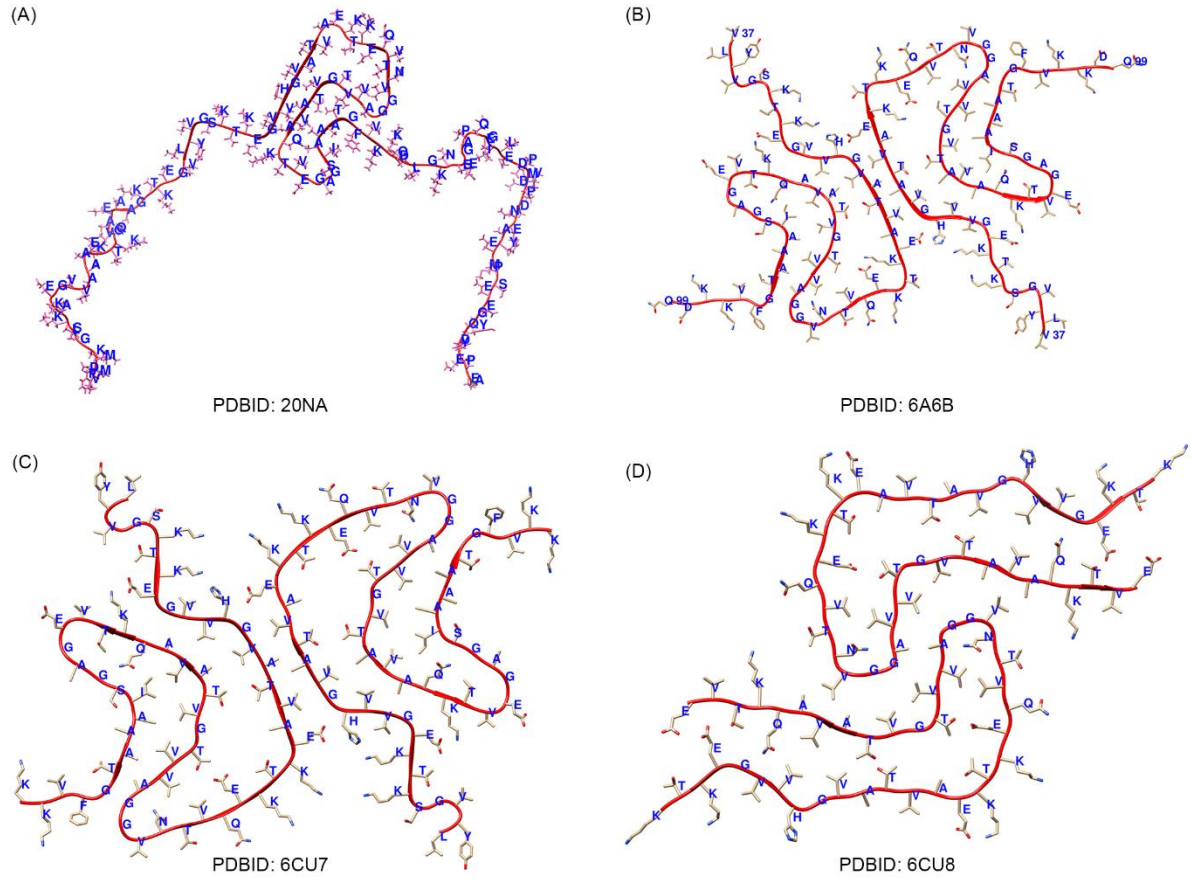

Fig. 1.9. The fibrillar structure of αS. Tuttle et al. reported the fibrillar structure of αS with parallel in-register β-sheet and a Greek key motif topology (Tuttle et al., 2016) (A), Li et al., in 2018, reported the cryo-EM derived amyloid fibril structure of αS (Y. Li et al., 2018) (B), The "rod"(C) and "twister" (D) shaped fibre polymorphs of αS were reported by Li et al. in 2018 (B. Li et al., 2018). The top chain of the fibril structures are shown to visualise the intermolecular interactions.

In the same year, Li et al. worked out a 3.7 Å resolution structure of a full-length αS fibril using cryo-EM (B. Li et al., 2018). The authors reported the presence of "twister" and "rod" like fibre polymorphs in their preparations. They found a preNAC steric zipper (^{47}GVVHGVTTVA^{56}) in their rod-shaped polymorphs and a steric homo-zipper (^{68}GAVVTGVTAVA^{78}) in their twister polymorphs. In the twister model, the αS parkinsonian mutations do not fall under the purview of the steric zipper. Hence, it is likely that the mutations will systematically promote a twister architecture rather than going for the rod-like polymorphs.

Ferreira et al., in 2019, reported two new polymorphs of αS (2a and 2b) (Guerrero-Ferreira et al., 2019). These structures are distinct from the earlier reported polymorphs. Here, the N-terminus wraps around the fibril and encloses the NAC. The electrostatics of the interface between the protofilaments is dominated by inter-molecular salt-bridges (K45 – E57 or K45 – E46). The αS parkinsonian mutants exhibit different fibrillar architecture (Table 1.4).

Table 1.4. The fibrillar architecture of αS's Parkinsonian variants probed through AFM. Adapted from (Y. Li et al., 2018).

	Fibril width (nm)	Periodicity	Fibril twist
WT-αS	10.5 ± 0.8 nm	120 ± 14 nm	Left-handed fibril
A30P-αS	10.5 ± 0.7 nm	120 ± 19 nm	Left-handed fibril
E46K-αS	9.0 ± 0.5 nm	60 ± 8 nm	Right-handed fibril
H50Q-αS	7.0 ± 0.5 nm		
G51D-αS	7.0 ± 0.4 nm		
A53E-αS	7.5 ± 0.4 nm	60–80 nm	
A53T-αS	9.5 ± 0.3 nm	80 ± 13 nm	Left-handed fibril

1.5 Research design and objectives

The polymorphic nature of αS allows it to switch between unordered conformation in solution to attain the α-helical conformation while it interacts with lipid vesicle. Getting inspired from the αS's ability to switch conformation, the interfacial properties of αS were investigated to understand the structural transition during conformational switching. Since the protein remains physiologically in N-terminally acetylated state, an objective comparison of the interfacial

properties among the NH_2-αS and the Ac-αS was carried out. Using the LB method, the surface activity of both these variants were ascertained. Further, the compression/expansion of the LB protein monolayer was carried out to understand the interfacial self-assembly. The Blodgett deposition of the LB monolayer onto a quartz slide/silicon wafer was carried out to understand the structural transition of the protein while it forms LB film. The structural analysis was carried out using CD and LD spectroscopic methods. The AFM characterization of LB thin film was carried out to visualise the self-assembled state of the protein.

The following objectives were undertaken in this thesis:

- To understand the effect of N-terminal acetylation on the αS's interfacial properties.
- To investigate the interfacial properties of αS's parkinsonian variants.
- To investigate the effect of polymyxin B on αS aggregation

CHAPTER 2

Materials and Methods

2.1 Materials

The plasmid pET21a-alpha-synuclein was a gift from Michael J Fox Foundation MJFF (Addgene plasmid # 51486), while the plasmid pNatB (pACYCduet-naa20-naa25) was a gift from Dan Mulvihill (Addgene plasmid # 53613) (Johnson, Coulton, Geeves, & Mulvihill, 2010). Reagents for protein expression, purification, and monolayer studies were procured from Himedia, Sigma Aldrich, Merck, and Sisco Research Laboratory. Polymyxin B analytical standard solution (1 mg/ml in H_2O, Product No. 81271) and Thioflavin T (Product No. T3516) were procured from Sigma Aldrich. The 1 mm thick high precision quartz slide, used for CD and LD analysis of Blodgett films, was procured from Hellma Analytics. The rotation mount from Thor Labs was kindly provided by Dr. Gagan Kumar, Department of Physics, IIT Guwahati. HiTrap QFF anion-exchange and HiLoad® 16/600 Superdex® 75 pg columns were procured from GE healthcare (Sweden). Chromatography was performed on an AKTA Prime Plus chromatography system, GE healthcare (Sweden).

2.2 Methods

2.2.1 Protein expression

Using the pET21a- alpha-synuclein plasmid and the oligonucleotides obtained from GenScript, USA (Table A1 in Appendix), we carried out the site-directed mutagenesis to obtain the six gene constructs having single αS mutations *viz.* A30P, E46K, H50Q, G51D, A53E, and A53T (H. Liu & Naismith, 2008). The sequences of the gene constructs were confirmed by sequencing the plasmid DNA at Agrigenome, India (Fig. A1). *E. coli* BL21(DE3) cells were transformed with the plasmid pET21a-alpha-synuclein (for NH_2-αS) and co-transformed with the plasmids pET21a-alpha-synuclein and pNatB (pACYCduet-naa20-naa25) (for Ac-αS) using standard transformation methodology (Sambrook, Fritsch, & Maniatis, 1989). Similarly, the *E. coli* BL21(DE3) cells were transformed with pET21a-αS-*A30P*, pET21a-αS-*E46K*, pET21a-αS-*H50Q*, pET21a-αS-*G51D*, pET21a-αS-*A53E*, and pET21a-αS-*A53T* plasmids. The primary inocula were prepared from single colonies of the transformed cells that were subsequently used as inocula in the 800 ml Luria-Bertani broth, containing 100 µg/ml Ampicillin and 50 µg/ml Chloramphenicol (for Ac-αS). Once the cultures attained an OD_{600} = 0.6, IPTG was added with a 1 mM effective concentration, and the cultures allowed to grow for 15 h at 25 °C with 150 rpm shaking. The cells were harvested by centrifuging the culture at 8000 rpm, and the pellets were resuspended in 60 ml of Buffer A (20 mM Tris-Cl, 5 mM EDTA, pH 8.0). After one round of washing with the same buffer, the cell suspensions were spiked with PMSF (1 mM effective concentration) and sonicated for 45 min with 8 s 'ON'

and 22 s 'OFF' cycle at 33% amplitude to obtain a clear suspension. The enrichment of the proteins was achieved using a well-established boiling method (Coelho-Cerqueira et al., 2013). Briefly, the sonicated clear suspensions were kept in the ice for 1 h before being quickly transferred to a 95 °C water bath. The suspensions turned turbid due to the precipitation of the insoluble proteins. After 20 min of incubation at 95 °C, the suspensions were centrifuged at 20,000×*g* for 30 min, and the clear supernatants (containing soluble NH_2-αS or Ac-αS or the mutants) were passed through 0.45 μm filters. The filtrates were used for isolating the proteins using ion-exchange and size exclusion chromatography.

2.2.2 Anion exchange chromatography

The proteins were enriched on the HiTrap QFF anion-exchange column from GE Healthcare using AKTA Prime Plus chromatography system. The filtered cell lysates were loaded on the anion-exchange column that was pre-equilibrated with Buffer B (20 mM Tris-Cl, 1 mM EDTA, pH 8.0). Elution was carried out using a linear gradient of Buffer C (20 mM Tris, 1 mM EDTA, 1 M NaCl, pH 8.0) at 5 ml/min flow rate.

2.2.3 Size exclusion chromatography (SEC)

The partially purified proteins were concentrated using Pierce 3 kDa MWCO centrifugal concentrators. The concentrated proteins were further purified on an AKTA Prime Plus chromatography system with HiLoad® 16/600 Superdex® 75 pg size exclusion column pre-equilibrated with 25 mM phosphate buffer, pH 7.5 using a flow rate of 1 ml/min. For the experiments carried out in chapter 5, the eluant from anion exchange was dialysed against Buffer D (25 mM phosphate buffer, 0.01% NaN_3, pH 7.4) using a pre-activated Thermo Scientific™ SnakeSkin™ Dialysis Tubing, 7 K MWCO. The dialysed sample volume was reduced to one-third using a Thermo Scientific™ Pierce 3 kDa MWCO centrifugal concentrator. The concentrated fraction was filtered through a 0.45 μm filter for clarification and ultra-centrifuged at 100,000 *g* for 1 h at 4 °C using a Thermo Scientific™ Sorvall™ WX+ ultracentrifuge. The SEC was carried out in the same Buffer D. The SEC fractions were analyzed using SDS-PAGE (Figs. 3.1 and A2). The purity of the protein fractions was ascertained using reversed-phase HPLC, and the identity was confirmed using MALDI-TOF mass spectrometry (Figs. A3, A4, A5, and A6; Table A2). The SEC fractions were used as the protein stocks for further experiments. As all the αS variants have identical aromatic amino composition, their concentrations were estimated by using the ε_{280} = 5,120 $M^{-1}cm^{-1}$ reported in the literature for the wild-type αS (Pfefferkorn & Lee, 2010).

2.2.4 Dynamic light scattering (DLS)

The DLS was recorded on a Malvern Zetasizer Nano-ZS instrument for the protein stock solutions in 25 mM phosphate buffer, pH 7.5. Twenty measurements were made at 25 °C in the 173° backscatter configuration. The DLS analyses of the αS Parkinsonaian variant's purified protein stock solutions were carried out using Malvern Zetasizer NANO-ZS90 DLS instrument with 90° measurement angle (Fig. A7). The size and the polydispersity index were determined using the inbuilt softwares.

2.2.5 Surface activity

The interfacial properties of the NH_2-αS and Ac-αS were investigated at the air/aqueous interface on a KSV NIMA Langmuir-Blodgett instrument (Code: KN 2002), Biolin Scientific, Sweden. The 10 mM phosphate buffer, 150 mM NaCl, pH 7.5 was taken as the aqueous subphase. The surface-seeking propensity of the proteins was investigated by injecting them in the subphase. Briefly, 10 ml buffer was added to a thoroughly-cleaned custom-made circular Teflon trough with 13.2 cm^2 area. The trough was set-up for gentle magnetic stirring at the bottom of the subphase. Once the surface of the subphase became stagnant, a paper Wilhelmy plate was dipped, and the set up was allowed to stabilize (Fig. 2.1). The surface pressure was set to zero and 0.1 nmoles of protein was injected into the subphase. The increase in surface pressure was monitored over time. Once the pressure began to stabilize, more protein was added, and changes in surface pressure recorded.

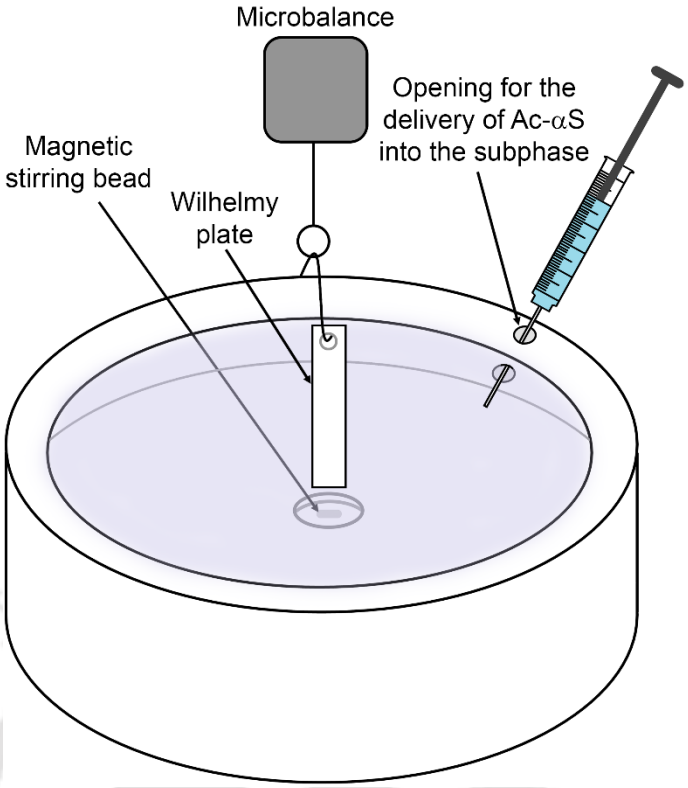

Fig. 2.1. The custom-made circular Teflon trough having a slot for a tiny magnetic bead and an opening through the wall for delivery material in the subphase.

The compression-expansion isotherms as well as the Blodgett deposition were carried out using the standard 200 ml rectangular Teflon trough. The barriers were expanded to encompass 234 cm^2 area. The surface pressure was set to zero, and a compression/expansion cycle was recorded to ascertain the absence of surfactants. The 40 µl of 50 µM protein stock solution was carefully layered on the aqueous subphase to obtain a two-dimensional monomolecular layer at the air-aqueous interface. The set-up was left undisturbed for 30 min. Three compression/expansion cycles were recorded with 20 cm^2/min barrier speed. The fourth and the final compression was made to achieve a surface pressure between 26 and 28 mN/m, followed by automatic single layer Blodgett deposition over a pre-cleaned quartz surface at a slow rate of 5 mm/min (1 mm/min for the αS Parkinsonan variants) to ensure uniform deposition with minimal defects (Fig. 2.2) (Chen & Liu, 2006; Kurniawan, Ventrici de Souza, Dang, Liu, & Kuhl, 2018). The surface pressure (π) was plotted against the molecular area (A), and the limiting molecular area (A_0) was determined using the first compression cycle by extrapolating the steep part of the compression isotherm. The compressibility modulus (C_s^{-1}) was calculated by multiplying the negative of the molecular area to the corresponding dπ/dA values.

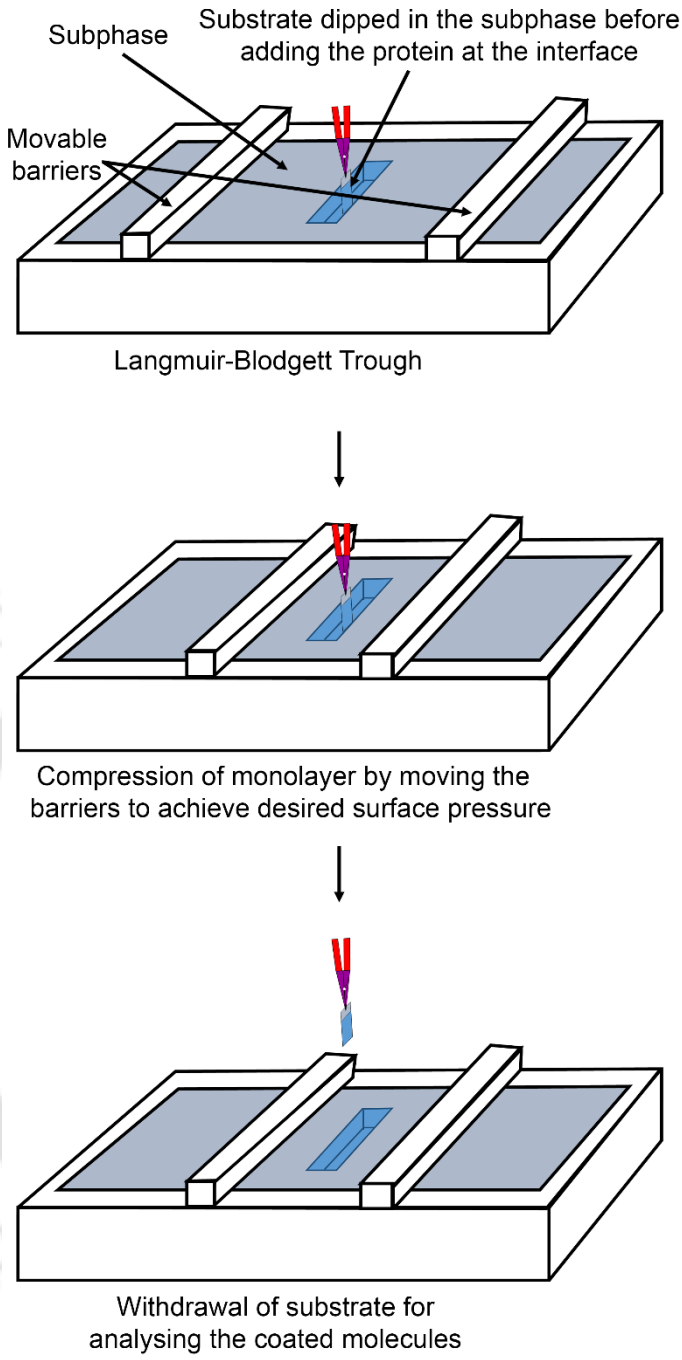

Fig. 2.2. The schematic diagram of Blodgett deposition on the pre-dipped substrate from a compressed monolayer.

2.2.6 Protein-lipid interaction

To probe the protein-lipid interaction, the custom-made circular trough was utilised in a different setting. Here, the lipids from 1.5 mM POPC or POPC:POPS (1:1) stock solutions, prepared in chloroform, were layered over the subphase (10 mM phosphate buffer, 150 mM NaCl, pH 7.5). The lipids were layered to attain the desired starting surface pressures. Once the initial surface pressure (π_i) stabilised, one nanomole of the purified protein was introduced

into the subphase through the orifice. The change in surface pressure was monitored till it reached the plateau (π_f). The $\Delta\pi$ (π_f - π_i) was plotted against π_i to understand the membrane-seeking propensity of the αS and its variants.

2.2.7 Circular dichroism (CD) spectroscopy of the LB film

After recording the three compression/expansion cycles, the monolayers were compressed (the 4th compression isotherm, 4^{C}) to π ~17-18 mN/m, and Blodgett-deposited on a pre-dipped quartz slide by retrieving it at 5 mm/min (1 mm/min for αS Parkinsonian variants) speed. The slow and steady retrieval assists in the uniform deposition of the LB film with minimal defects. The secondary structures of the proteins in the LB films were investigated using far-UV CD spectroscopy. The CD spectra were recorded on a Jasco J-1500 CD spectropolarimeter. As only two monolayers (one monolayer on each side of the quartz slide) are deposited upon single Blodgett deposition, 48 accumulations were collected for each spectrum to obtain a good signal to noise ratio. The spectra were recorded with a 0.05 nm data pitch at a speed of 100 nm/min and 1 nm bandwidth. The CD spectra of the proteins (2 μM) were also recorded in the subphase. Twelve accumulations were acquired for each spectrum. To monitor the secondary structure transition during aggregation of αS, aliquots from the aggregation reactions were diluted 50-fold in 25 mM phosphate buffer pH 7.4 to obtain a 2 μM effective αS protein concentration. The CD spectra were recorded with 0.1 nm data pitch and 1 nm bandwidth in a 1 mm path length quartz cell. Each spectrum is the average of 8 accumulations. The spectra were smoothed using the second-order polynomial Savitzky-Golay algorithm with a 20 points window in Origin 2018 software. The mean residue ellipticity ([θ]MRE) was calculated as described elsewhere [27].

2.2.8 Linear dichroism (LD) spectroscopy of the LB films

The linear dichroism (LD) is a chiral sample's differential absorption of parallel and perpendicularly polarized light (Rodger). LD spectroscopy was employed to investigate the orientation of the protein deposited as LB films on the quartz slide. The quartz slides having LB films were placed on a rotation mount and kept in the light path in the Jasco J-1500 CD spectropolarimeter. The LD [dOD] spectra were recorded with one accumulation from 260 to 190 nm with 0.1 nm data pitch, 1 nm bandwidth, 2 s digital integration time, and a scan speed of 100 nm/min. The reduced linear dichroism (LD^r) was calculated by dividing the obtained LD values by isotropic absorbance (A_{iso}) of the sample. The LD^r plot against wavelength represents the LD value, which is independent of the path length and the concentration of the sample.

2.2.9 Atomic force microscopy (AFM)

AFM images of the coverslip/silicon wafer-deposited LB films were recorded in non-contact mode on a Cypher Asylum Research AFM. The WSxM 5.0 Developer 9.2 software was used to plane, flatten, and equalize the images reported in chapter 3 (Horcas et al., 2007). The images for αS Parkinsonian variants (the images reported in chapter 4) were analysed using Gwyddion open source STM software with the plane, flatten, and equalisation tools.

2.2.10 Thioflavin T (ThT) fluorescence assay

The αS aggregation kinetics in the absence or presence of PMB was monitored for 120 h using ThT fluorescence assay. The PMB stock solution (1 mg/ml in H2O) with formula weight 1385.61 Da (C55H96N16O13.2H2SO4) corresponds to 721 µM concentration. Aggregation was set up with 100 µM αS protein in 25 mM phosphate buffer pH 7.4, 0.01% sodium azide at room temperature with continuous agitation using PTFE-coated magnetic microbeads. The aliquots were drawn at different time points and ThT fluorescence was measured effectively with 1 µM αS in 25 mM phosphate buffer pH 7.4 in the presence of 10 µM ThT on a Jasco FP8500 spectrofluorometer with λex = 440 nm, 2.5 nm slit width. Fluorescence emission spectra were recorded from 460 to 600 nm, with a slit width of 5 nm and the data pitch of 0.5 nm. The fluorescence intensity at 482 nm was extracted from the spectra and plotted against the incubation time. Data from three independent experiments were used to compute the mean fluorescence intensity and standard deviation. The sigmoidal fitting of the aggregation kinetics data was done using the Boltzmann function with Levenberg Marquardt iteration algorithm.

2.2.11 Transmission electron microscopy (TEM)

The aggregation of αS was examined using TEM on a JEOL JEM-2100F FE-TEM instrument at 200 kV. Briefly, the 5 µl aliquots were taken from the aggregation reactions (100 µM αS with or without 100 µM PMB). The aliquots were diluted five times with Buffer D and deposited on the carbon-coated copper grids (Electron Microscopy Sciences, Hatfield, USA). The grids were then washed with deionized water five times, air-dried, and 5 µl of 2% uranyl acetate solution was added. The grids were dried overnight under a desiccator and analysed by TEM.

2.2.12 Neuronal cell viability assay

Mice neuro-2a cells were procured from National Centre for Cell Science (NCCS), Pune, India. Cells were maintained in Dulbecco's Modified Eagle's Medium (DMEM) supplemented with 10% fetal bovine serum (Invitrogen, Grand Island, NY) at 37 °C in 5% CO_2. The 3-(4,5-

dimethylthiazol-2-yl)-2,5-diphenyltetrazolium (MTT) bromide formazan conversion assay was performed to determine cytotoxicity. The cells (10^4 /well) were seeded in a 96-well microtiter plate, 12 h prior to the treatment. The αS aggregation reactions, with and without equimolar PMB, were set up at 100 μM protein concentration in 25 mM phosphate buffer, pH 7.4 with constant stirring using a micromagnetic bar. The cytotoxicity was assayed for the 0 h (freshly prepared samples), 25 h, 70 h, and 120 h aged samples. Briefly, the αS aggregation samples were diluted 12.5-fold in a separate V-bottom plate using DMEM medium (without FBS). The cells were washed with phosphate-buffered saline and incubated with the diluted samples for 4 h. Following incubation, the treatment medium was replaced with 100 μl/well of the working solution of MTT. The plates were incubated for 3 h in a CO_2 incubator at 37 °C. The 100 μl/well of DMSO was subsequently added, and the plates were incubated in a CO_2 incubator at 37 °C for 5 min. Finally, the absorbance was measured at 570 nm on a microplate reader (Thermo Scientific™ Multiskan™). The percentage cell viability of the samples was calculated compared to the control (the untreated cells).

CHAPTER 3

The Effect of N-terminal Acetylation on the αS's Interfacial Properties

3.1 Summary

Alpha-synuclein (αS) is a membrane-binding protein found predominantly in neurons and erythrocytes. The protein remains unordered in aqueous solutions but folds into an α-helical structure when bound to membranes. Besides, it gets deposited as β-sheet rich aggregates in diseases known as synucleinopathies. The native αS has been reported to be acetylated at the N-terminus. Here, we compare the interfacial properties of the N-terminal acetylated αS (Ac-αS) with non-acetylated αS (NH_2-αS) at the air-water interface. Both the protein forms are highly surface-active, with surface pressure reaching up to ~30 mN/m upon compression. The pressure-area isotherms obtained from the repeated compression-expansion cycles display large hysteresis suggesting self-assembly at higher surface pressures. The expansion isotherm is characterized by a rapid decrease in surface pressure followed by a slower transition phase starting around 15–17 mN/m. These data suggest that the compressed monolayer breaks into small clusters upon expansion, followed by these clusters' loosening. The circular dichroism spectroscopic analysis of the Blodgett-deposited films suggests the protein to be in largely α-helical conformation. The linear dichroism investigations suggest the protein to be anisotropically deposited. Blodgett deposition of the Langmuir films, therefore, is a rather simple method for preparing oriented monolayers of surface-active macromolecules.

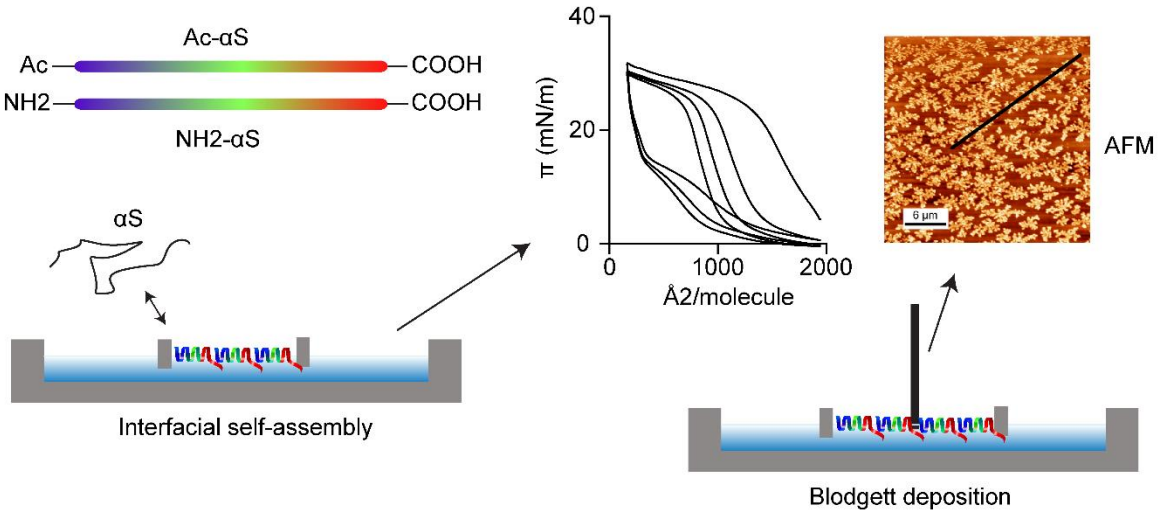

3.2 Introduction

Even though the function of αS in neurons is not fully understood, the protein's localization on synaptic vesicles is well-established. For this reason, the interaction of αS with micelles and liposomes has been investigated in reasonably great detail (T. Das & Eliezer, 2019). Synaptic vesicles are highly curved vesicles, and the αS is known to interact with the vesicles having comparable curvatures strongly. The αS is indeed a curvature-sensing protein (Jensen et al., 2011; Middleton & Rhoades, 2010). Langen and coworkers investigated the conformation of the small unilamellar vesicle-bound αS by EPR spectroscopy of the spin-labeled αS derivatives. They revealed that the N-terminal αS region, encompassing the seven repeats, folds into a non-canonical extended helix with 3.67 residues per turn (Jao et al., 2004; Jao, Hegde, Chen, Haworth, & Langen, 2008). The N-terminal 98 residues of the SDS micelle-bound αS, on the other hand, form two antiparallel helices (Chandra et al., 2003), possibly to optimize the binding to the micelles that are far more curved than vesicles (Kurniawan et al., 2018).

Langen and co-workers have investigated the curvature induction properties of αS using giant multilaminar vesicles (Varkey et al., 2010). The αS, BS and apolipoprotein A-1 share conserved functionality to induce curvature in large vesicles. The above proteins produce morphologically similar curvature produced by amphiphysin, a well-known curvature inducing protein. However, αS lacks any curvature induction domain. The property is mediated by membrane penetration and wedging (Varkey et al., 2010). The protein, therefore, has a curvature-inducing property as well.

In 2011, Selkoe and coworkers demonstrated that the αS exists as an aggregation-resisting helically-folded tetramer (Bartels et al., 2011). However, very few research groups have been able to isolate the helical αS tetramer. Lashuel and coworkers, in 2012, reported that the protein exists predominantly as an intrinsically disordered monomer (Fauvet et al., 2012). The great difficulty in isolating the quaternary αS reveals that the Selkoe's helical tetramer could be a less-populated transient structure. The strategies for isolating the metastable helical tetrameric αS in adequate amounts are under investigation. The amino-terminus of most eukaryotic proteins is acetylated, and αS is no exception (Anderson et al., 2006; Johnson et al., 2010). The tetrameric αS reported by Selkoe and coworkers was, therefore, the *N*-acetylated αS (Ac-αS). As most in vitro studies on αS had been carried out with non-acetylated αS (NH_2-αS), the role of acetylation on helical propensity was quickly investigated. It turned out that the N-terminal acetylation indeed confers higher helical propensity (Bartels, Kim, Luth, & Selkoe, 2014). *N*-acetylation of αS, however, resulted in little success in isolating the quaternary protein

(Maltsev, Ying, & Bax, 2012). Like NH_2-αS, it is difficult to obtain the tetrameric form of the Ac-αS. Fernández and Lucas, however, reported the isolation of tetrameric Ac-αS using mild purification methods; a 1 litre *E. coli* culture yielded ~2 mg tetrameric protein of >98% tetrameric Ac-αS (Fernandez & Lucas, 2018a).

The interfacial properties of NH_2-αS have been reported in the literature. The protein rapidly adsorbs at the air-water interface causing a maximal surface pressure around 25 mN/m (Chaari et al., 2013; C. Wang et al., 2010). The interface-adsorbed protein was found to fold into α-helical conformation wherein the α-helices were oriented parallel to the surface. Although the monomeric NH_2-αS is prone to aggregation in aqueous buffers, it behaves very differently at the air-aqueous interface by resisting the aggregation over a prolonged period (C. Wang et al., 2010). As native αS is acetylated at N-terminus, we compared the interfacial properties of Ac-αS with NH_2-αS. The interfacial properties was studied using the Langmuir-Blodgett (LB) method. Repeated compression/expansion cycles of the monolayers at the interface were carried out to understand the protein's self-assembly at the air/water interface. The Blodgett-deposited monolayers were investigated using circular dichroism (CD) and linear dichroism (LD) spectroscopy to understand the αS conformation and orientation.

3.3 Results and discussion

3.3.1 Characterization of the purified protein

The purified NH_2-αS and Ac-αS were analyzed by SDS-PAGE. The SEC peak with elution volume ~ 54 ml in Fig. 3.1A was ascertained to be that of Ac-αS while that with elution volume ~ 55 ml in Fig. 3.1B was ascertained to be that of NH_2-αS. The purity and the identity of the proteins were established by reversed-phase HPLC and MALDI-TOF mass spectrometry (Figs. A3 and A4). To ascertain that the protein preparations were free from oligomers, native as well as the amyloid, the purified proteins in 25 mM phosphate buffer, pH 7.5 were characterized using DLS. Twenty DLS measurements were made for both the proteins. The size distributions from the representative measurements are shown in Fig. 3.1C and D. Single peaks corresponding to the hydrodynamic diameters of 8.6 ± 2.6 nm for Ac-αS and 10.65 ± 1.85 nm for NH_2-αS were observed. Based on small-angle X-ray scattering data, Fink and coworkers have reported a radius of gyration of 40 Å for NH_2-αS (V. N. Uversky, Li, & Fink, 2001). The hydrodynamic diameters observed in DLS, therefore, suggest monomeric protein preparations.

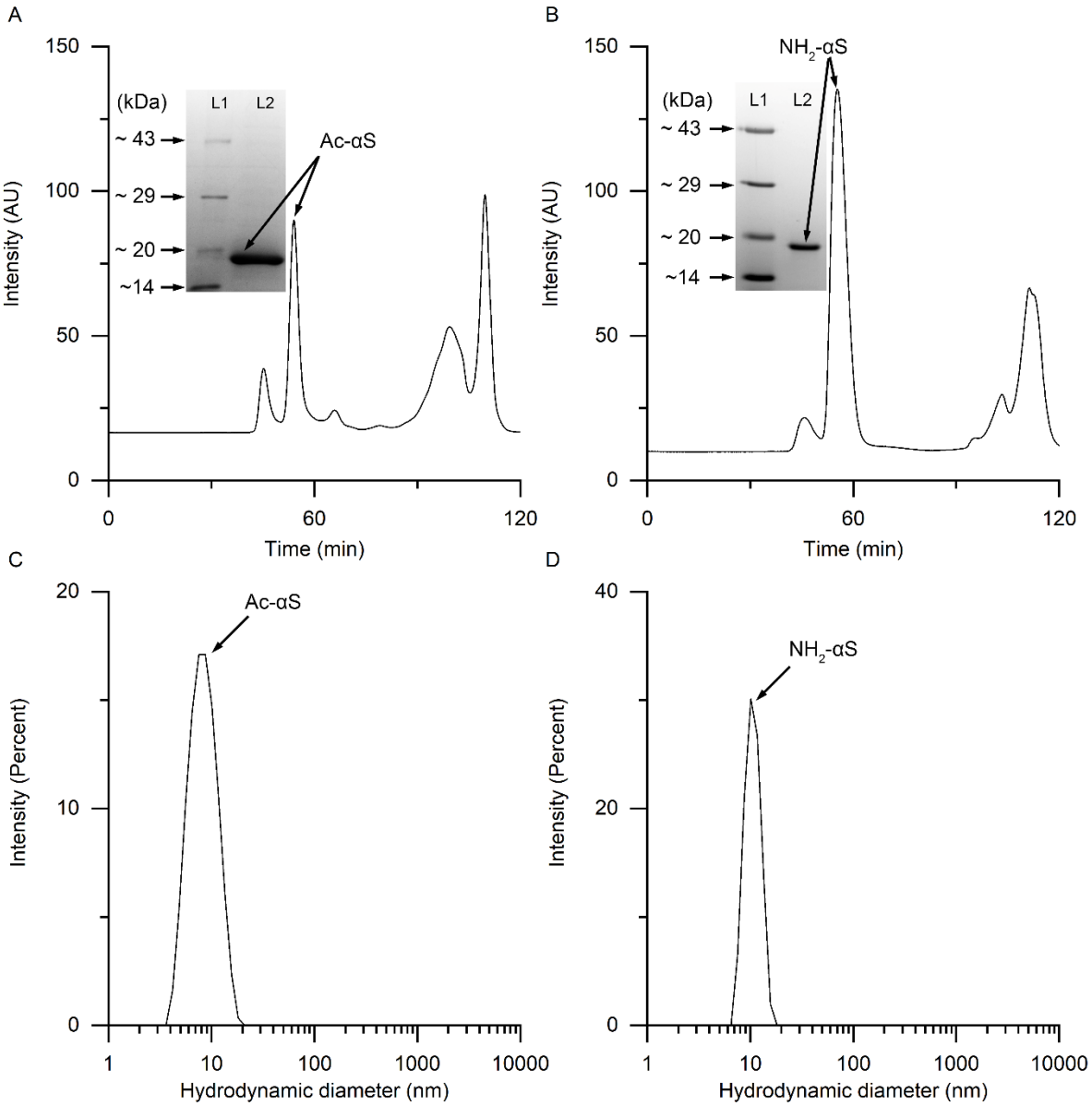

Fig. 3.1. Purification and characterization of Ac-αS and NH2-αS. The SEC profile showing elution of Ac-αS (A) and NH2-αS (B) at 54 ml and 55 ml, respectively. The inset shows the 12% SDS-PAGE of the purified fractions. The DLS-derived size distributions of freshly-prepared Ac-αS (C) and NH2-αS (D) stock solutions.

3.3.2 Surface activity

The adsorption of the proteins at the air-aqueous interface was examined in a small volume custom-made trough. The proteins were delivered to the bulk of the subphase through an opening, as shown in Fig. 3.2.1 (Chapter 2), and the change in surface pressure was monitored over time. The addition of 0.1 nmoles of protein in the 10 ml subphase, i.e., an effective concentration of 10 nM did not cause any appreciable increase in the surface pressure for either protein (Fig. 3.2A and B). Subsequent addition of 0.9 nmoles (effective concentration: 100 nM)

caused very large increase (~20 mN/m) in surface pressure. Both Ac-αS and NH_2-αS show a comparable surface pressure caused by 1 nmole of protein. This increase in surface pressure is in agreement with that reported in the literature (Chaari et al., 2013). The addition of proteins beyond 1 nmole caused small enhancements in the surface pressure.

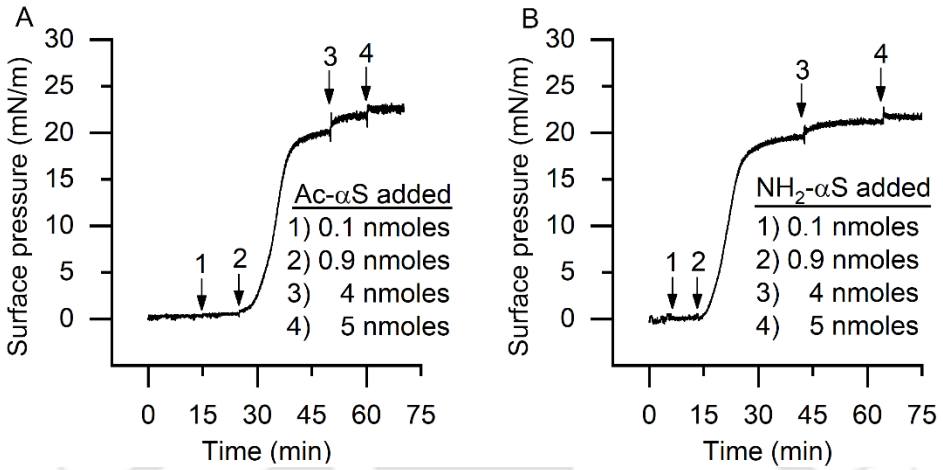

Fig. 3.2. The surface activity of Ac-αS and NH2-αS. Kinetic adsorption of Ac-αS (A) and NH2-αS (B) at the air-aqueous interface.

3.3.3 Compression/expansion isotherms

The surface pressure vs. molecular area (π-A) isotherms were recorded at room temperature by repeated compression/expansion of the proteins deposited at the air-aqueous interface (Fig. 3.3). The molecular areas were calculated by assuming all the protein molecules to be at the interface. Fig. 3.3A shows the isotherms recorded for Ac-αS. The first compression isotherm 1^C starts from a surface pressure of ~5 mN/m at the molecular area of ~1933 $Å^2$/molecule, reaches an inflection around 19 mN/m pressure at 1440 $Å^2$/molecule, and enters a condensed phase, with surface pressure reaching beyond 30 mN/m at areas ≤ 500 $Å^2$/molecule. The expansion of the monolayer causes a rapid drop in surface pressure. The pressure quickly drops to ~18 mN/m at a molecular area of approximately 292 $Å^2$/molecule, followed by a gradual fall in surface pressure as the barriers expand (1^E, Fig. 3.3A). The isotherms recorded for NH_2-αS are shown in Fig. 3.3B. The isotherms are very similar to those observed for Ac-αS. The limiting molecular areas calculated from the steep region of the first compression isotherms of Ac-αS and NH_2-αS are 1940 $Å^2$/molecule and 1983 $Å^2$/molecule, respectively. These data indicate similar interfacial properties of Ac-αS and NH_2-αS. The hysteresis observed in the compression/expansion cycle is attributed in the literature to the protein compaction, self-assembly, or depletion of the molecules from the interface. The large hysteresis observed between 1^C and 1^E suggests molecular self-assembly. Self-assembling peptides have been

reported in the literature to exhibit such large hysteresis (Chaudhary & Nagaraj, 2011). The isotherms shifted towards lower molecular areas with subsequent compression/expansion cycles, indicating the added irreversible molecular event with each compression isotherm. In addition, the hysteresis becomes smaller with each subsequent compression/expansion cycle, suggesting a smaller contribution to self-assembly with each passing cycle. The phase transition points are easily identified by analyzing the data in terms of compressibility modulus. The compressibility moduli for all the compression isotherms were plotted against the surface pressure (Fig. 3.3C–F). The C_s^{-1} vs. π plots obtained from the first compression isotherms of Ac-αS and NH_2-αS are shown in Fig. 3.3C. The plots show different compressibility below the inflections (~19 mN/m for Ac-αS and ~16 mN/m for NH_2-αS) but reach the same compressibility modulus of ~60 mN/m at the inflection points. The change in the sign of the slope dC_s^{-1}/dx, i.e. the inflection point, indicates phase transitions. The C_s^{-1} at high surface pressures decreases and approaches zero, indicating high interfacial elasticity of the condensed phase. The subsequent compression isotherms are very different from the first one. There is only one inflection point, indicating two distinct phases. Another interesting feature to note is the lack of monolayer collapse even upon compression near the saturation surface area. This could be due to a relatively smooth partitioning of the protein to subphase at large pressures, a high propensity of structural reorganization at the interface, or both.

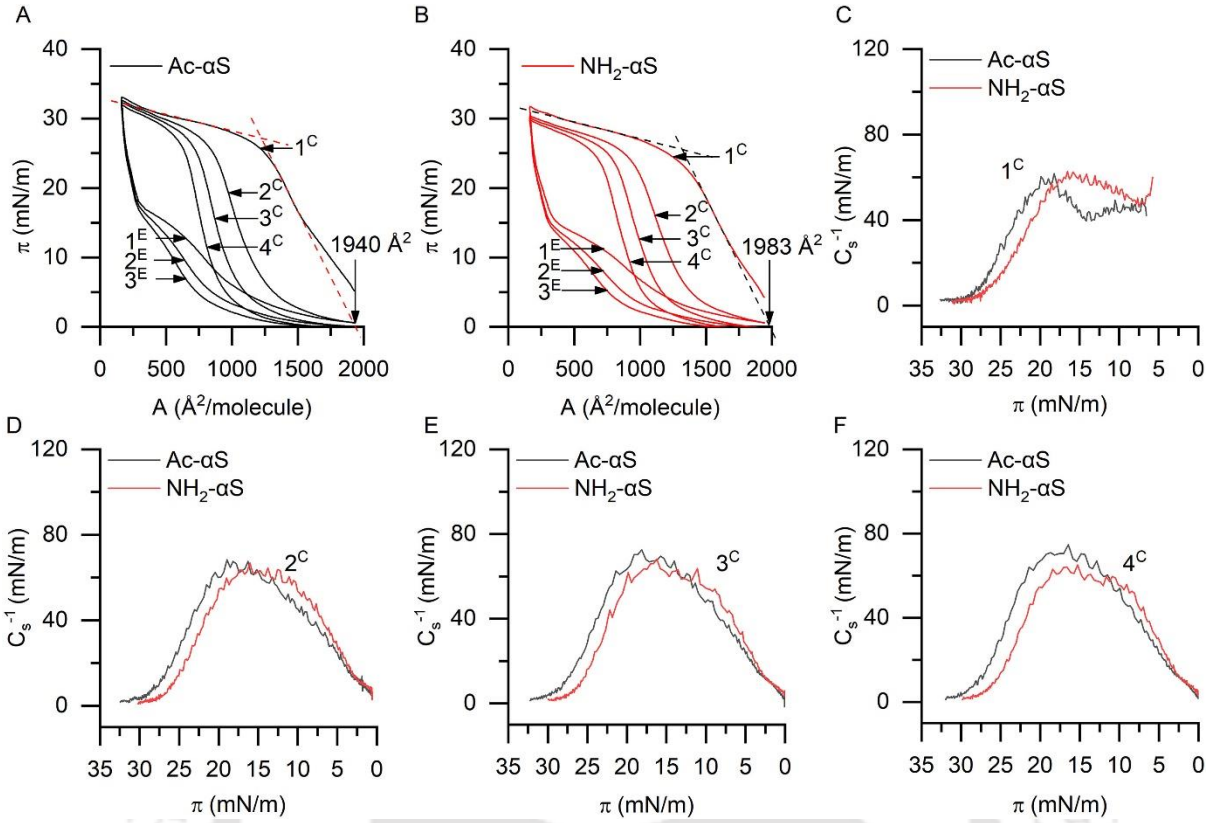

Fig. 3.3. Langmuir compression/expansion isotherms. The repeated compression/expansion isotherms for Ac-αS (A) and NH2-αS (B). The π-A isotherms from successive compression are labeled as 1C, 2C, 3C, and 4C. The three successive expansion isotherms are labeled as 1E, 2E, and 3E. The 4C-compressed monolayers were used for Blodgett depositions. The Cs^{-1} vs. π plots for the 1C (C),2C (D), 3C (E), and 4C (F) isotherms.

3.3.4 Blodgett deposition and CD spectroscopy

The monolayers were Blodgett-deposited on both the sides of a quartz slide by retrieving the pre-dipped quartz slide from the subphase after fourth compression 4^C (Fig. 2.2, Chapter 2). The secondary structures of the Ac-αS and NH_2-αS in the LB films were investigated using CD spectroscopy. Fig. 3.4A shows the CD spectrum of the Ac-αS LB films. The spectrum is characterized by the negative bands around 222 nm and 208 nm with a positive band around 193 nm, the characteristic features of an α-helix. The CD spectrum of the NH_2-αS LB films also displays predominantly α-helical conformation, albeit with a less pronounced band around 222 nm and a more intense positive band around 193 nm (Fig. 3.4B). Even though there are subtle differences in the CD spectra of the two forms of the protein, both take up predominantly α-helical conformation at the air-water interface.

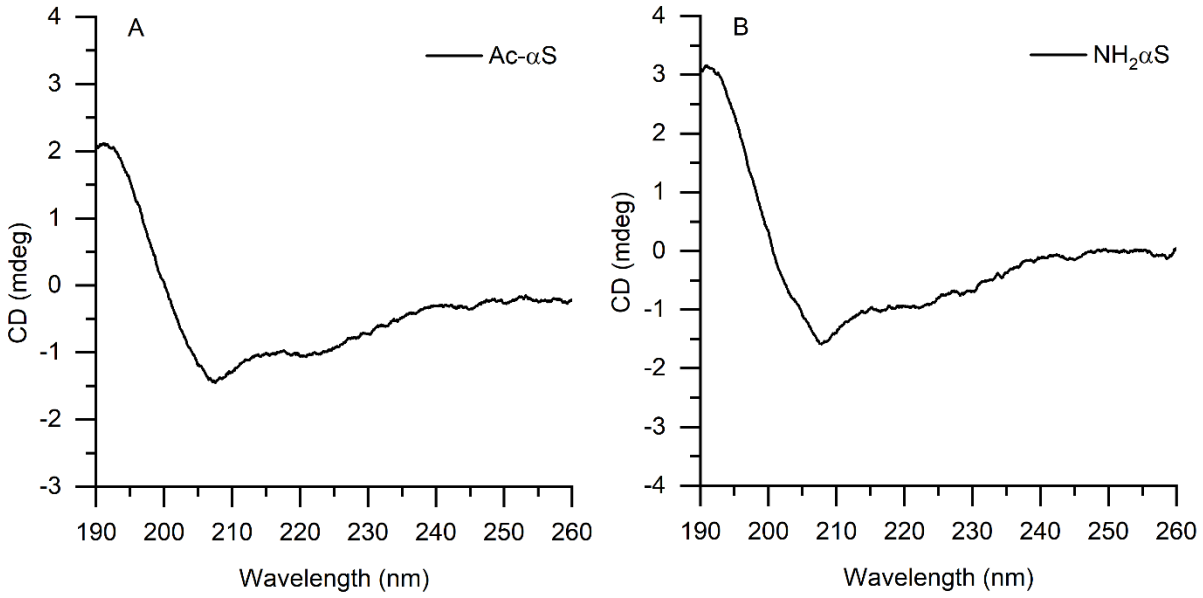

Fig. 3.4. The far-UV CD spectroscopic characterization of the LB film. The far-UV CD spectroscopic characterization of the Ac-αS (A) and NH2-αS (B) LB films.

3.3.5 LD spectroscopy of the LB films

The LD spectra were recorded to gain insights into the orientation of the α-helices in the LB films. An α-helix is characterized by three transitions viz. n → π* transition around 222 nm perpendicular to the helix axis, a π → π* transition around 190 nm perpendicular to the helix axis, and a π → π* transition around 210 nm parallel to the helix axis (Bulheller et al., 2009). The data for Ac-αS (Fig. 3.5A) and NH_2-αS (Fig. 3.5B) are presented as plots of LD^r against the angle of rotation (azimuth) of the sample. The LD^r at 193 nm and 208 nm for 360° rotation of the LB films with 10° steps are shown in Fig. 3.5. When measured without changing the orientation of the LB substrate after retrieval from the subphase (zero azimuth), both Ac-αS and NH_2-αS display a positive band around 193 nm and a negative band around 210 nm, indicating a distinct orientation of the protein's α-helical region. Rotation of the sample shows a gradual decrease in the amplitudes of the bands with little LD^r observed at 40° (Fig. 3.5, A8, and A9). The sinusoidal nature of the plots suggests the anisotropic nature of the protein films. The data indicate that the protein molecules get deposited on the quartz substrate, with the helical axis being roughly perpendicular to the direction of the substrate withdrawal from the subphase.

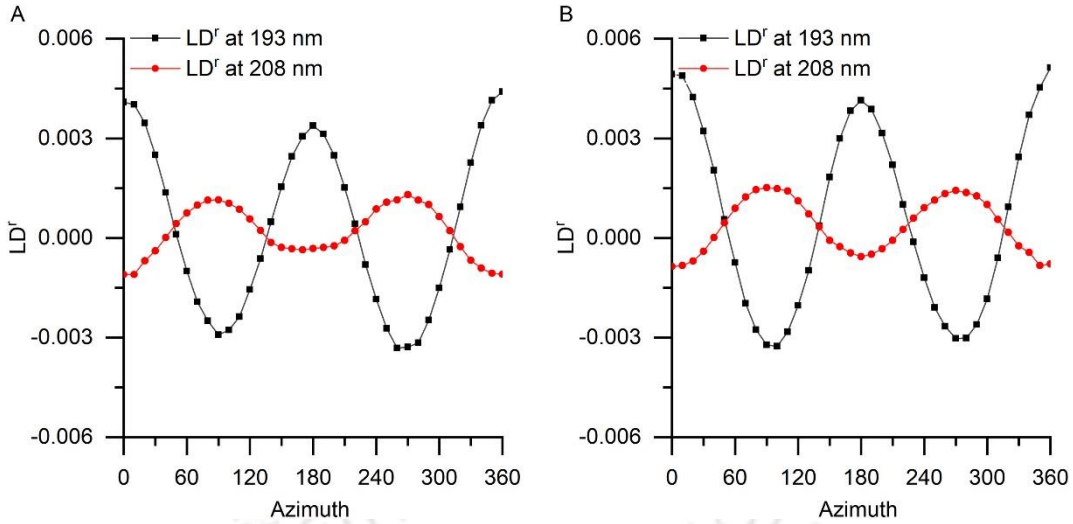

Fig. 3.5. LD spectroscopy of the LB films at different angles with 10° intervals. LD spectroscopy of the LB films at different angles with 10° intervals. The LDr at 193 nm and 208 nm plotted against the azimuth for the Ac-αS (A) and NH2-αS (B) LB films.

3.3.6 AFM of the LB film

The AFM image of the Ac-αS LB film deposited on a glass coverslip was recorded (Fig. 3.6). The image reveals Ac-αS clusters formed upon compression. The clusters are uniformly spread out on the slide (Fig. 3.6A) and have ~4–8 nm thickness (Fig. 3.6B). A close examination of the individual clusters reveals 'bead-like' structures stuck together in the AFM micrograph. The compression of the monolayer, therefore, causes self-assembly of the protein at the air-water interface to form small α-helical oligomers that form a gel-like phase near the maximal surface pressure. The rapid drop in surface pressure observed during the expansion (Fig. 3.6A) is attributed to the breaking of the gel-phase into two-dimensional microclusters. The subsequent gradual decrease in surface pressure is attributed to the further breaking of these clusters. The oligomerization of a protein upon compression would cause shifting of the subsequent compression isotherms to lower molecular areas, as is observed for both Ac-αS and NH_2-αS (Fig. 3.6A and B). Upon compression, the protein appears to form oligomers that do not disassemble on the compression/expansion timescale.

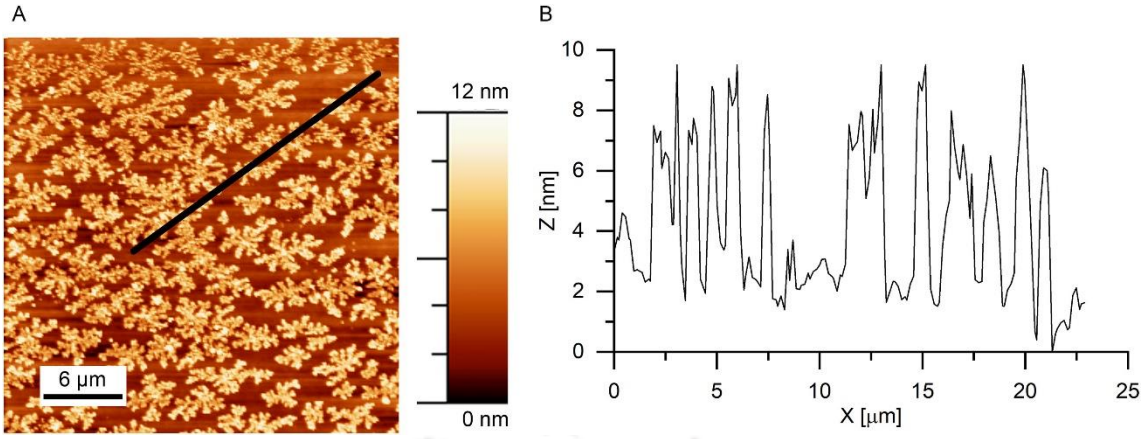

Fig. 3.6. The AFM imaging of the Ac-αS LB film. Surface topography (A) and the Z-height vs. distance plot for the line segment shown in panel A (B).

3.4 Conclusion

The αS, irrespective of the N-terminal acetylation, was found to possess a high surface activity. The interface-adsorbed protein adopts a largely α-helical conformation. Recent advances in αS structure suggest the N-terminal acetylation does not cause appreciable structural changes in the membrane-bound form of αS (Runfola et al., 2020). The compression of the monolayer causes self-assembly forming α-helix-rich oligomers. The protein monolayers displayed a maximal surface pressure of ~30 mN/m. Further compression did not cause any appreciable increase in surface pressure. Still, the monolayers did not show distinct collapse suggesting molecular arrangement at the interface or gradual depletion of the protein from the interface into the subphase. The LD spectroscopy of the LB films reveals a distinct helix orientation. The αS gets deposited on the quartz substrate with the helical axis perpendicular to the direction of the substrate retrieval. The data suggest that the helices on the air-water interface lie parallel to the interface, as expected from the amphipathic helices. The deposited LB layer possesses crystallinity that is manifested in the anisotropic deposition on the quartz substrate. AFM imaging of the Blodgett-deposited Ac-αS film revealed particles with ~4–8 nm thickness. Petsko and coworkers, using electron microscopy, have previously reported ~8–11 nm diameter for the natively-folded α-helical αS oligomers (W. Wang et al., 2011). As the sizes are comparable, it would be interesting to investigate if the helical oligomers formed at the interface are similar to the native oligomeric αS. We investigated the potential membrane-disrupting ability of these oligomers by incubating the calcein-loaded POPG LUVs (100 nm) on the LB films. No disruption of lipid vesicles was observed (data not shown). This study also reinforces the potential that Langmuir-Blodgett possesses for achieving ordered thin layers of

biomolecules that may find application in medicine. Macromolecules for LD spectroscopic analysis are usually prepared using a Couette flow system. Here we demonstrate that the surface-active biomolecules can be oriented by Langmuir-Blodgett deposition, and the LB films so deposited are amenable for LD characterization

CHAPTER 4

Interfacial Properties of αS's Parkinsonian Variants

4.1 Summary

The human alpha-synuclein (αS) protein is associated with the occurrence of Parkinson's disease. In the past decade, six autosomally dominant mutations have been identified in the αS (SNCA) gene that translate into A30P, E46K, H50Q, G51D, A53E, and A53T mutations in the protein. These mutations alter the electrostatics and hydrophobicity of a cardinal region of the protein. A comprehensive comparison of the interfacial properties of these Parkinsonian αS variants is crucial to understand their membrane dynamics. Here, we investigated the interfacial activity of these αS variants at the air-aqueous interface. The lipid-penetration activity was also investigated using zwitterionic and negatively-charged lipid monolayers. All the αS variants were found to possess comparable surface activity of ~20-22 mN/m. Compression/expansion isotherms reveal a very distinct behaviour of the A30P variant compared to others. The Blodgett-deposited films were analysed using CD and LD spectroscopy as well as the atomic force microscopy. All the variants adopted predominantly α-helical conformation in these films. Atomic force microscopy of the Langmuir-Blodgett films revealed self-assembly at the interface.

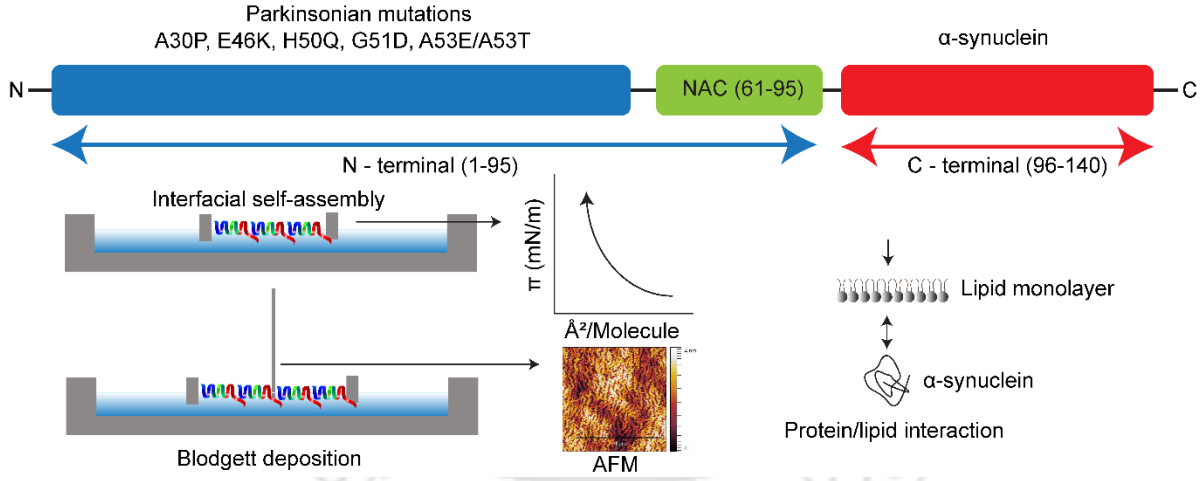

4.2 Introduction

Six autosomal dominant mutations in the SNCA have been documented, namely A30P, E46K, H50Q, G51D, A53E, and A53T (Mohite et al., 2018). The six mutations occur upstream of the NAC region. The NAC's hydrophobicity drives the protein's aggregation and toxicity (Waxman, Mazzulli, & Giasson, 2009). The NAC region is followed by a highly acidic C-terminal 96-140 amino acid stretch. The αS remains largely unstructured in the aqueous solutions. It has been reported to bind the sodium dodecyl sulfate micelles, wherein the N-terminal occupy ~two-third region of the protein folds into a broken helix (Chandra et al., 2003). The N-terminal region of the liposome-bound αS, on the other hand, adopts an extended helical conformation (Jao et al., 2004; Jao et al., 2008). The protein has a high affinity to interact with highly curved membranes. Varkey et al. showed that the protein induces highly curved membrane tubules from the giant unilamellar vesicles (Varkey et al., 2010). The αS, therefore, is a curvature-sensing and curvature inducing protein. The lysine residues flanking the consensus sequence stabilise the polar head groups during the protein-lipids interaction, and the hydrophobic face dives into the interior of the membrane (Choi, Han, Heo, Lee, & Kim, 2018). The αS displays a preference to bind the anionic lipids over the zwitterion groups (Pfefferkorn et al., 2012). This is largely attributed to the multiple lysine residues in the N-terminal region (Pfefferkorn et al., 2012). Although the lipid head group's electrostatics dictates the phase separation, the head group's size also plays a vital role by facilitating the space for the protein's insertion into the membrane (Brummel, Braun, & Sachs, 2017; Jo et al., 2000). Phosphatidic acid, phosphatidylethanolamine and phosphatidylinositol are known to allure αS more as compared to the other lipids with similar electrostatics (Jo et al., 2000; Middleton & Rhoades, 2010; Rhoades, Ramlall, Webb, & Eliezer, 2006; Shvadchak, Falomir-Lockhart, Yushchenko, & Jovin, 2011; van Rooijen, Claessens, & Subramaniam, 2009). The presence of raft-like composition containing cholesterol and ganglioside GM1 facilitates αS penetration (Fortin et al., 2004; Martinez, Zhu, Han, & Fink, 2007). In a nutshell, αS binds to curved membranes, and the structural transition happens in a step-wise manner (Bartels et al., 2010). First, the long-range electrostatic interaction facilitates the binding of the N-terminal αS to the curved membrane. Later, the local rearrangements dictate sheering and introduction of the hydrophobic side chain into the bilayer (Bartels et al., 2010; Pfefferkorn et al., 2012). Meanwhile, the electrostatic interaction of the lysine residues stabilises the interaction with the polar head groups (Bartels et al., 2010). Finally, the polypeptide transitions into a helix (Bartels et al., 2010). The NMR-based SDS micelles binding study reaffirms the importance of αS's N-

terminal mediated helix-formation upon membrane interaction and rejects the involvement of the C-terminal region (Bartels et al., 2010). αS binds to many membrane types, including planar supported bilayers, micelles, gel phase vesicles, and fluid phase vesicles (Middleton & Rhoades, 2010). In the patients with E46K SNCA mutation, an altered membrane affinity towards anionic lipids confers toxicity (Auluck, Caraveo, & Lindquist, 2010; Rovere et al., 2019). In a helical wheel model, the E46K mutation disposes the lysine residue to the helix's solvent-exposed face. Thus, with a gain of +2 charge, E46K-αS gets electrostatically attracted towards negatively charged membranes; however, the mutation does not contribute in partitioning into the membrane (Middleton & Rhoades, 2010). Middleton et al. suggested A30P-αS mutant to have a low binding affinity than WT-αS towards membranes (Middleton & Rhoades, 2010). This property of A30P-αS is accredited to the proline residue-induced kink in the protein's helical domain. Moreover, alanine-to-proline mutation imparts reduced hydrophobicity leading to reduced beneficial hydrophobic interaction with the lipid membrane (Middleton & Rhoades, 2010). However, the A30P-αS mutant is reported to have a higher affinity towards a highly curved membrane than the WT-αS protein (Middleton & Rhoades, 2010). Interfaces can also have strong effects on the protein structure (Macritchie, 1978). It is a well-established fact that proteins lose their tertiary structure when subjected to interfaces. However, the air-water interface can induce folding if the folded structure is amphipathic. The proteins having amphipathic regions partion to the air-water interface. The αS, which is disordered in aquous solutions, rapidly partions to the air-aqueous interface, wherein it take up an α-helical conformation (Chaari et al., 2013; Mohapatra & Chaudhary, 2021; C. Wang et al., 2010). The interfacial properties of the Parkinsonian αS variants, however, has not been reported in the literature. In this study, we report the interfacial properties and lipid penetration of six Parkinsonian variants.

4.3 Results and discussion

4.3.1 Surface activity

The adsorption of αS and its variants at the air-aqueous interface was investigated by measuring the change in the surface pressure, when the protein was introduced into the subphase. When 0.1 nmole of the protein was added to the subphase, no appreciable increase in the surface pressure was observed for any of the protein variants (Fig. 4.1). The subsequent addition of 0.9 nmoles of the proteins caused a rapid increase in the surface pressure that plateaued around 20 mN/m. The wild type αS (WT-αS) has been reported in the literature to be highly-surface active (Chaari et al., 2013; Mohapatra & Chaudhary, 2021). The data in Fig. 4.1 show that the point

mutations associated with αS protein variants do not significantly affect the surface activity. All the αS variants display comparable surface pressures at 0.1 μM protein concentration. Addition of more protein caused only a little increase in the surface pressure. Thus, further addition of the protein would increase the subphase concentration of the protein.

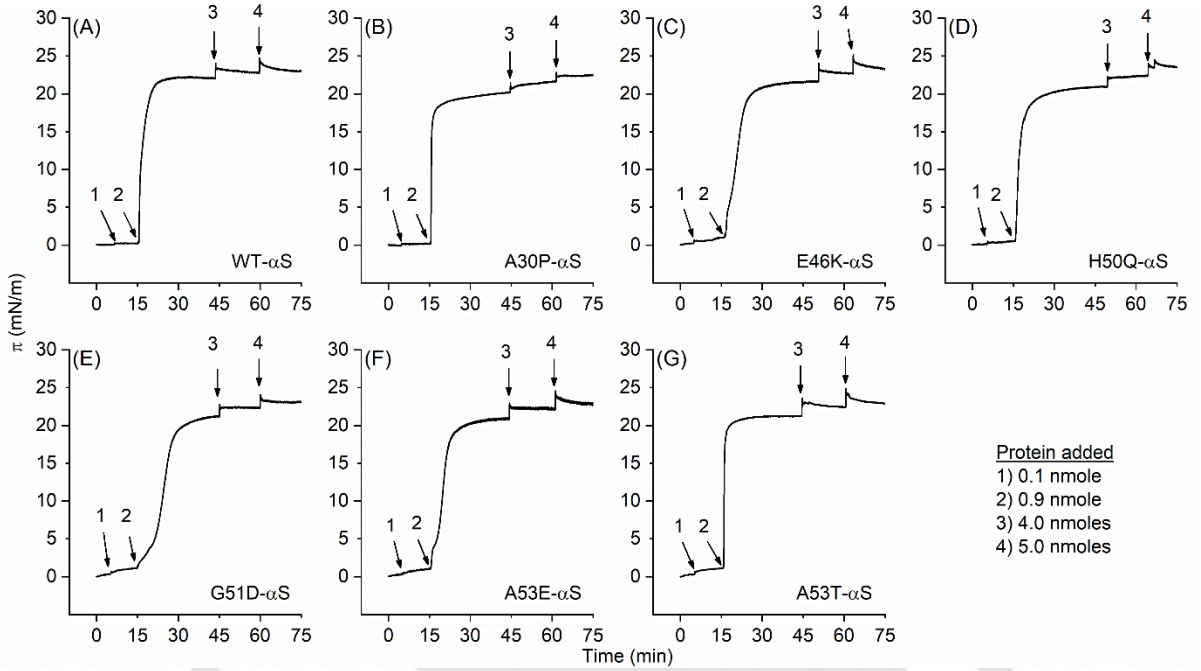

Fig. 4.1. The surface activity of the αS protein variants. The adsorption kinetics of αS protein variants at air-aqueous interface, monitored by the change in the surface pressure after injecting the protein in the subphase. WT-αS (A), A30P-αS (B), E46K-αS (C), H50Q-αS (D), G51D-αS (E), A53E-αS (F), and A53T-αS (G).

4.3.2 Compression/expansion isotherms

The monolayers of αS protein variants at the air-aqueous interface were subjected to compression/expansion cycles. Briefly, on a standard 200 ml trough, 20 μl of 100 μM protein was carefully layered at the interface. The monolayer was left undisturbed for 30 minutes to facilitate molecular rearrangements. The calculations were carried out assuming all the protein to be at the air-aqueous interface. For WT-αS, the initial surface pressure after spreading (π_I) was found to be around 5 mN/m (Fig. 4.2A). Similarly, initial surface pressures of around 3-5 mN/m were observed for the αS protein variants (Fig 4.2B–G). Three compression/expansion isotherms were recorded for the monolayers. The limiting molecular areas A_0 were estimated by extending the steep region of the first compression isotherm, labelled as 1^C. The WT-αS shows a characteristic A_0 ~1997 $Å^2$/molecule as reported earlier (Mohapatra & Chaudhary, 2021). Comparable limiting molecular areas were observed for A53E-αS and E46K-αS. The

first compression isotherm of the WT-αS and the variants other than A30P-αS, show a gradual rise in surface pressure upon compression, indicating a rather smooth transition from liquid-expanded (LE) to liquid-condensed (LC) state. A30P-αS, unlike all other αS variants investigated here, displays three phases. Compression of the liquid-expanded phase beyond ~18 mN/m pressure results in a less compressible state. However, further compression results in a phase transition, rendering the monolayer more compressible. Compared to the other variants that resulted in a surface pressure of ~30-32 mN/m at ~500 $Å^2$/molecule, the minimum molecular surface area that we could reach with our set-up, A30P-αS reached a surface pressure ~36 mN/m. A common feature to each of the protein variants is the large hysteresis between the compression and expansion isotherms. Such large hysteresis could arise from molecular reorientation, conformational changes, or self-assembly. Subsequent compressions (2^C–4^C) shifted the isotherms to lower molecular areas, indicating the compression-induced molecular events that do not fully reverse on our experimental time-scales. The expansion isotherms are characterised by a large drop in surface pressure i.e. a large dπ/dA at lower molecular areas. This rapid drop in pressure is suggestive of a "spring" kind of behaviour of the compressed monolayer. The release of the stored potential energy during the monolayer's expansion seems to drive the instant drop in the surface pressure. The monolayer expands with a gradual drop in the surface pressure until it reaches 0 mN/m at a fully expanded position.

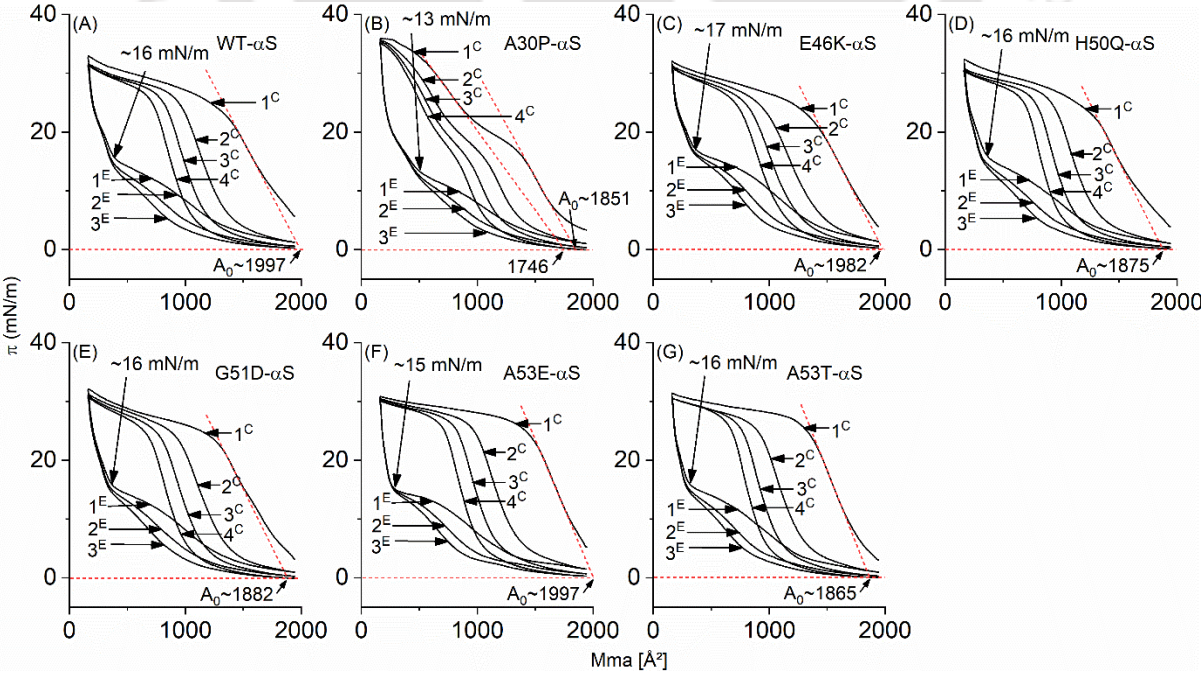

Fig. 4.2. The compression-expansion isotherms of αS protein variants. The π-A isotherm of compression/expansion profiles are shown for WT-αS (A), A30P-αS (B), E46K-αS (C), H50Q-αS (D), G51D-αS (E), A53E-αS (F), and A53T-αS (G).

4.3.3 The compressibility modulus

The compressibility or the compressibility coefficient (C_s) is the relative change in the area in response to the pressure. The compressibility modulus (C_s^{-1}) is simply the reciprocal of the compressibility coefficient. To better understand the phase transitions observed in the π-A plots (Fig. 4.2), the compressibility moduli were evaluated. The C_s^{-1} vs π plots of the 1^C, 2^C, 3^C, and 4^C compression isotherms show distinct phase transition features (Fig. 4.3). The starting C_s^{-1} (at π = 5 mN/m) for the WT-αS monolayer was found to be ~48 mN/m. The C_s^{-1}–π plots obtained from the first compression isotherms (1^C) show differences in the initial C_s^{-1} values among the αS variants. The A30P-αS stood out with a very low C_s^{-1} of ~10 mN/m compared to all other variants that displayed the starting C_s^{-1} (around π = 3–5 mN/m) of 35 mN/m or more. The 1^C C_s^{-1}–π curves show variable inflection points and compressibility moduli among the αS variants. Such variation could arise due to the differences in the initial conformations of the αS variants at the air-aqueous interface. The first compression/expansion cycle alleviate these variations, except for the A30P-αS. The C_s^{-1}–π curves obtained from the second compression onward are quite consistent (Fig. 4.3B-D). For 2^C isotherms, the C_s^{-1} of all αS variants is ~5 mN/m at a low surface pressure of ~2-3 mN/m, suggesting high compressibility (Fig. 4.3B). The C_s^{-1} of all, but A30P-αS, variants gradually increase up to π ~15-18 mN/m, before decreasing to close to the initial values, suggesting a phase change. A30P-αS, on the other hand, displays a very different C_s^{-1}–π plot. The C_s^{-1} reaches a maximum of around 50 mN/m near π ~10 mN/m, before dropping down to ~15 mN/m near π ~20 mN/m. The C_s^{-1} further rises and reaches another peak of ~20 mN/m near π ~25 mN/m. These data clearly indicate three distinct phases, compared to the two phases observed for all other variants.

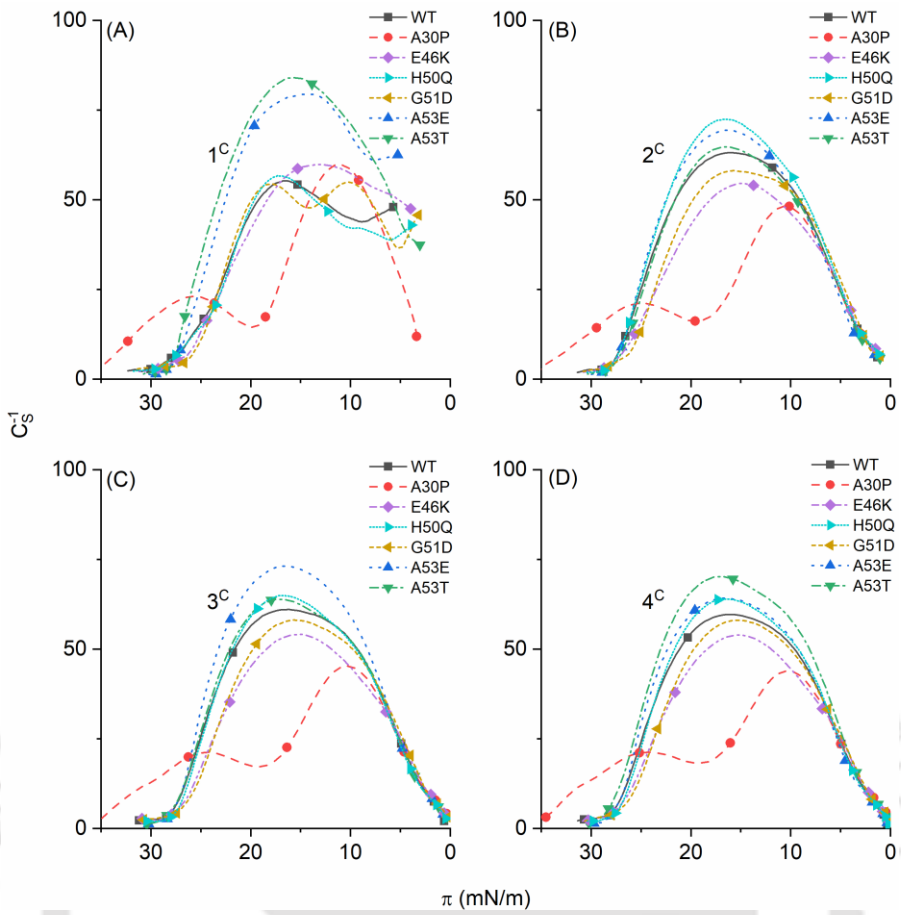

Fig. 4.3. The C_s^{-1} vs π plots for the compression part in the π-A isotherm. 1^C (A), 2^C (B), 3^C (C), and 4^C (D).

4.3.3.1 Penetration into phospholipid monolayers

Interactions of αS synuclein with lipid vesicles and detergent micelles have been investigated in detail (Middleton & Rhoades, 2010). The αS has been reported to strongly interact with highly curved membranes. The membrane-binding involves the folding of the disordered αS into α-helical conformation. Besides, the protein displays a higher affinity towards negatively charged lipids compared to the zwitterionic lipids (Middleton & Rhoades, 2010). Here, we investigated the affinity of αS and its Parkinsonian variants towards flat membranes (essentially the lipid monolayers) composed of POPC and POPC:POPS (1:1). The lipid monolayers with different starting surface pressures (π_i) were prepared, and the protein (1 nmole) was added to the subphase. The penetration of the protein into the lipid monolayers resulted in an increase in the surface pressure that eventually plateaued (π_f). The π_f - π_i ($\Delta\pi$) was plotted against the π_i (Fig. 4.4). When the π_i is 5 mN/m, all the αS variants cause a large increase in pressure wherein $\Delta\pi$ is around 20-22 mN/m. It is important to note that the 1 nmole of αS variants, in the absence of lipids, tends to achieve the maximal surface pressure higher than 20-22 mN/m. This implies

that the αS variants display affinity towards the lipid bilayer, taking the initial surface pressure from 5 mN/m to ~27-29 mN/m.

It is imperative that the protein's penetration into the lipid monolayer would be higher at lower π_i, as the lipid molecules are loosely packed. A higher π_i implies better-packed lipids, that need to be displaced by the penetrating molecule. Not surprisingly, therefore, we see a drop in $\Delta\pi$ as the π_i is increased. The data could be well fitted using linear regression and the critical pressure of insertion (π_c) estimated by extrapolating the line to $\Delta\pi=0$. The π_c represents the surface pressure at which no penetration takes place. The data indicate the preferential insertion of all αS variants into the negatively charged lipid monolayer. The π_c values are reported in Table 4.1. All the variants show higher π_c values for the POPC/POPS monolayers indicating the involvement of electrostatic interactions in membrane interaction. The E46K-αS variant has +2 charge more compared to the wild-type peptide and displays the maximum π_c (37.4 mN/m) for the negatively charged monolayers among all the αS variants. The π_c for the WT-αS is also comparable (36.9 mN/m).

Middleton et al. have investigated the binding of αS and some of its Parkinsonian variants with small and large unilamellar vesicles (Middleton & Rhoades, 2010). A direct comparison of the binding to liposomes with that to lipid monolayers may not be very relevant. However, it is important to note that Middleton et al. found E46K-αS to have the highest binding strength among all the αS variants studied. The electrostatic contribution to the binding, however, was lesser than expected. This was attributed to the location of E46, which is on the solvent-exposed face of the αS helix. The A30P-αS penetration is also noteworthy. It shows the lowest π_c (31 mN/m) for the POPC monolayers. A distinct preference for negatively charged lipids is observed at all initial pressures (Fig. 4.4B, Table 4.1). A proline substitution does not give any extra charge to the mutant A30P-αS. However, proline introduces a kink in the α-helices, thereby affecting their properties. Middleton et al. reported the lower affinity of the A30P-αS towards SUVs and LUVs compared to the WT-αS. Thus, the binding of the αS is dictated by the electrostatic interaction between the αS and the negatively charged lipids, and is sensitive to the conformational changes introduced by the mutations such as A30P.

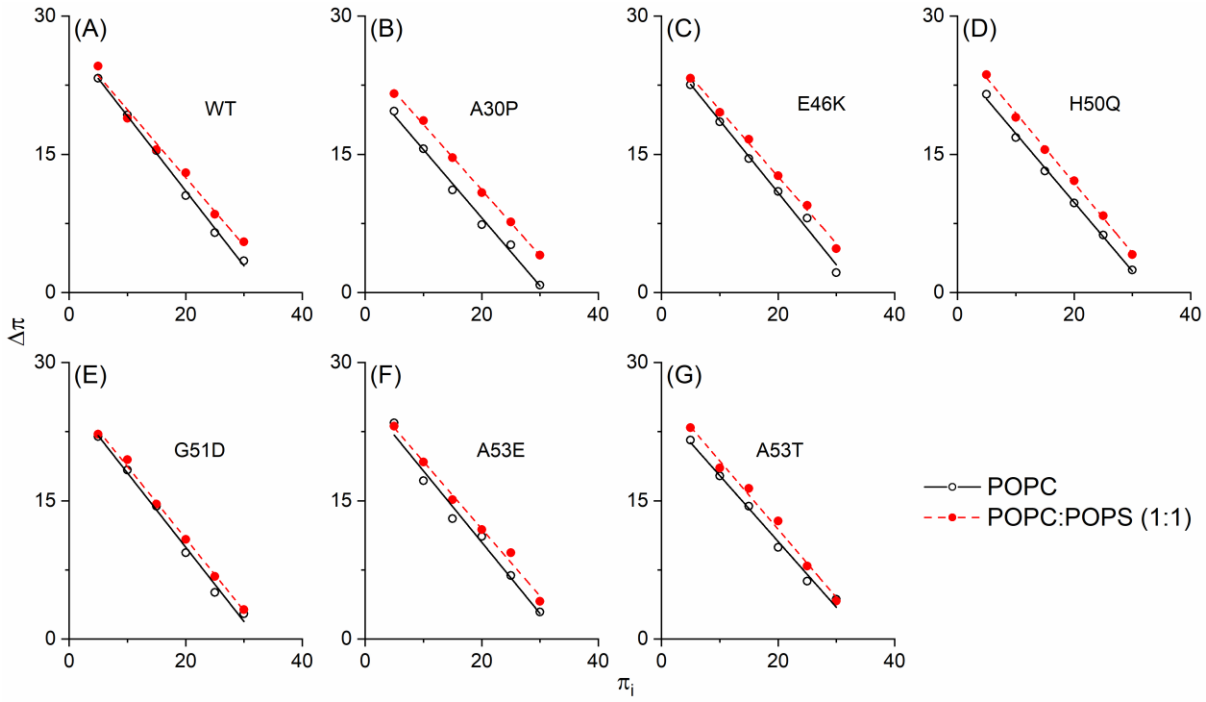

Fig. 4.4. The lipid monolayer penetration by αS protein variants. The Δπ vs π_i plots for the POPC and POPC:POPS (1:1) monolayer penetration are shown for WT-αS (A), A30P-αS (B), E46K-αS (C), H50Q-αS (D), G51D-αS (E), A53E-αS (F), and A53T-αS (G).

Table 4.1. The critical pressure of insertion for the αS variants.

αS variant	π_c (mN/m)	
	POPC	POPC/POPS
WT-αS	33.6	36.9
A30P-αS	31.0	35.6
E46K-αS	33.8	37.4
H50Q-αS	33.1	35.6
G51D-αS	32.4	34.0
A53E-αS	33.6	36.4
A53T-αS	34.8	36.1

4.3.4 CD spectroscopy

The CD spectra of the αS variants in solution (dotted lines) and in the LB films (solid line) are shown in Fig. 4.5. The CD spectra of the Langmuir films are characterised by the negative bands around 208 and 222 nm alongside a positive band around 192 nm, a signature characteristic of α-helical conformation. The solution CD spectra, on the other hand, show a

negative band around 198 nm, suggesting a predominantly unordered conformation. These data suggest that all the αS variants studied in this study remain largely unordered in bulk solution but fold into predominantly α-helical conformation at the air-water interface.

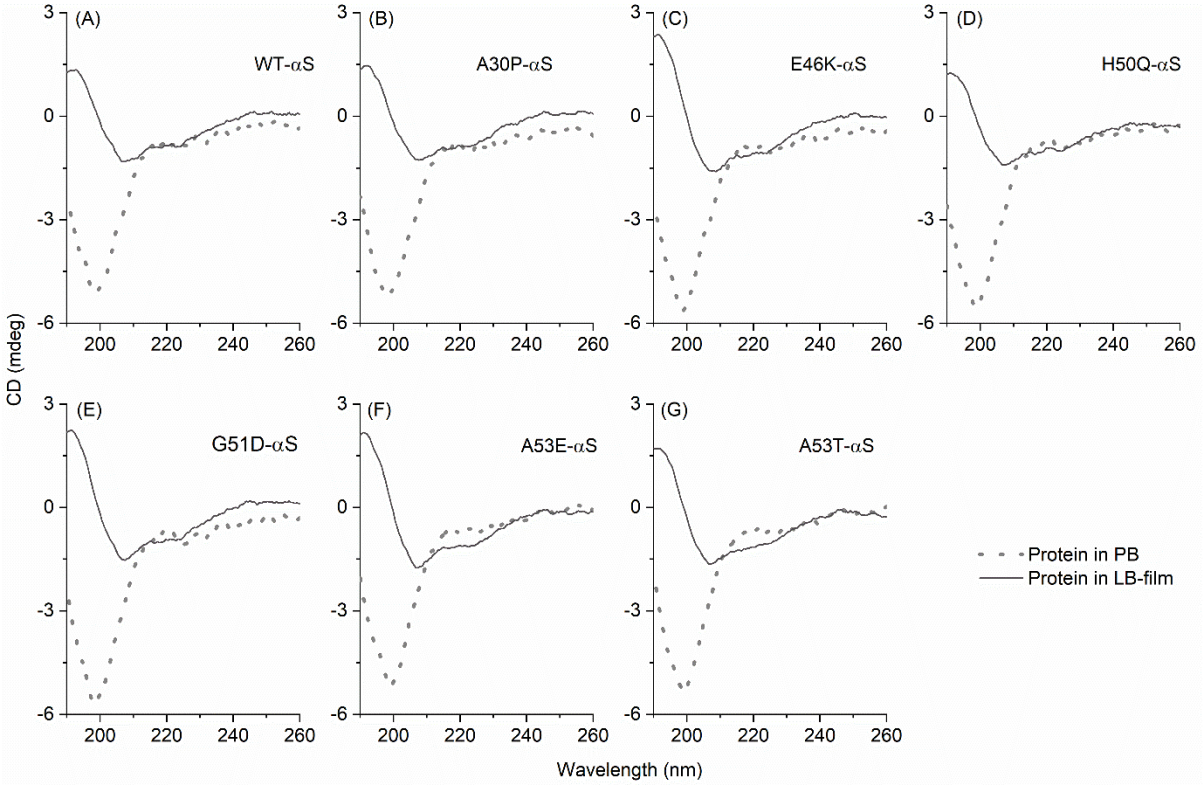

Fig. 4.5. The far-UV CD spectra of αS protein variants. The CD spectra in solution (dotted lines) and in LB films (solid lines) for WT-αS (A), A30P-αS (B), E46K-αS (C), H50Q-αS (D), G51D-αS (E), A53E-αS (F), and A53T-αS (G).

4.3.5 LD spectroscopy

The monolayer was very carefully Blodgett-deposited over the substrate (a 1 mm quartz slide). The LD spectra were recorded to gain insight into the protein's orientation in the Blodgett films. The spectroscopic origin of the LD spectrum is described in Section 3.3.5. The LD values at 208 and 193 nm were derived from the LD spectra. The reduced LD (LD^r) at 208 and 193 nm are plotted against the azimuth (angle of rotation) (Fig. 4.6, and A10). A sinusoidal change in the LD^r at both the wavelengths was observed. The LD^r becomes zero near 40-50° azimuth. This signifies a roughly perpendicular orientation of the helical axis to the substrate withdrawal direction.

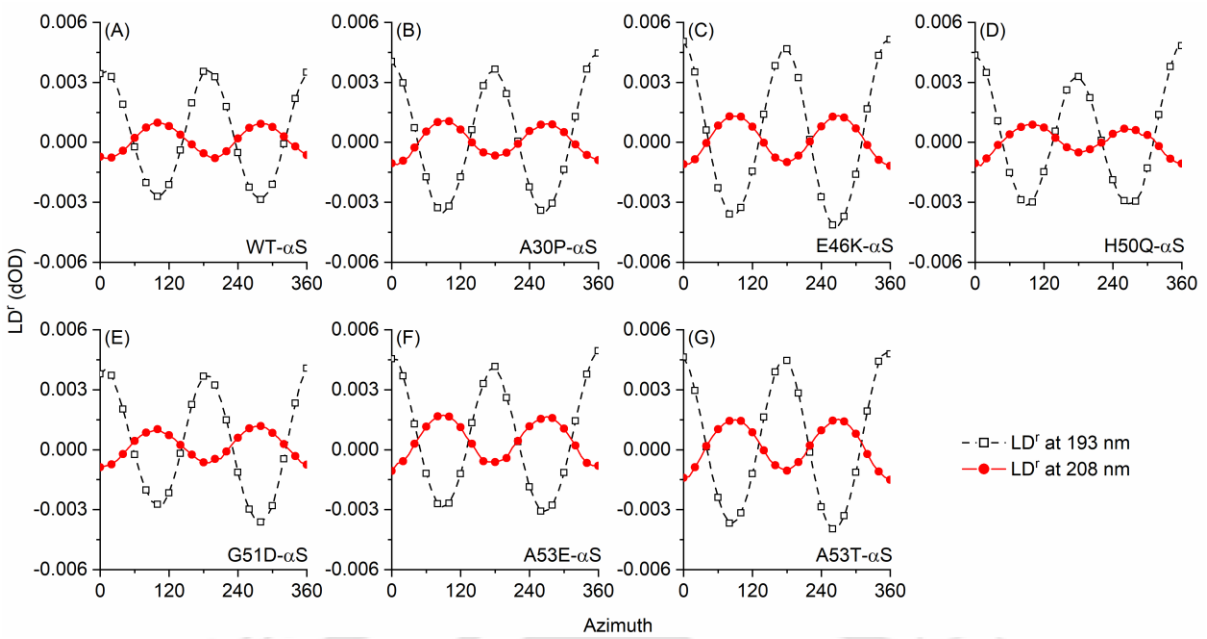

Fig. 4.6. LD spectroscopy of the LB films. The LDr at 193 nm and 208 nm plotted against the azimuth for the WT-αS (A), A30P-αS (B), E46K-αS (D), H50Q-αS (E), G51D-αS (F) A53E-αS (C), and A53T-αS (G).

4.3.6 AFM of the LB films

The surface topography of the LB films deposited over the n-type silicon wafers was investigated using AFM. The AFM micrographs show uniform deposition of the LB films over the silicon substrate (Fig. 4.7). The mesh-like microstructures were observed for WT-αS (panel A), A30P-αS (Panel B), E46K-αS (Panel C), H50Q-αS (Panel D), G51D-αS (Panel E), A53E-αS (Panel F), and A53T-αS (Panel G). The mesh-like microstructures seem to make carpet-like structures, with the partial alignment of the underlying filamentous structures. The average height of these structures is around 2-3 nm. There are some variations to note *viz.* the individual filaments formed by the E46K-αS are very narrow while those formed by A53T-αS are quite broad compared to the filaments observed for WT-αS. The AFM images obtained for the A30P-αS were very different; no filamentous structures were observed. Instead, intermittent holes were observed in the otherwise homogeneously spread-out film. The structures observed in the AFM micrograph give us information about the compressed monolayers of protein.

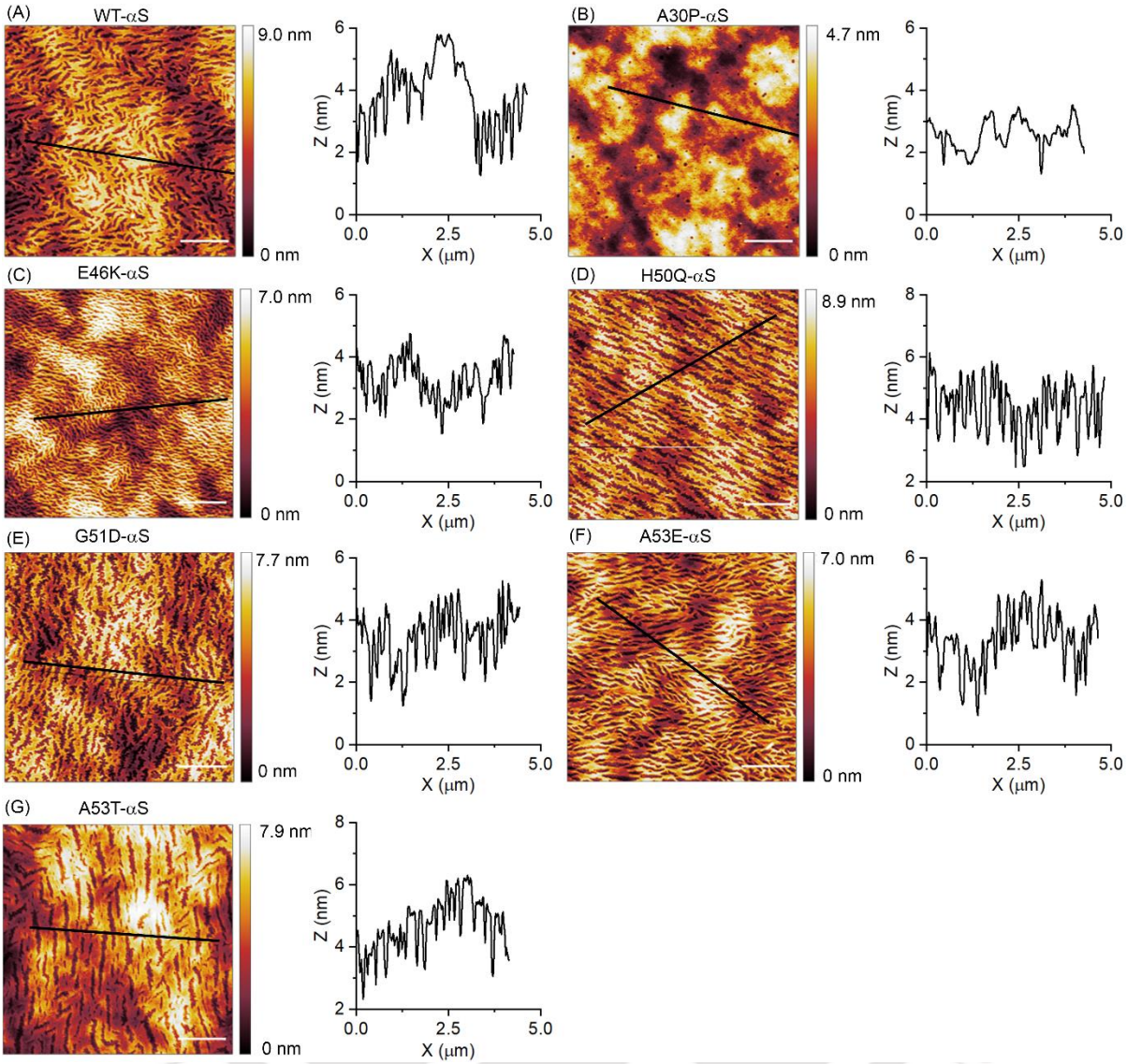

Fig. 4.7. The AFM micrograph of LB film. The surface topography of LB film deposited on a silicon wafer are shown for WT-αS (A), A30P-αS (B), E46K-αS (C), H50Q-αS (D), G51D-αS (E), A53E-αS (F), and A53T-αS (G). The z-height vs distance plots for the lines drawn on the AFM micrographs are shown to the right of the micrographs.

4.4 Conclusion

In this study, the interfacial properties of αS protein variants at the air-aqueous interface were investigated. The results show that the αS protein variants rapidly get adsorbed at the air-aqueous interface, attaining very high surface pressure (π ~20-22 mN/m). The PD mutations do not appreciably alter the surface activity of the mutant proteins. The compression appears to cause self-assembly of the protein into α-helix rich superstructures. Non-dispersion of the protein molecules from the self-assembled structures on the time scale of isotherms results in large hysteresis observed in the compression/expansion cycles. Compared to the WT-αS and

all other variants that displayed two distinct phases, the A30P-αS variant displayed three phases. The LD spectroscopy of the Blodgett deposited LB film reveals the presence of oriented α-helix. The AFM analysis of the LB films shows mesh-like uniform microstructures formed with a 2-3 nm height profile among the αS protein variants. The A30P mutant has a distinct fluid-like microstructure in the LB film with the presence of intermittent holes. The αS protein variants interact and penetrate the lipid monolayers composed of zwitterionic and negatively charged lipids. The protein variants show a higher affinity towards the negatively charged monolayers.

CHAPTER 5

Polymyxin B-catalysed αS Aggregation

5.1 Summary

Parkinson's disease (PD) is a progressive neurodegenerative disorder caused by the loss of dopaminergic neurons. It is characterised by the deposition of insoluble α-synuclein aggregates in the brain. Constipation is a common PD-associated condition, and the treatment of constipation with certain antibiotics seem to improve the PD symptoms. Polymyxin B, a last resort drug in treating the life-threatening Gram-negative bacterial infections, is one such antibiotic. The administration of polymyxin B in PD patients is known to alleviate the movement disorder symptoms; the mechanism of action, however, remains unclear. We, therefore, wondered if polymyxin B could modulate the aggregation of α-synuclein. We find that the polymyxin B promotes the aggregation of α-synuclein into amyloid fibrils. At equimolar polymyxin B concentration, the lag phase was reduced to around one-third of that in the absence of polymyxin B.

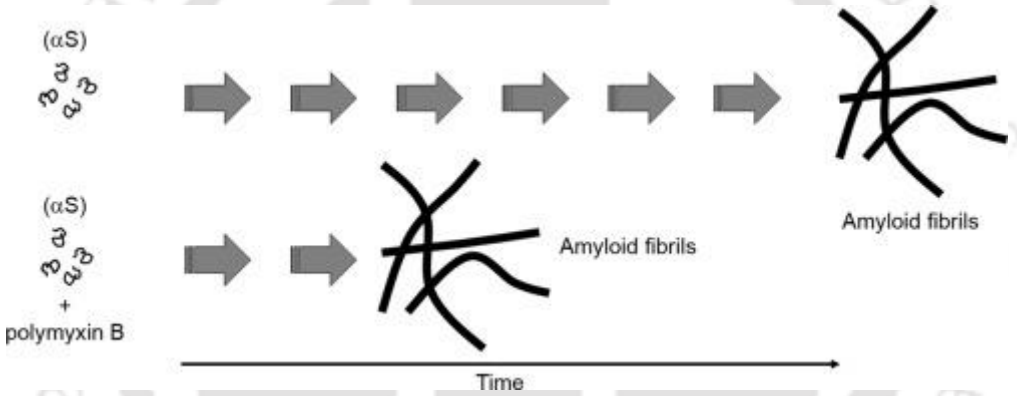

5.2 Introduction

The deposition of αS in the gut precedes the appearance of PD symptoms, and constipation happens to be a rather common condition in the PD patients. Constipation, therefore, is sometimes considered an early symptom of PD. Antibiotic treatment of constipation in PD patients is reported to alleviate movement disorder symptoms; vancomycin, metronidazole, colchicine and neomycin combination, and the metronidazole and polymyxin B combination improve the PD symptoms (Ovallath & Sulthana, 2018).

The polymyxins are amphipathic cyclic lipopeptide antibiotics that display strong activity against Gram-negative bacteria (Zavascki, Goldani, Li, & Nation, 2007). Due to their toxicity, however, their use is mostly limited to either multidrug resistance bacteria or specific cystic fibrosis cases (Landman, Georgescu, Martin, & Quale, 2008; Poirel, Jayol, & Nordmann, 2017). The routine usage includes topical application and as a bactericidal agent during irrigation in medical procedures (Kumar, Singh, Yadav, Mathur, & Bhadani, 2018; Poirel et al., 2017). The polymyxin class of antibiotics houses several closely related compounds (Fig. 5.1) (Orwa et al., 2001). Despite their inherent toxicity, polymyxin B and polymyxin E (colistin) are in clinical practice, albeit under serious circumstances (Satlin & Jenkins, 2017). Studies on polymyxin-administered patients suggest that the toxicity was due to their relatively higher daily doses than the currently recommended dosage (Sandri et al., 2013; Trimble, Mlynarcik, Kolar, & Hancock, 2016). Improved pharmaceutical manufacturing technology accompanied with better patient care has been instrumental in bringing down the polymyxin's toxicity over the recent years (Dai et al., 2017). Polymyxin B (PMB), a mixture of closely related fatty-acylated peptides, is isolated from *Bacillus polymyxa*, an anaerobic Gram-positive soil bacterium (Fig. 5.1) (Stansly & Schlosser, 1947). During multidrug resistant (MDR) or extensively drug resistant (XDR) bacterial infection in the central nervous system, the PMB is administered through the intrathecal (ITH) and intraventricular (ITV) routes (Pan et al., 2018). Such administration routes bypass the blood-brain barrier and are the only available treatment for the MDR, XDR, and other unresponsive Gram-negative infections. The crossing of blood-brain barrier by PMB made us wonder about its role, if any, in the neurodegenerative diseases.

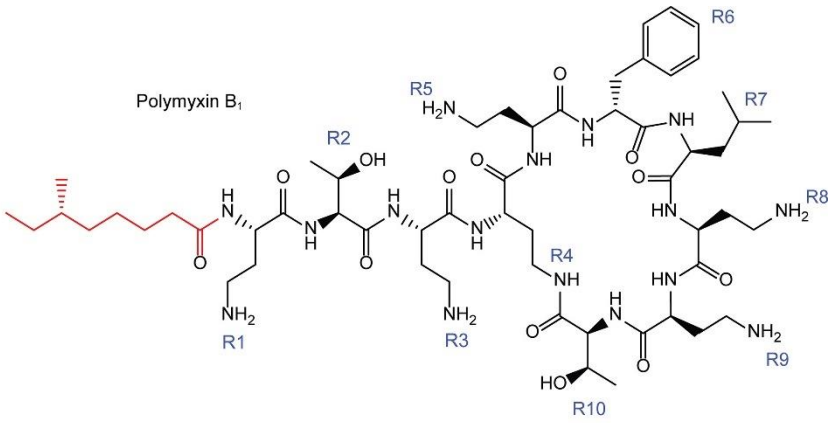

Polymyxins and their derivatives	Fatty acyl tail	R
B_1	6-methyloctanoyl	
Ile-B_1	6-methyloctanoyl	R7: Ile
B_2	6-methylheptanoyl	
B_3	octanoyl	
B_4	heptanoyl	
B_5	nonanoyl	
B_6	3-hydroxy-6-methyloctanoyl	
Colistin A	6-methyloctanoyl	R6: D-Leu
Colistin B	6-methylheptanoyl	R6: D-Leu
PMBN	absent	R1: absent
NAB7061	octanoyl	R1: absent, R3: aminobutyric acid
NAB/SPR741	acetyl	R1: absent, R3: D-Ser
SPR206	(3S)-4-amino-3-(3-chlorophenyl)butanoyl	R1: absent, R3: diaminobutyric acid
NAB739	octanoyl	R1: absent, R3: D-Ser
NAB815	octanoyl	R3: D-Thr, R8: aminobutyric acid
MicuRx-12	3-(2,2-dimethyl-butanoyloxy)-propanoyl	
CA824	(S)-1-(2-methylpropyl)-piperazine-2-carbonyl	R1: absent
FADDI-287	octanoyl	R3: diaminopropionic acid, R6: D-Leu, R7: aminobutyric acid
FADDI-002	octanoyl	R7: aminodecanoic acid
CB-182,804	2-chloro-phenylamino-carbonyl	

Fig. 5.1. The structure of polymyxin B1 (top). The related naturally-occurring and synthetic polymyxin analogs (bottom). The differences in the fatty acyl chain and the peptidic moiety are mentioned.

In recent years, the PMB analogues/derivatives with lower toxicity have emerged as the promising drugs (Vaara, 2019b). Researchers have engineered the primary lipopeptide's charge and hydrophobicity to reduce its toxicity (Fig. 5.1 and Table A3). *In vitro* studies have indicated that certain antibiotics can reduce pathogenic oligomeric species during the αS aggregation (González-Lizárraga et al., 2017; J. Li, Zhu, Rajamani, Uversky, & Fink, 2004; Mahapatra, Sarkar, Biswas, & Chattopadhyay, 2019; Török, Majláth, Szalárdy, & Vécsei, 2016). This is in line with the clinical reports of improved motor functions in the antibiotic-treated PD patients. It would, therefore, be interesting to investigate the role of PMB in the PD biomarker αS aggregation, if any. Considering the net positive charge and hydrophobicity of the peptide, we hypothesised that PMB might influence the aggregation propensity of αS. In this study, we examined the self-assembly of αS in the presence of different molar ratios of PMB. We find

that PMB accelerates the aggregation of αS; the lag phase shortens to around one-third in the presence of equimolar PMB.

5.3 Results

5.3.1 Characterisation of the purified protein

The size exclusion chromatogram of αS purification is shown in Fig. 5.2A. The 54 min fraction was collected and characterised using analytical reversed-phase HPLC and MALDI-TOF mass spectrometry. The HPLC chromatogram shows a single peak suggesting a high purity protein preparation (Fig. 5.2B). The MALDI-TOF mass spectrum shows peaks at 7232.23 and 14,474.01 *m*/*z* values (Fig. 5.2C). The observed mass at 14474.01 corresponds to the $[M + Na]^+$ adduct of αS (Mohapatra & Chaudhary, 2021). The smaller m/z value corresponds to the doubly-charged αS. The protein preparation was further characterised using DLS. A single peak corresponding to the hydrodynamic diameter of 8.72 nm with PDI of 0.13 was observed, indicating a monodispersed protein preparation (Fig. 5.2D).

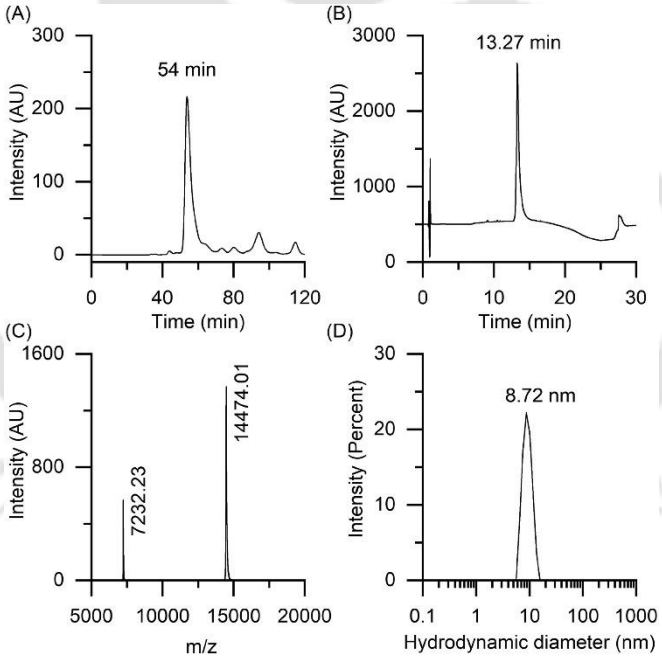

Fig. 5.2. Characterisation of αS protein. (A) The SEC profile of the anion exchange-purified αS, (B) the analytical reversed-phase HPLC profile of the SEC-purified αS, (C) the MALDI-TOF mass spectrum of the HPLC fraction at 13.27 min, and (D) the DLS-derived hydrodynamic diameter distribution of the 54 min SEC fraction.

5.3.2 Aggregation kinetics of αS in the presence of PMB

The 100 µM αS protein in the presence of different PMB concentrations (0 µM, 12.5 µM, 25 µM, 50 µM, and 100 µM) was set up for aggregation at room temperature in buffer D. The aggregation was monitored by drawing the 10 µl aliquots at 5 h intervals and recording ThT fluorescence with 10 µM effective ThT concentration. Intercalation of ThT into the developing β-sheets results in an enhanced fluorescence at around 482 nm when excited at 440 nm. As the aggregation reaction proceeded, we observed a sigmoidal increase in the fluorescence intensity over time.

In the absence of PMB, the amyloid formation by αS was characterised by a lag phase of around 60 h (Fig. 5.3). After the lag-phase, the self-assembly of the protein attains an exponential phase. Here, the self-assembly is autocatalytic, and the fibrils start forming rapidly. In the presence of 12.5 µM PMB (PMB:αS ratio of 1:8), there is no significant change in the lag phase but the exponential phase turns very steep and a higher ThT fluorescence is observed. This could be due to an increase in the primary nucleation and elongation rates of αS self-assembly in the presence of PMB. At higher PMB concentrations, there is a gradual decrease in the lag phase. At equimolar concentrations, the lag phase reduces to around 20 h. Besides, there is a considerable increase in the saturation phase ThT fluorescence intensity compared to that of the αS that aggregates without PMB. This could be due to the presence of higher fraction of αS in the fibrillar form.

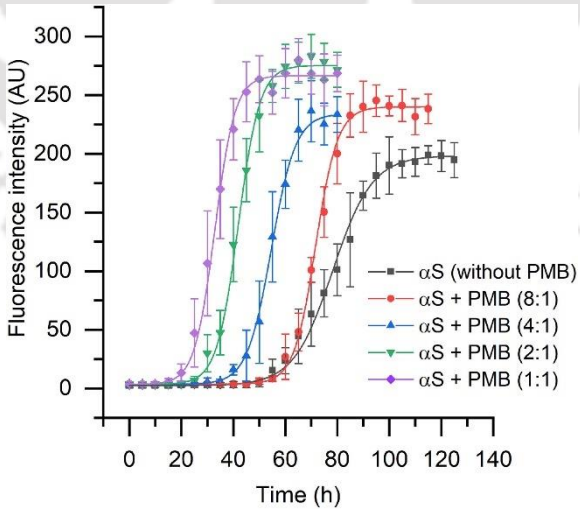

Fig. 5.3. Aggregation kinetics of αS in the presence of PMB. ThT fluorescence intensity at 482 nm is plotted against the time.

5.3.3 CD spectroscopy

The structural transition during αS aggregation in the presence or absence of the PMB was studied using CD spectroscopy in 25 mM phosphate buffer, pH 7.4. The CD spectrum of the freshly-prepared protein shows a broad negative band near 200 nm (Fig. 5.4A). The spectrum suggests an unordered secondary structure and hence corroborates with that of established intrinsically disordered conformation of αS in an aqueous solution (C.-H. Lee et al., 2006). There is no appreciable change in the ellipticity after 48 h of incubation. After 150 h of incubation, the αS shows a positive band around 195 nm and a broad negative band around 215 nm, indicating β-sheet conformation. The CD data for the αS incubated with equimolar PMB was profoundly different (Fig. 5.4B). The CD spectrum recorded for the freshly prepared sample showed a broad negative band around 200 nm, suggesting unordered αS. The 48 h incubated sample, on the other hand, displayed a positive band around 196 nm with a broad band centred around 218 nm, indicating a distinct β-sheet conformation. The CD spectrum obtained for 150 h old sample was nearly identical to that of 48 h sample. The CD data for αS and αS + PMB (1:1) are in sharp contrast to each other, where the 48 h spectrum of αS is similar to that of the freshly prepared sample, while that of αS + PMB (1:1) is nearly identical to 150 h sample. These data are in excellent correlation with the aggregation kinetics, wherein the αS is very much in the lag phase after 48 h whereas αS + PMB (1:1) nears aggregation completion. Besides, the ellipticity of the αS + PMB (1:1) sample after 150 h incubation is higher than that of the αS sample. These data clearly suggest that PMB accelerates the aggregation of PMB into amyloid fibrils. Besides, the PMB-induced aggregates display higher ThT fluorescence and the ellipticity compared to the αS that aggregates in the absence of PMB.

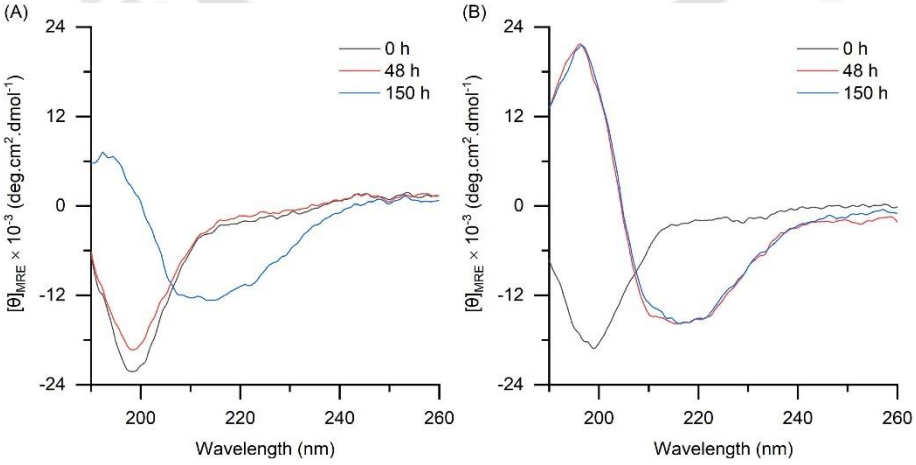

Fig. 5.4. CD spectroscopy of αS incubated with or without PMB. (A) αS incubated without PMB and (B) αS incubated with equimolar PMB.

5.3.4 TEM imaging

The aggregation of αS was further examined using TEM imaging. The freshly prepared αS and αS + PMB (1:1) were free from any discernible aggregates (Fig. 5.5A and D, respectively). The 48 h-old αS was also free from any amyloid-like aggregates (Fig. 5.5B). The αS + PMB (1:1), on the other hand, shows distinct fibrillar aggregates after 48 h of incubation (Fig. 5.5E). After 120 h of incubation, both αS and αS + PMB (1:1) show fibrillar aggregates (Fig. 5.5C and F, respectively).

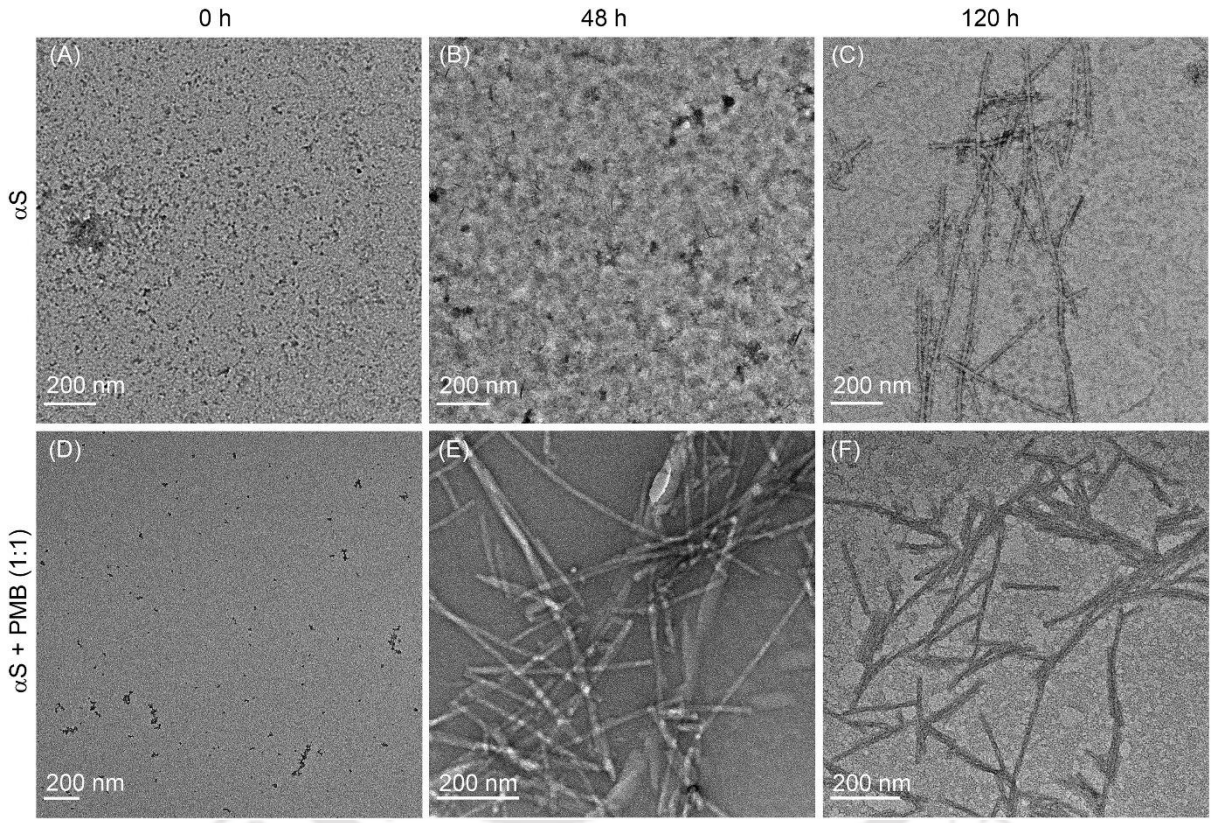

Fig. 5.5. TEM images of αS incubated with or without PMB. (A), (B), and (C) represent the images of αS incubated for 0 h, 48 h, and 120 h, respectively. (D), (E), and (F) show images of αS incubated with equimolar PMB for 0 h, 48 h, and 120 h, respectively.

5.3.5 Cell viability assay

Owing to its nephro- and neurotoxicity, the PMB is used as the last resort drug to treat the infections. As PMB accelerated the αS aggregation, we investigated if the PMB neurotoxicity is mediated *via* αS aggregation. The cytotoxicity of the αS, incubated without or with equimolar PMB, was investigated against the mouse neuronal cell line Neuro-2a. The toxicity was assayed at different time points, essentially the time points that correspond to the lag phase (freshly prepared samples, 0 h incubation), the start of the exponential phase where the prefibrillar

structures are expected to be populated (70 h for αS, 25 h for αS + PMB), and the saturation phase (120 h for αS, 70 and 120 h for αS + PMB). The cell viability data is shown in Fig. 5.6.

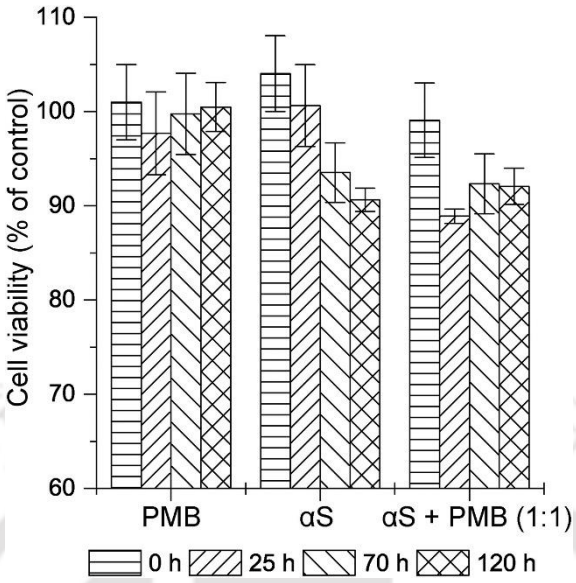

Fig. 5.6. The αS and PMB + αS-induced cytotoxicity. The histograms show cell viability (% of control) of mice neuro-2a cells treated with 0 h, 25 h, 70 h, and 120 h aged samples. The error bars represent standard deviation.

The PMB was found to be largely non-toxic at our working concentration. The αS displayed no cytotoxicity after 25 h incubation. The 70 h incubated αS, however, shows ~6% toxicity. The 120 h incubated αS sample also exhibited toxicity comparable to the 70 h sample. The αS + PMB (1:1) sample, on the other hand, displays ~10% toxicity after 25 h incubation. The data is consistent with the aggregation kinetics assay (Fig. 5.2). As the aggregation enters the exponential phase around this time, the sample is expected to be rich in oligomers. The samples incubated for longer durations (70 h and 120 h) resulted in somewhat better viability. Overall, the data do not suggest any significant difference in the viability of the cells treated with αS and αS + PMB (1:1).

5.3.6 Surface activity of PMB and PMB-αS interaction

As PMB is an amphipathic molecule, we got interested in investigating the αS interaction with PMB monolayers. The surface adsorption of PMB at the air-aqueous interface was carried out to understand the surface activity of the cationic lipopeptide. Progressively, a small amount of PMB was added to the subphase (10 mM PB, 150 mM NaCl, pH 7.5) while the increase in the surface pressure was recorded. The saturation π obtained at different amounts of PMB added to the subphase were extracted and plotted against the number of moles added to the subphase.

The lipopeptide displays low surface activity with 320 nmoles giving π ~7.5 mN/m (Fig. 5.7). No saturation in π could be achieved up to 320 nmoles. The interaction of αS with PMB monolayers was carried out with PMB monolayers (in 25 mM PB, pH 7.4) with 320 nmoles lipopeptide that gave a π ~7 mN/m. Injecting 2 nmoles of αS causes rapid rise in the π, that saturates ~20 mN/m (Fig. 5.7 B). It is important to note that a π ~20 mN/m has been obtained from 1 nmoles of αS alone (Fig. 3.2B, Chapter 3).

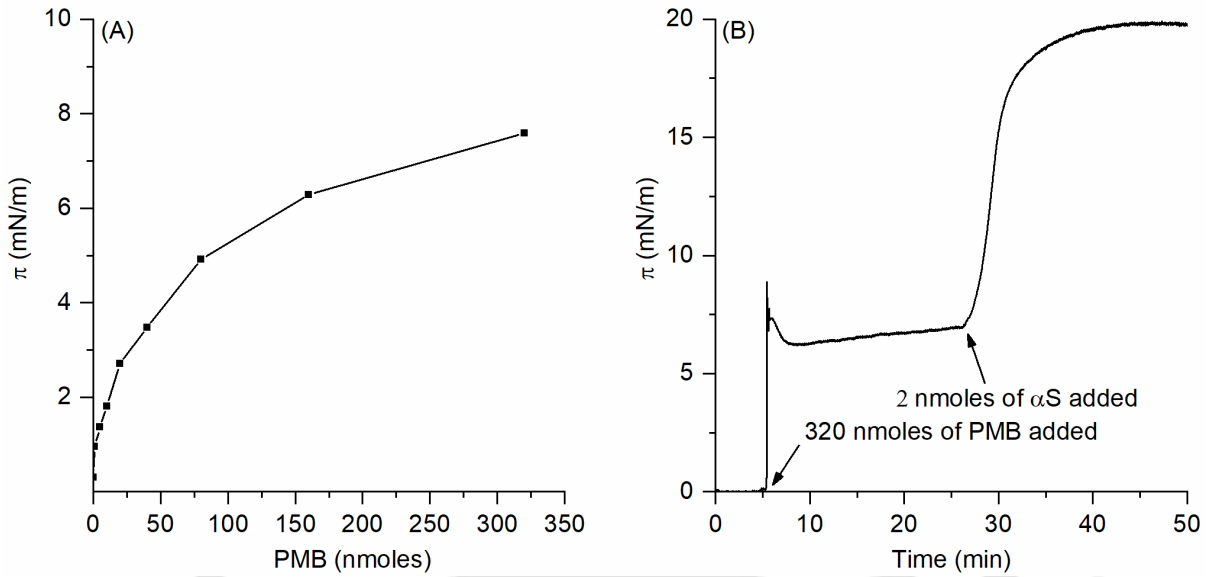

Fig. 5.7. Surface activity of PMB, and interaction with αS. The plot of π against the amount of PMB to the subphase (A). The penetration of αS into a monolayer of PMB at around 7 mN/m (B).

5.3.7 Compression/expansion isotherms

As the αS inhibits the αS aggregation at equimolar concentration, the compression/expansion isotherms of αS with and without equimolar PMB were recorded. The 10 mM PB, 150 mM NaCl, pH 7.5 was taken as the subphase. In a series of experiments, a mixture of 2 nmoles of αS along with 0 or 2 nmoles of PMB (αS:PMB = 1:1) was carefully layered on the interface. The monolayers were left undisturbed for 30 minutes, followed by continuous 3 cycles of compression/expansion of the monolayer at a rate of 20 cm^2/min. Considering all the protein at the interface, the π-A isotherms were computed (Fig. 5.8A-B). The initial surface pressure (π_i) after spreading the monolayer turned out to be around 3 to 5 mN/m The limiting molecular areas A_0 were calculated from the first compression (1^C) isotherms (Fig. 5.8A-B). Comparable limiting molecular areas were observed for the WT-αS in the absence (A_0 ~2020) or presence of PMB (A_0 ~1989). The first compression isotherms, in both the experiments, show a gradual

rise in surface pressure during compression, indicating a rather smooth transition from liquid-expanded (LE) to liquid-condensed (LC) phase. The compression isotherm reached a maximum surface pressure of around 32-33 mN/m. The compression and expansion isotherms do not retrace themselves in these experiments, thus a hysteresis could be seen. The large hysteresis originates from molecular reorientation, conformational changes, or self-assembly of the molecules at the interface. In the subsequence compression cycles, the compression isotherm (2^C-4^C) shifted to lower molecular areas. This signifies that the molecular events due to the compression does not reverse on the timescale of the experiment. The expansion isotherms (1^E-3^E) start with a rapid drop (up to π~15 mN/m) in the surface pressure, signifying an elastic behaviour. Further expansion leads a gradual drop in the surface pressure and reaches the minimum.

The C_S^{-1} vs π plots (Fig. 5.8C-F) represent the 1^C, 2^C, 3^C, and 4^C compression isotherms respectively. The initial isotherms (1^C) have distinctive features than rest of the isotherms. The deposited monolayers display low compressibility with C_s^{-1} above 70 mN/m A variable inflection point is seen which represents phase change from LE to LC. From the second compression, the C_s^{-1} is around 5 mN/m at lower surface pressure, suggesting higher compressibility. The C_s^{-1} increases with π, and reaches a plateau near π ~15 mN/m, and then decreases. This clearly indicate the two distinct phases in the monolayers. The isotherms as well as the C_s^{-1}-π plots are very similar, indicating that the contribution of PMB in the interfacial activity is insignificant. This is not unexpected as 1 nmoles of αS reaches up to 20 mN/m surface pressure (Fig. 3.2B, Chapter 3) whereas the that of PMB results in ~0.5 mN/m surface pressure (Fig. 5.7A).

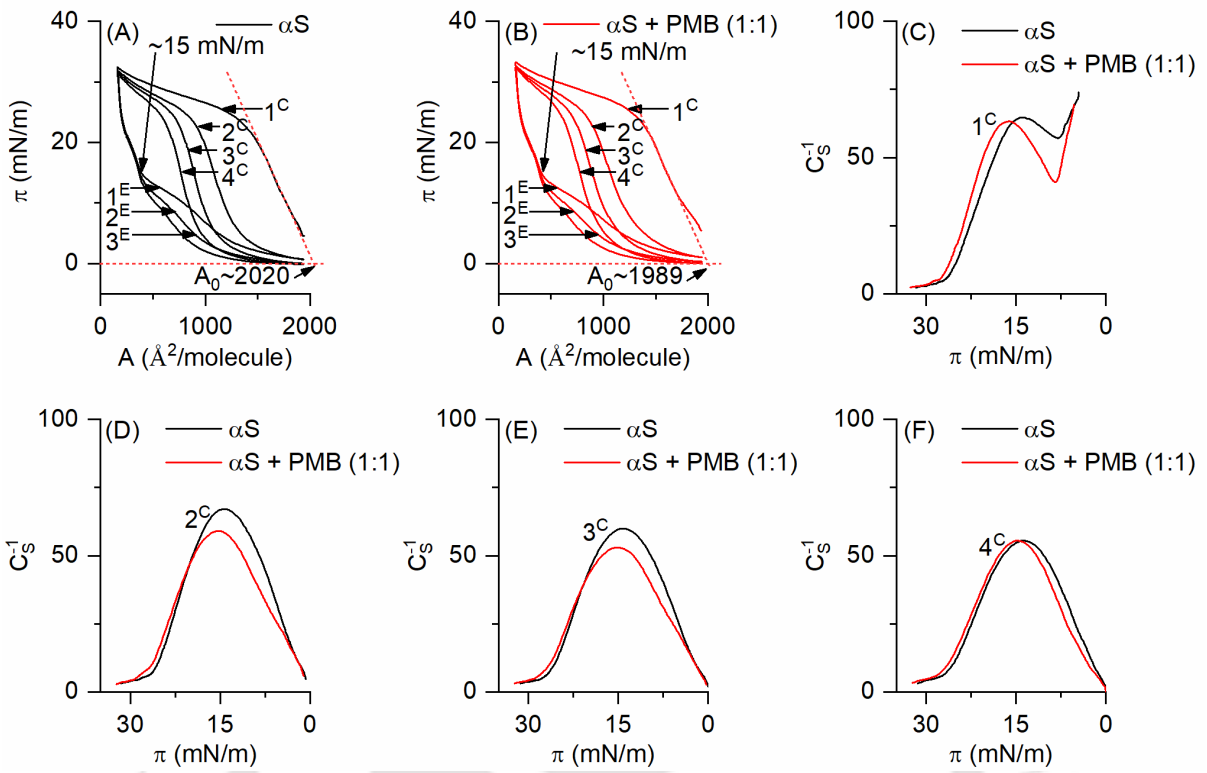

Fig. 5.8. Langmuir compression/expansion isotherms of αS in the absence or presence of equimolar PMB. The π-A isotherm of αS in the absence of PMB (A) and in the presence of PMB (1:1) (B). The compressibility moduli of 1^C, 2^C, 3^C and 4^C are shown in panels C-F, respectively.

5.3.8 Circular dichroism (CD) of the LB film

The Langmuir monolayers are the fourth compression were Blodgett-deposited on quartz slides for CD spectroscopy. The CD spectra of the Blodgett-deposited films are shown in Fig. 5.9. Both the CD spectra show a positive band around 192 nm, and negative bands around 208 and 222 nm, which is a characteristic α-helical signature. These data suggest that the αS predominantly remains in the α-helix rich conformation at the air-aqueous interface, and PMB has little influence, if any at all.

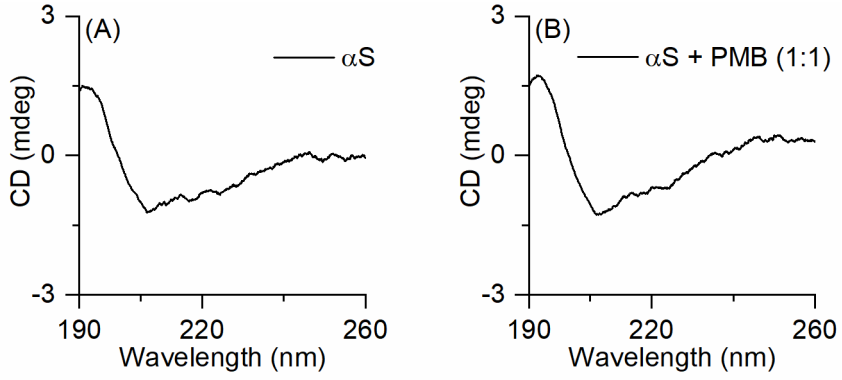

Fig. 5.9. CD spectra of the Blodgett films. The CD spectra of αS in the absence of PMB (A) and in the presence of PMB (1:1) (B).

5.4 Discussion

Polymyxins display excellent bactericidal activity against Gram-negative bacteria but their potential is marred due to their neuro- and nephrotoxicity. As PMB features in the list of antibiotics reported to improve PD symptoms, we investigated its role in the αS aggregation. PMB was found to promotes the αS aggregation. αS is an intrinsically disordered protein in aqueous solutions. However, it binds to the negatively charged membranes, wherein the N-terminal region (up to ~95 residues) folds into an amphipathic helix (Bartels et al., 2010; Jao et al., 2004; Jao et al., 2008). The protein binds to the SDS micelles wherein the N-terminal region takes up a broken-helix conformation with the two helical regions lying roughly antiparallel to each other (Chandra et al., 2003; Lokappa & Ulmer, 2011). Lee and coworkers reported that the membrane-bound αS has a higher aggregation tendency, and the aggregates formed on the membrane can seed the aggregation of free αS (H.-J. Lee, Choi, & Lee, 2002). PMB is a cyclic lipopeptide that can form micelles. The critical micelle concentration (CMC) of PMB is not properly reported in the literature. Lawrence et al. reported the PMB's CMC to be slightly lower than 6 wt% (~43 mM) but did not report the data (Lawrence, Alpar, McAllister, & Brown, 1993). Boyd and coworkers have reported the CMC of colistin (polymyxin E) as 1.5 mM in deionized water (Wallace et al., 2010). PMB and colistin are very similar, the only difference being the presence of D-phenylalanine in PMB instead of D-leucine in colistin (Kwa, Kasiakou, Tam, & Falagas, 2007). As we have carried out the αS aggregation assays with ≤100 μM PMB concentrations, we are way below the reported CMC values for polymyxins. The faster kinetics of PMB-induced aggregation, therefore, is unlikely to be micelle-induced.

Fink and coworkers reported partial folding of αS at lower pH or higher temperatures (V. N. Uversky et al., 2001). Both these conditions enhanced the αS aggregation kinetics indicating that the partially-folded species could be a fibril precursor. Eliezer and coworkers further investigated the αS structural changes under acidic conditions (McClendon et al., 2009). The low pH causes protonation of the acidic side chains, thereby eliminating electrostatic repulsions, and leading to a collapse of the C-terminal region. The C-terminal tail of αS was found to be fully protonated at pH 3 and existed as an ensemble of compact conformations. A slight increase in the interaction of the C-terminal tail with the NAC region was also reported. Lapidus and coworkers investigated the role of intramolecular diffusion upon αS aggregation

kinetics (Ahmad, Chen, & Lapidus, 2012). They proposed that the fast intramolecular reconfiguration does not allow stable bimolecular association. They found that the charge neutralization of the C-terminal tail has profound effects on the NAC. It appears that the high hydrophobicity of NAC would enforce significant compaction, unless countered by the charged C-terminal tail. The acidic pH induced slowdown in reconfiguration was proposed to enhance aggregation propensity. The C-terminal tail of αS, therefore, is an essential qualifier to its aggregation propensity. The amount of net negative charge dictates the lag phase length in aggregation kinetics (Afitska, Fucikova, Shvadchak, & Yushchenko, 2017). Jovin and coworkers have reported enhancement in the αS aggregation kinetics by polyamines, wherein the faster kinetics is a direct consequence of polyamine binding to the C-terminal tail (Fernández et al., 2004). PMB being a positively charged lipopeptide, with an effective +5 charge at pH 7.4, is highly likely to interact with the negatively charged C-terminal region (net charge: −12) of the αS. The amphipathic αS, that takes up an α-helix rich conformation at the air-aqueous interface is highly likely to have its C-terminal tail exposed to the subphase. The PMB has low surface activity, and does not affect the strong interfacial activity of αS. Further, it is likely that the PMB binds to the αS C-terminal domain, and therefore, does not contribute to the interfacial activity. The faster aggregation kinetics observed in the presence of PMB could, therefore, be due to the C-terminal tail's charge neutralization. Our cell viability data did not suggest any significant difference in the neurotoxicity of the αS and the αS + PMB. We found that that an enhancement in the aggregation propensity by PMB could reduce the critical aggregation concentration of the αS, thereby shifting the equilibrium towards aggregation. It would, therefore, be worth investigating if the PMB causes αS fibrillation at the otherwise non-aggregation conditions.

CHAPTER 6

Conclusions and Future Prospects

CONCLUSION AND FUTURE DIRECTIONS

Intrinsically disordered proteins (IDPs) have dynamic three-dimensional structure in solution and influence several physiological functions of the cells (Vladimir N. Uversky, 2019). In fact, several folded proteins also contain intrinsically disordered regions, that might fold depending upon the function (Babu, 2016). The αS is a well-studied intrinsically disordered protein (Fakhree, Nolten, Blum, & Claessens, 2018). Even though Selkoe and coworkers reported that the native αS might exist as folded α-helical tetramer, subsequent studies support an equilibrium between the α-helical oligomeric and disordered monomeric αS (Bartels et al., 2011; Lucas & Fernandez, 2020). When the intrinsically disordered αS encounters a membrane, depending upon the curvature of the lipid bilayer, it attains an extended helix or a broken helix-rich state (Lokappa & Ulmer, 2011). As up to around two-thirds of the protein can fold into an amphipathic α-helix, we explored the interfacial activity of the αS, its Parkinsonian variants, and the role of N-terminal acetylation on the interfacial activity.

In eukaryotes, almost all the proteins are acetylated, so is the case with αS (Johnson et al., 2010). Further, it is noteworthy that the N-terminal acetylation has been shown to be helix-inducing in the peptide fragments of αS (Bartels et al., 2014). The full-length acetylated αS is also reported in the literature to form the metastable tetrameric form of the protein (Fernandez & Lucas, 2018a). In chapter 3, we investigated the interfacial activity of the αS, and the role of N-terminal acetylation on that, if any. The data suggested that N-terminal acetylation does not have any noticeable effect on the protein's interfacial activity. Based on these data, the studies reported in the chapters 4 and 5 were carried out using unacetylated αS and its parkinsonian variants. The reason for choosing the unacetylated protein over the acetylated one was the higher protein yield of NH_2-αS over Ac-αS. The interfacial activity of the parkinsonian variants and their interaction with zwitterionic and negatively-charged lipid monolayers were investigated in chapter 4. The interfacial activity of the mutants, except the A30P-αS, were comparable to that of wild-type αS. The compression isotherms indicated two phases. The A30P-αS isotherms, however, displayed three distinct phases. All the αS variant, not surprisingly, displayed higher affinity towards the negatively-charged monolayers. The Blodgett-deposition of the αS and its variants' Langmuir films showed far-UV linear dichroism indicating anisotropic deposition of the protein. The LB, could, therefore be used for ordered deposition of amphipathic molecules, including biomolecules.

Chapter 5 discusses the Polymyxin-B catalysed aggregation of αS in solution. The antibiotic reduces the lag phase in the aggregation kinetics of αS, thus producing early fibrillation of the protein. The early fibrillation was ascertained using several biophysical methods *viz.* ThT fluorescence, CD spectroscopy, and TEM imaging. Using the Langmuir-Blodgett technique, the PMB's inability to influence interfacial properties of αS was discussed. The data, though indirectly, indicates that the cationic lipopeptide PMB may bind to the acidic C-terminal of the αS protein, thus not affecting its interfacial properties. Recently, several old antibiotics have been repurposed for various diseases (Bortolanza et al., 2018; Zheng, Sun, & Simeonov, 2018). In-spite of known effectiveness of the PMB, the neuro- and nephrotoxicity restricts it's use to only cystic fibrosis and bacterial meningitis like cases (Crass, Rutter, Burgess, Martin, & Burgess, 2017; Segal-Maurer, Mariano, Qavi, Urban, & Rahal, 1999). Due to growing antibiotic resistance, several derivatives of PMB are currently being explored for their efficacy and toxicity (Vaara, 2019a). It would be interesting to investigate their influence of the αS aggregation. There are several interesting aspects that can be looked at:

1. The effect of PMB administration in the PD mice model would be worth investigating
2. The detailed mechanism of the dramatic influence of PMB on αS aggregation remains unknown.
3. If the effect of PMB on αS aggregation is mediated through electrostatic interactions, it would be worthwhile to investigate the effect of other cationic molecules such as cationic antimicrobial peptides (AMP).
4. An interesting study could be to investigate the expression of AMPs in the PD patients or PD mouse models.

Appendix

Table A1. DNA oligonucleotides used for the site-directed mutagenesis.

Mutation	Primer sequence	No. of bases
aSyn-A30P-FP	5`-GGCGGAAGCGCCAGGCAAAACGAAAGAAGGTG-3`	32
aSyn-A30P-RP	5`-CGTTTTGCCTGGCGCTTCCGCCACGC-3`	26
aSyn-E46K-FP	5`-GCAAAACCAAAAAAGGCGTGGTTCATGG-3`	28
aSyn-E46K-RP	5`-CCACGCCTTTTTTGGTTTTGCTGC-3`	24
aSyn-H50Q-FP	5`-CGTGGTTCAAGGTGTGGCCACCGTTGC-3`	27
aSyn-H50Q-RP	5`-GGCCACACCTTGAACCACGCCTTCTTTGG-3`	29
aSyn-G51D-FP	5`-GGTTCATGACGTGGCCACCGTTGC-3`	24
aSyn-G51D-RP	5`-GGTGGCCACGTCATGAACCACGCC-3`	24
aSyn-A53E-FP	5`-GGTGTGGAAACCGTTGCAGAAAAAACG-3`	27
aSyn-A53E-RP	5`-GCAACGGTTTCCACACCATGAACCACG-3`	27
aSyn-A53T-FP	5`-GGTGTGACAACCGTTGCAGAAAAAACG-3`	27
aSyn-A53T-RP	5`-GCAACGGTTGTCACACCATGAACCACG-3`	27

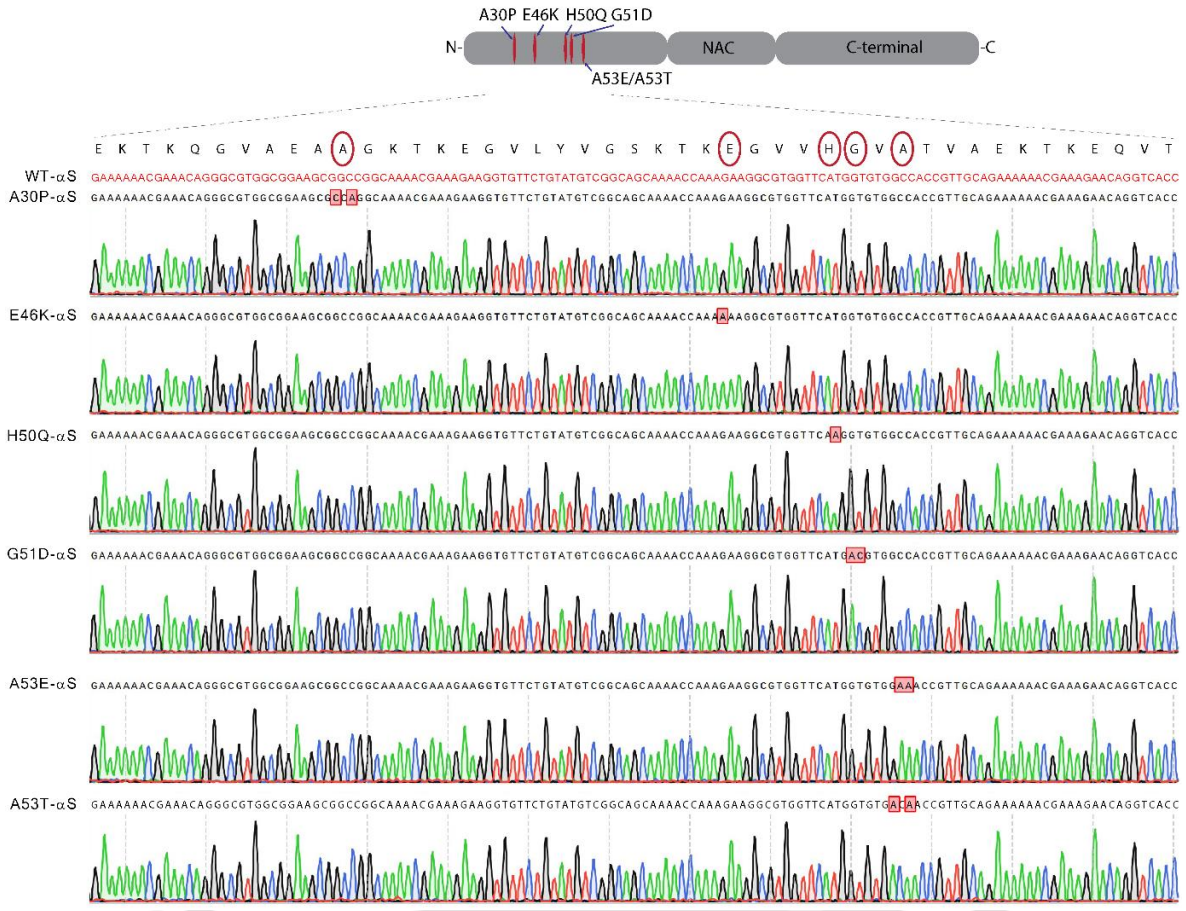

Fig. A1. The sequencing snapshot of the αS parkinsonian mutations made using SDM. The nucleotide sequences were analysed using Snapgene software. The nucleotide changes are marked with red boxes.

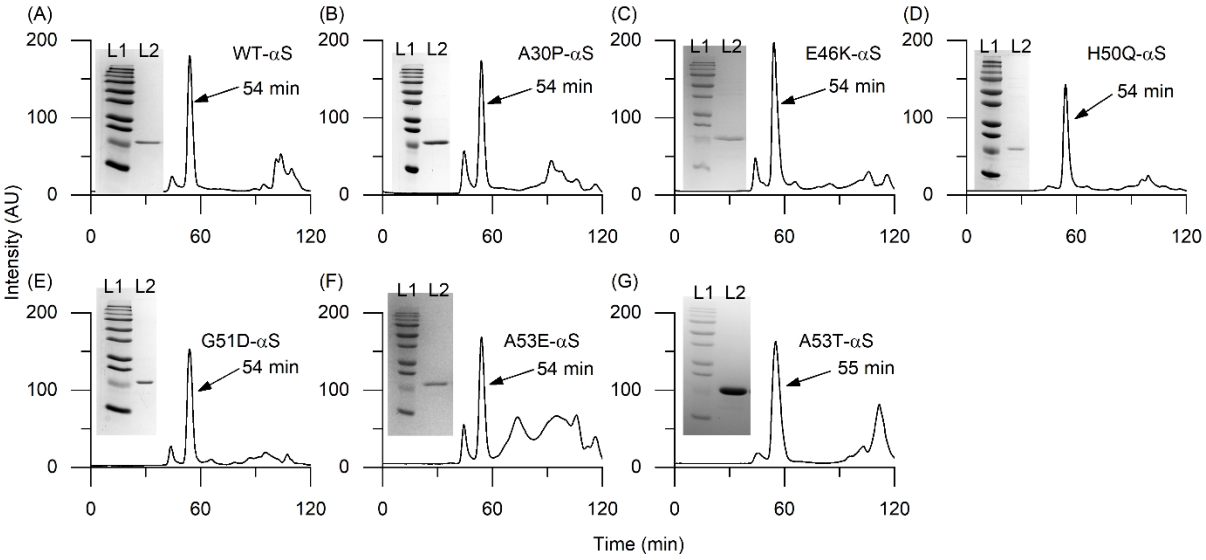

Fig. A2. The size exclusion chromatographic profiles of the αS variantsThe WT-αS elutes at 54 min (A), A30P-αS elutes at 54 min (B), E46K-αS elutes at 54 min (C), H50Q-αS elutes at 54 min (D), G51D-αS elutes at 54 min (E) A53E-αS elutes at 54 min (F), and A53T-αS elutes at 55 min (G). The insets show 15 % SDS-PAGE analysis of the SEC-purified protein. The BioRad Precision Plus Protein™ ladder is in L1, whereas the SEC-purified protein is in L2. L1 ladder size (from bottom): ~10 kDa, ~15 kDa, ~20 kDa, ~25 kDa, ~37 kDa, ~50 kDa, ~75 kDa, ~100 kDa, ~150 kDa, ~250 kDa. The protein bands in L2 correspond to ~15 kDa.

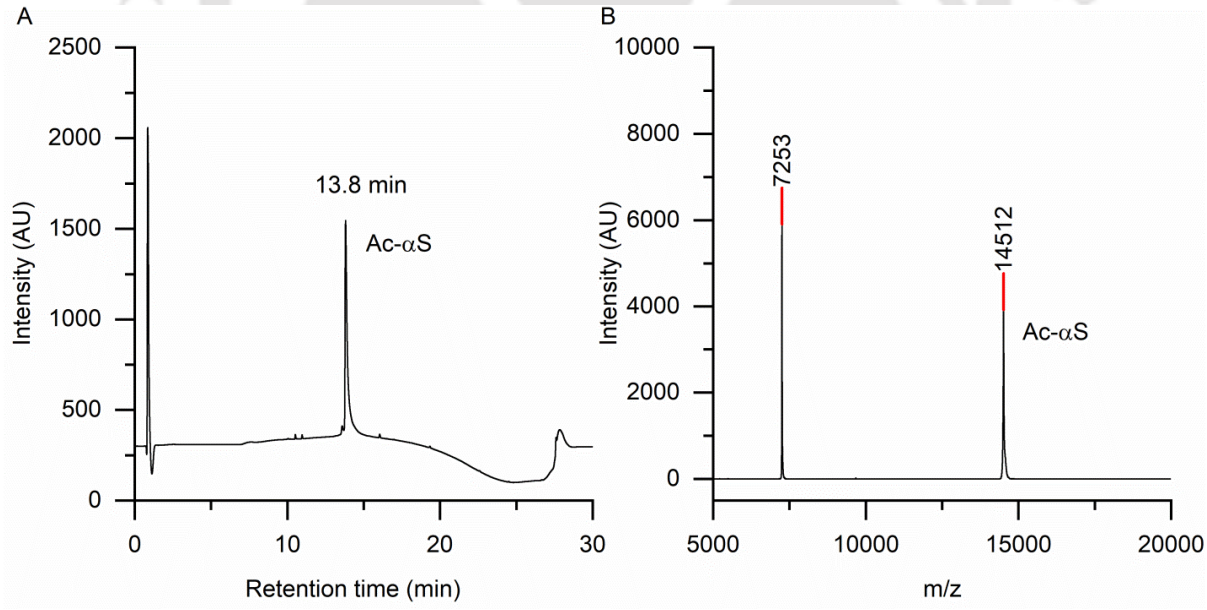

Fig. A3. (A) Analytical reversed-phase HPLC chromatogram of N-terminal acetylated α-synuclein (Ac-αS). (B) MALDI-TOF mass spectrum of reversed-phase HPLC-purified Ac-αS. We observed a peak at 14512 Da, which is a Na^+ adduct of Ac-αS. The Ac-αS has a theoretical

monoisotopic mass of 14493.229 Da [1]. The z = 2 peak is also observed at m/z of 7253. The mass spectrum was obtained using a Bruker, Autoflex Speed MALDI TOF/TOF.

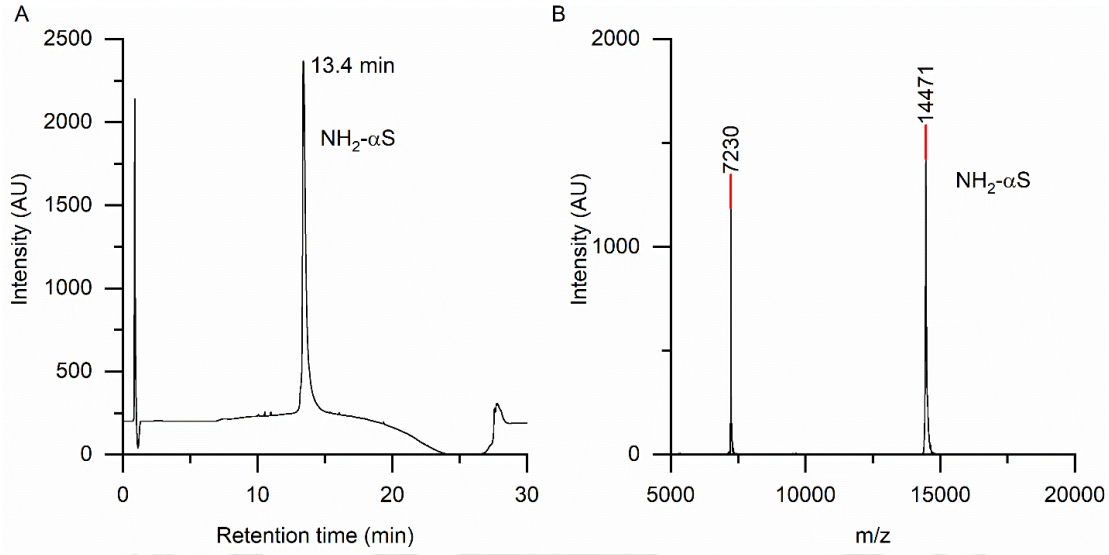

Fig A4. (A) Analytical reversed-phase HPLC chromatogram of NH_2-αS. (B) MALDI-TOF mass spectrum of reversed-phase HPLC-purified NH_2-αS. We observed a peak at 14471 Da, which is a Na^+ adduct of NH_2-αS. The NH_2-αS has a theoretical monoisotopic mass of 14451.22 Da [1]. The z = 2 peak is also observed at m/z of 7230. The mass spectrum was obtained using a Bruker, Autoflex Speed MALDI TOF/TOF.

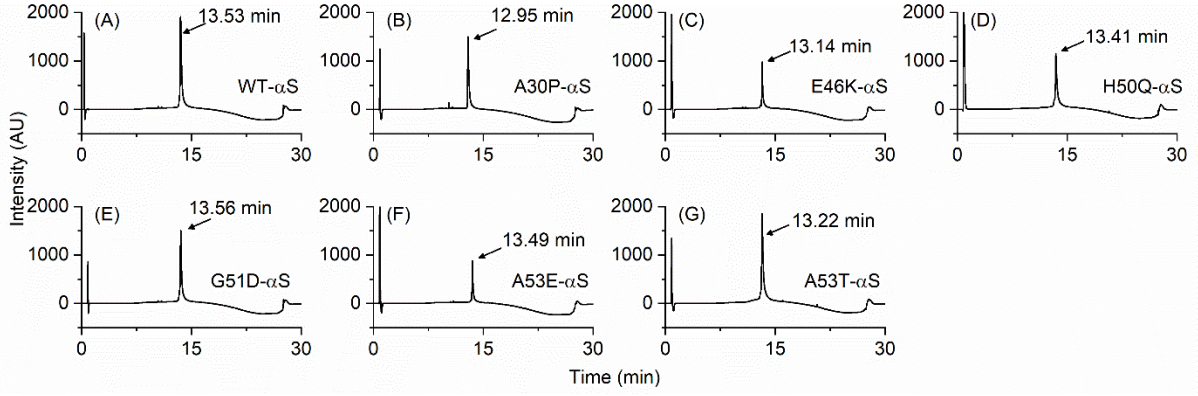

Fig. A5. Reversed-phase UHPLC chromatograms of αS protein variants. WT-αS elutes at 13.53 min (A), A30P-αS elutes at 12.95 min (B), E46K-αS elutes at 13.14 min (C), H50Q-αS elutes at 13.41 min (D), G51D-αS elutes at 13.56 min (E), and A53E-αS elutes at 13.49 min (F), A53T-αS elutes at 13.22 min (G).

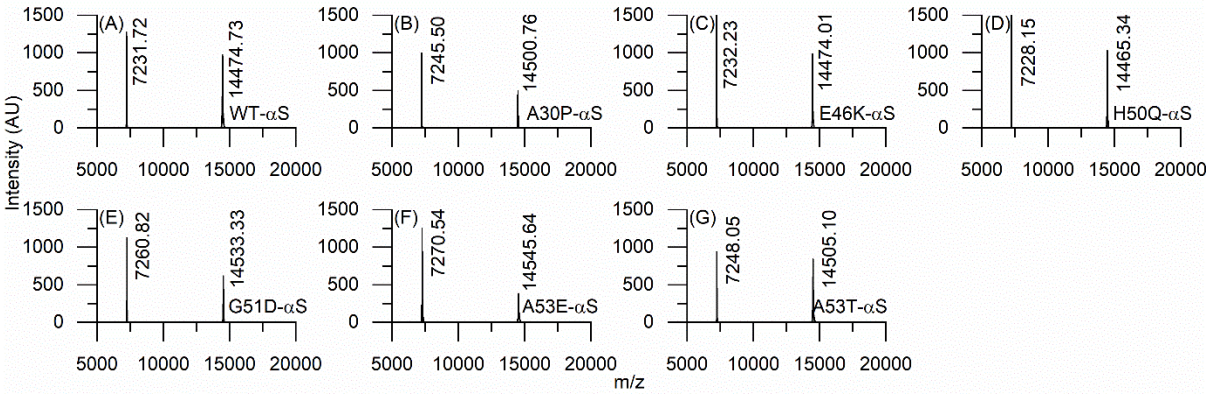

Fig. A6. MALDI-TOF mass spectrometric analyses of αS protein variants. The MALDI-TOF mass spectrum of WT-αS (A), A30P-αS (B), E46K-αS (C), H50Q-αS (D), G51D-αS (E) A53E-αS (F), and A53T-αS (G).

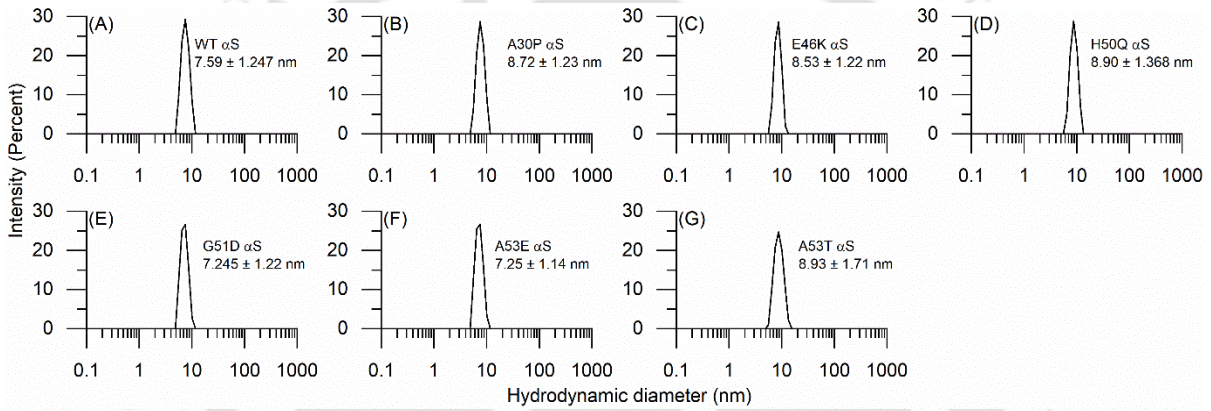

Fig. A7. DLS-derived hydrodynamic diameters of the freshly-prepared protein variants. WT-αS size was 7.59 ± 1.24 nm (A), A30P-αS size was 8.72 ± 1.24 nm (B), E46K-αS size was 8.53 ± 1.22 nm (C), H50Q-αS size was 8.90 ± 1.368 nm (D), G51D-αS size was 7.24 ± 1.22 nm (E) A53E-αS size was 7.25 ± 1.14 nm (F), and A53T-αS size was 8.93 ± 1.71 nm (G).

Table A2. Mass spectrometric analyses of the αS protein variants.

Protein	Monoisotopic mass (Da)	Identified species	Expected mass (Da)	Observed mass (Da)
Wt-αS	14451.22	$[M + Na]^+$	14474.22	14474.73
A30P-αS	14477.23	$[M + Na]^+$	14500.23	14500.76
E46K-αS	14450.27	$[M + Na]^+$	14473.27	14474.0
H50Q-αS	14442.25	$[M + Na]^+$	14465.25	14465.34
G51D-αS	14509.23	$[M + Na]^+$	14532.23	14533.33
A53E-αS	14509.22	$[M + K]^+$	14548.22	14545.64
A53T-αS	14481.23	$[M + Na]^+$	14504.23	14505.10

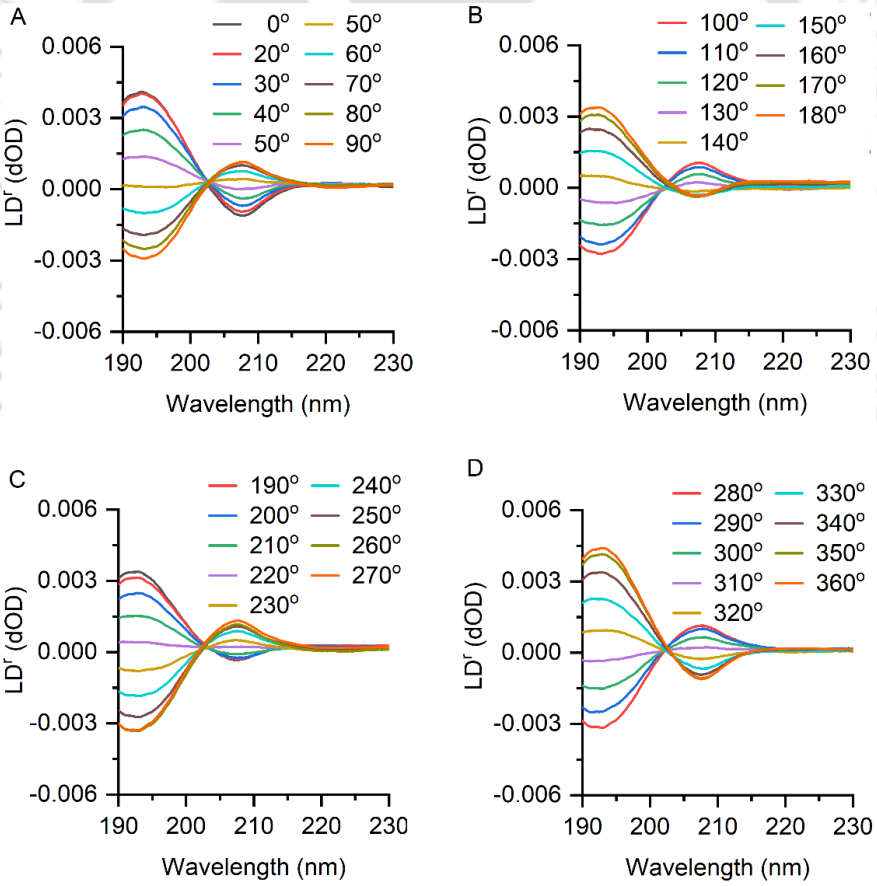

Fig. A8. (A-D) LD^r spectra of the Ac-αS LB film at different angles with 10° intervals. The 0° LD^r spectrum corresponds to the LD spectrum wherein the substrate retrieved from the subphase was used for recording the spectrum without any rotation.

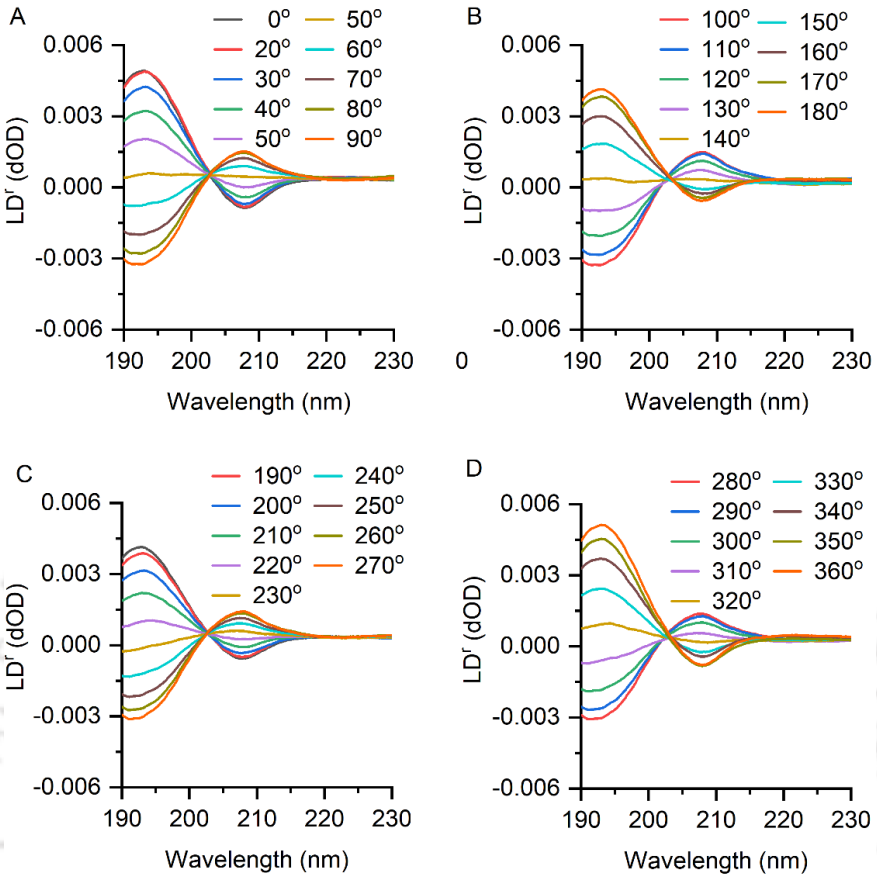

Fig A9. (A-D) LD^r spectra of the NH_2-αS LB film at different angles with 10° intervals. The 0° LD^r spectrum corresponds to the LD spectrum wherein the substrate retrieved from the subphase was used for recording the spectrum without any rotation.

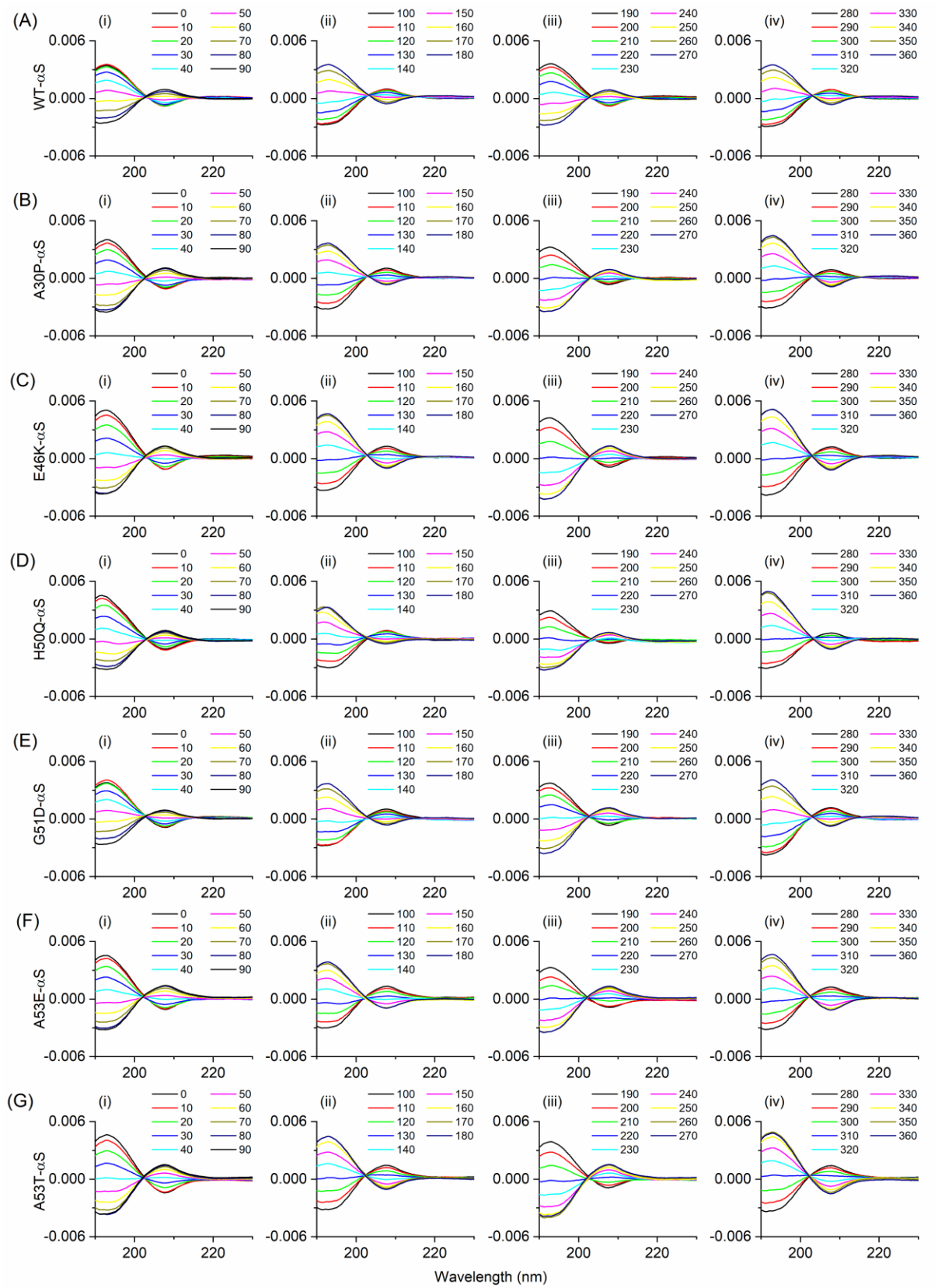

Fig. A10. LD spectra of αS protein variants. WT-αS (A), A30P-αS (B), E46K-αS (C), H50Q-αS (D), G51D-αS (E), A53E-αS (F), and A53T-αS (G).

Table A3. Synthetic derivatives of polymyxins

Molecule name	Chemical substitution	*In-vitro* activity	References
Colistin methanesulfonate	Sulfomethylation of amino groups	Administered parenterally, less toxic than colistin.	(Bergen, Li, Rayner, & Nation, 2006; Pirri, Giuliani, Nicoletto, Pizzuto, & Rinaldi, 2009)
Polymyxin B nonapeptide	FA tail is absent; R1 is absent	Outer membrane disorganising activity in serum against *E. coli*, potent sensitiser when used with hydrophobic antibiotics such as fusidic acid.	(Pirri et al., 2009; Vaara, Siikanen, Apajalahti, Frimodt-Moller, & Vaara, 2010; Vaara, Viljanen, Vaara, & Makela, 1984)
NAB7061	FA is octanoic acid; R1 is absent; R3 is aminobutyric acid	Outer membrane-permeabilising activity, potent sensitiser when used with rifampicin and clarithromycin against polymyxin-resistant strain *K. pneumoniae.*	(Pirri et al., 2009; Vaara et al., 2010)
NAB739	FA is octanoic acid; R1 is absent; R3 is D-serine	Works against PMB-resistant *Enterobacteriaceae* and *Acinetobacter baumannii as a potent sensitiser even at sub-MIC.*	(Vaara, 2009)
SPR741/NAB741	FA is acetic acid; R1 is absent; R3 is D-serine	Undulation of outer membrane, potent sensitiser, decreases the MIC of rifampicin and clarithromycin	(Mingeot-Leclercq, Tulkens, Denamur, Vaara, & Vaara, 2012; Pirri et al., 2009)

SPR206	FA tail was replaced by (S)-4-amino-3-(3-chlorophenyl)butanoic acid, R1 is absent, R3 is diaminobutyric acid	Broad spectrum Gram-negative antibacterial activity	(P. Brown et al., 2019)
NAB815	FA tail is octanoic acid; R3 is D-threonine, R8 is aminobutyric acid	Able to control urinary tract infection in mouse models.	(Vaara, Vaara, & Vingsbo Lundberg, 2018)
MicuRx-12	FA tail is 3-(2,2-dimethyl-butanoyloxy)-propanoic acid	*Effective against E. coli* systemic infections.	(Vaara, 2019b)
CA824	FA tail is (S)-1-(2-methylpropyl)-piperazine-2-carbonic acid; R1 is absent	Efficacy was superior than PMB in lung infection models against *A. baumannii* and *P. aeruginosa*, less cytotoxic than PMB.	(P. Brown & Dawson, 2017)
FADDI-287	FA is octanoic acid; R3 is diaminopropionic acid; R6 is D-Leucine; R7 is aminobutyric acid	Similar activity as PMB with reduced toxicity in mouse.	(P. Brown & Dawson, 2017)
FADDI-002	FA is octanoic acid; R7 is aminodecanoic acid	Effective against polymyxin-resistant *P. aeruginosa* and *A. baumannii*	(P. Brown & Dawson, 2017)
CB182, 804	FA is 2-chloro-phenylamino-carbonyl	Similar activity as PMB with lesser toxicity` in Cynomolgus monkey.	(P. Brown & Dawson, 2017)
Abbreviations: FA tail: Fatty acid tails, R1-10: R position denoted in Fig. 5.1			

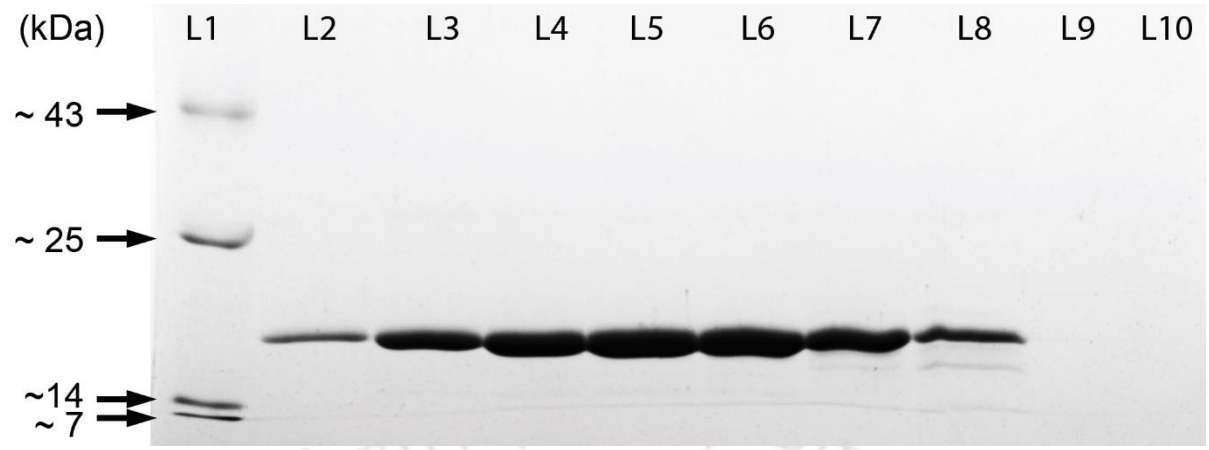

Fig. A11. The 12 % SDS-PAGE analysis of SEC fractions. L2-L8 correspond to the 0.5 ml fractions collected from 52 ml retention volume onwards.

References

Abeliovich, A., Schmitz, Y., Farinas, I., Choi-Lundberg, D., Ho, W. H., Castillo, P. E., . . . Rosenthal, A. (2000). Mice lacking alpha-synuclein display functional deficits in the nigrostriatal dopamine system. *Neuron, 25*(1), 239-252.

Afitska, K., Fucikova, A., Shvadchak, V. V., & Yushchenko, D. A. (2017). Modification of C Terminus Provides New Insights into the Mechanism of α-Synuclein Aggregation. *Biophysical journal, 113*(10), 2182-2191.

Aguzzi, A., & Heppner, F. L. (2000). Pathogenesis of prion diseases: a progress report. *Cell Death Differ, 7*(10), 889-902.

Ahmad, B., Chen, Y., & Lapidus, L. J. (2012). Aggregation of α-synuclein is kinetically controlled by intramolecular diffusion. *Proceedings of the National Academy of Sciences of the United States of America*.

Alam, P., Bousset, L., Melki, R., & Otzen, D. E. (2019). alpha-synuclein oligomers and fibrils: a spectrum of species, a spectrum of toxicities. *J Neurochem, 150*(5), 522-534.

Alexander, G. E. (2004). Biology of Parkinson's disease: pathogenesis and pathophysiology of a multisystem neurodegenerative disorder. *Dialogues Clin Neurosci, 6*(3), 259-280.

Alexander, G. E. (2004). Biology of Parkinson's disease: pathogenesis and pathophysiology of a multisystem neurodegenerative disorder. *Dialogues in Clinical Neuroscience, 6*(3), 259-280.

Anderson, J. P., Walker, D. E., Goldstein, J. M., de Laat, R., Banducci, K., Caccavello, R. J., . . . Chilcote, T. J. (2006). Phosphorylation of Ser-129 is the dominant pathological modification of alpha-synuclein in familial and sporadic Lewy body disease. *J Biol Chem, 281*(40), 29739-29752.

Atsmon-Raz, Y., & Miller, Y. (2015). A Proposed Atomic Structure of the Self-Assembly of the Non-Amyloid-beta Component of Human alpha-Synuclein As Derived by Computational Tools. *J Phys Chem B, 119*(31), 10005-10015.

Auluck, P. K., Caraveo, G., & Lindquist, S. (2010). alpha-Synuclein: membrane interactions and toxicity in Parkinson's disease. *Annu Rev Cell Dev Biol, 26*, 211-233.

Babu, M. M. (2016). The contribution of intrinsically disordered regions to protein function, cellular complexity, and human disease. *Biochem Soc Trans, 44*(5), 1185-1200.

Barbour, R., Kling, K., Anderson, J. P., Banducci, K., Cole, T., Diep, L., . . . Chilcote, T. J. (2008). Red blood cells are the major source of alpha-synuclein in blood. *Neurodegener Dis, 5*(2), 55-59.

Bartels, T., Ahlstrom, L. S., Leftin, A., Kamp, F., Haass, C., Brown, M. F., & Beyer, K. (2010). The N-terminus of the intrinsically disordered protein alpha-synuclein triggers membrane binding and helix folding. *Biophys J, 99*(7), 2116-2124.

Bartels, T., Choi, J. G., & Selkoe, D. J. (2011). alpha-Synuclein occurs physiologically as a helically folded tetramer that resists aggregation. *Nature, 477*(7362), 107-110.

Bartels, T., Kim, N. C., Luth, E. S., & Selkoe, D. J. (2014). N-alpha-acetylation of alpha-synuclein increases its helical folding propensity, GM1 binding specificity and resistance to aggregation. *PLoS One, 9*(7), e103727.

Bendor, J. T., Logan, T. P., & Edwards, R. H. (2013). The function of alpha-synuclein. *Neuron, 79*(6), 1044-1066.

Bergen, P. J., Li, J., Rayner, C. R., & Nation, R. L. (2006). Colistin methanesulfonate is an inactive prodrug of colistin against Pseudomonas aeruginosa. *Antimicrob Agents Chemother, 50*(6), 1953-1958.

Bisaglia, M., Mammi, S., & Bubacco, L. (2009). Structural insights on physiological functions and pathological effects of alpha-synuclein. *FASEB J, 23*(2), 329-340.

Blaszczyk, J. W. (2016). Parkinson's Disease and Neurodegeneration: GABA-Collapse Hypothesis. *Front Neurosci, 10*, 269.

Bohdanowicz, M., & Grinstein, S. (2013). Role of phospholipids in endocytosis, phagocytosis, and macropinocytosis. *Physiol Rev, 93*(1), 69-106.

Booth, P. J., & Curnow, P. (2009). Folding scene investigation: membrane proteins. *Curr Opin Struct Biol, 19*(1), 8-13.

Borbat, P., Ramlall, T. F., Freed, J. H., & Eliezer, D. (2006). Inter-helix distances in lysophospholipid micelle-bound alpha-synuclein from pulsed ESR measurements. *J Am Chem Soc, 128*(31), 10004-10005.

Bortolanza, M., Nascimento, G. C., Socias, S. B., Ploper, D., Chehin, R. N., Raisman-Vozari, R., & Del-Bel, E. (2018). Tetracycline repurposing in neurodegeneration: focus on Parkinson's disease. *J Neural Transm (Vienna), 125*(10), 1403-1415.

Brown, M. F. (2017). Soft Matter in Lipid-Protein Interactions. *Annu Rev Biophys, 46*, 379-410.

Brown, P., Abbott, E., Abdulle, O., Boakes, S., Coleman, S., Divall, N., . . . Dawson, M. J. (2019). Design of Next Generation Polymyxins with Lower Toxicity: The Discovery of SPR206. *ACS Infect Dis, 5*(10), 1645-1656.

Brown, P., & Dawson, M. J. (2017). Development of new polymyxin derivatives for multi-drug resistant Gram-negative infections. *J Antibiot (Tokyo), 70*(4), 386-394.

Brummel, B. E., Braun, A. R., & Sachs, J. N. (2017). Polyunsaturated chains in asymmetric lipids disorder raft mixtures and preferentially associate with alpha-Synuclein. *Biochim Biophys Acta Biomembr, 1859*(4), 529-536.

Bulheller, B. M., Rodger, A., Hicks, M. R., Dafforn, T. R., Serpell, L. C., Marshall, K. E., . . . Hirst, J. D. (2009). Flow linear dichroism of some prototypical proteins. *J Am Chem Soc, 131*(37), 13305-13314.

Burre, J. (2015). The Synaptic Function of alpha-Synuclein. *J Parkinsons Dis, 5*(4), 699-713.

Burre, J., Sharma, M., & Sudhof, T. C. (2014). alpha-Synuclein assembles into higher-order multimers upon membrane binding to promote SNARE complex formation. *Proc Natl Acad Sci U S A, 111*(40), E4274-4283.

Bussell, R., Jr., & Eliezer, D. (2003). A structural and functional role for 11-mer repeats in alpha-synuclein and other exchangeable lipid binding proteins. *J Mol Biol, 329*(4), 763-778.

Bussell, R., Jr., Ramlall, T. F., & Eliezer, D. (2005). Helix periodicity, topology, and dynamics of membrane-associated alpha-synuclein. *Protein Sci, 14*(4), 862-872.

Cabin, D. E., Shimazu, K., Murphy, D., Cole, N. B., Gottschalk, W., McIlwain, K. L., . . . Nussbaum, R. L. (2002). Synaptic vesicle depletion correlates with attenuated synaptic responses to prolonged repetitive stimulation in mice lacking alpha-synuclein. *J Neurosci, 22*(20), 8797-8807.

Casares, D., Escriba, P. V., & Rossello, C. A. (2019). Membrane Lipid Composition: Effect on Membrane and Organelle Structure, Function and Compartmentalization and Therapeutic Avenues. *Int J Mol Sci, 20*(9).

Castano, E. M., Prelli, F., Soto, C., Beavis, R., Matsubara, E., Shoji, M., & Frangione, B. (1996). The length of amyloid-beta in hereditary cerebral hemorrhage with amyloidosis, Dutch type. Implications for the role of amyloid-beta 1-42 in Alzheimer's disease. *J Biol Chem, 271*(50), 32185-32191.

Caughey, B., & Chesebro, B. (1997). Prion protein and the transmissible spongiform encephalopathies. *Trends Cell Biol, 7*(2), 56-62.

Chaari, A., Horchani, H., Frikha, F., Verger, R., Gargouri, Y., & Ladjimi, M. (2013). Surface behavior of alpha-Synuclein and its interaction with phospholipids using the Langmuir monolayer technique: a comparison between monomeric and fibrillar alpha-Synuclein. *Int J Biol Macromol, 58*, 190-198.

Chandra, S., Chen, X., Rizo, J., Jahn, R., & Sudhof, T. C. (2003). A broken alpha -helix in folded alpha -Synuclein. *J Biol Chem, 278*(17), 15313-15318.

Chandra, S., Gallardo, G., Fernandez-Chacon, R., Schluter, O. M., & Sudhof, T. C. (2005). Alpha-synuclein cooperates with CSPalpha in preventing neurodegeneration. *Cell, 123*(3), 383-396.

Chaudhary, N., & Nagaraj, R. (2011). Self-assembly of short amyloidogenic peptides at the air-water interface. *J Colloid Interface Sci, 360*(1), 139-147.

Chen, C. W., & Liu, T. J. (2006). Maximum withdrawal speed for Langmuir-Blodgett film deposition of arachidic acid. *J Colloid Interface Sci, 298*(1), 298-305.

Choi, T. S., Han, J. Y., Heo, C. E., Lee, S. W., & Kim, H. I. (2018). Electrostatic and hydrophobic interactions of lipid-associated alpha-synuclein: The role of a water-limited interfaces in amyloid fibrillation. *Biochim Biophys Acta Biomembr, 1860*(9), 1854-1862.

Coelho-Cerqueira, E., Carmo-Goncalves, P., Pinheiro, A. S., Cortines, J., & Follmer, C. (2013). alpha-Synuclein as an intrinsically disordered monomer--fact or artefact? *FEBS J, 280*(19), 4915-4927.

Coelho, T. (1996). Familial amyloid polyneuropathy: new developments in genetics and treatment. *Curr Opin Neurol, 9*(5), 355-359.

Cole, M. A., & Seabrook, G. R. (2020). On the horizon-the value and promise of the global pipeline of Alzheimer's disease therapeutics. *Alzheimers Dement (N Y), 6*(1), e12009.

Cole, N. B., Dieuliis, D., Leo, P., Mitchell, D. C., & Nussbaum, R. L. (2008). Mitochondrial translocation of alpha-synuclein is promoted by intracellular acidification. *Exp Cell Res, 314*(10), 2076-2089.

Collinge, J. (2001). Prion diseases of humans and animals: their causes and molecular basis. *Annu Rev Neurosci, 24*, 519-550.

Comellas, G., Lemkau, L. R., Nieuwkoop, A. J., Kloepper, K. D., Ladror, D. T., Ebisu, R., . . . Rienstra, C. M. (2011). Structured regions of alpha-synuclein fibrils include the early-onset Parkinson's disease mutation sites. *J Mol Biol, 411*(4), 881-895.

Crass, R. L., Rutter, W. C., Burgess, D. R., Martin, C. A., & Burgess, D. S. (2017). Nephrotoxicity in Patients with or without Cystic Fibrosis Treated with Polymyxin B Compared to Colistin. *Antimicrob Agents Chemother, 61*(4).

Dai, C., Ciccotosto, G. D., Cappai, R., Wang, Y., Tang, S., Xiao, X., & Velkov, T. (2017). Minocycline attenuates colistin-induced neurotoxicity via suppression of apoptosis, mitochondrial dysfunction and oxidative stress. *Journal of Antimicrobial Chemotherapy, 72*(6), 1635-1645.

Danzer, K. M., Haasen, D., Karow, A. R., Moussaud, S., Habeck, M., Giese, A., . . . Kostka, M. (2007). Different species of alpha-synuclein oligomers induce calcium influx and seeding. *J Neurosci, 27*(34), 9220-9232.

Das, M., Mei, X., Jayaraman, S., Atkinson, D., & Gursky, O. (2014). Amyloidogenic mutations in human apolipoprotein A-I are not necessarily destabilizing - a common mechanism of apolipoprotein A-I misfolding in familial amyloidosis and atherosclerosis. *FEBS J, 281*(11), 2525-2542.

Das, T., & Eliezer, D. (2019). Membrane interactions of intrinsically disordered proteins: The example of alpha-synuclein. *Biochim Biophys Acta Proteins Proteom, 1867*(10), 879-889.

Davidson, W. S., Jonas, A., Clayton, D. F., & George, J. M. (1998). Stabilization of alpha-synuclein secondary structure upon binding to synthetic membranes. *J Biol Chem, 273*(16), 9443-9449.

de Oliveira, G. A. P., & Silva, J. L. (2019). Alpha-synuclein stepwise aggregation reveals features of an early onset mutation in Parkinson's disease. *Commun Biol, 2*, 374.

Dennison, S. R., Harris, F., & Phoenix, D. A. (2014). Chapter Three - Langmuir–Blodgett Approach to Investigate Antimicrobial Peptide–Membrane Interactions. In A. Iglič & C. V. Kulkarni (Eds.), *Advances in Planar Lipid Bilayers and Liposomes* (Vol. 20, pp. 83-110): Academic Press.

DiFiglia, M., Sapp, E., Chase, K. O., Davies, S. W., Bates, G. P., Vonsattel, J. P., & Aronin, N. (1997). Aggregation of huntingtin in neuronal intranuclear inclusions and dystrophic neurites in brain. *Science, 277*(5334), 1990-1993.

Eisenberg, D., & Jucker, M. (2012). The amyloid state of proteins in human diseases. *Cell, 148*(6), 1188-1203.

Eliezer, D., Kutluay, E., Bussell, R., Jr., & Browne, G. (2001). Conformational properties of alpha-synuclein in its free and lipid-associated states. *J Mol Biol, 307*(4), 1061-1073.

Emmertsen, K. (1985). Medullary thyroid carcinoma and calcitonin. *Dan Med Bull, 32*(1), 1-28.

Fakhree, M. A. A., Nolten, I. S., Blum, C., & Claessens, M. (2018). Different Conformational Subensembles of the Intrinsically Disordered Protein alpha-Synuclein in Cells. *J Phys Chem Lett, 9*(6), 1249-1253.

Fanning, S., Selkoe, D., & Dettmer, U. (2020). Parkinson's disease: proteinopathy or lipidopathy? *NPJ Parkinsons Dis, 6*, 3.

Fauerbach, J. A., Yushchenko, D. A., Shahmoradian, S. H., Chiu, W., Jovin, T. M., & Jares-Erijman, E. A. (2012). Supramolecular non-amyloid intermediates in the early stages of alpha-synuclein aggregation. *Biophys J, 102*(5), 1127-1136.

Fauvet, B., Mbefo, M. K., Fares, M. B., Desobry, C., Michael, S., Ardah, M. T., . . . Lashuel, H. A. (2012). alpha-Synuclein in central nervous system and from erythrocytes, mammalian cells, and Escherichia coli exists predominantly as disordered monomer. *J Biol Chem, 287*(19), 15345-15364.

Fernández, C. O., Hoyer, W., Zweckstetter, M., Jares-Erijman, E. A., Subramaniam, V., Griesinger, C., & Jovin, T. M. (2004). NMR of α-synuclein–polyamine complexes elucidates the mechanism and kinetics of induced aggregation. *The EMBO Journal, 23*(10), 2039-2046.

Fernandez, R. D., & Lucas, H. R. (2018a). Isolation of recombinant tetrameric N-acetylated alpha-synuclein. *Protein Expr Purif, 152*, 146-154.

Fernandez, R. D., & Lucas, H. R. (2018b). Mass spectrometry data confirming tetrameric alpha-synuclein N-terminal acetylation. *Data Brief, 20*, 1686-1691.

Ferreon, A. C., Gambin, Y., Lemke, E. A., & Deniz, A. A. (2009). Interplay of alpha-synuclein binding and conformational switching probed by single-molecule fluorescence. *Proc Natl Acad Sci U S A, 106*(14), 5645-5650.

Fink, A. L. (2006). The aggregation and fibrillation of alpha-synuclein. *Acc Chem Res, 39*(9), 628-634.

Fortin, D. L., Troyer, M. D., Nakamura, K., Kubo, S., Anthony, M. D., & Edwards, R. H. (2004). Lipid rafts mediate the synaptic localization of alpha-synuclein. *J Neurosci, 24*(30), 6715-6723.

Fröhlich, F. (2016). Chapter 23 - Parkinson's Disease. In F. Fröhlich (Ed.), *Network Neuroscience* (pp. 291-296). San Diego: Academic Press.

Gath, J., Habenstein, B., Bousset, L., Melki, R., Meier, B. H., & Bockmann, A. (2012). Solid-state NMR sequential assignments of alpha-synuclein. *Biomol NMR Assign, 6*(1), 51-55.

Gejyo, F. (2001). [Beta 2-microglobulin and dialysis-related amyloidosis]. *Rinsho Byori, 49*(3), 244-248.

George, J. M., Jin, H., Woods, W. S., & Clayton, D. F. (1995). Characterization of a novel protein regulated during the critical period for song learning in the zebra finch. *Neuron, 15*(2), 361-372.

Giasson, B. I., Murray, I. V., Trojanowski, J. Q., & Lee, V. M. (2001). A hydrophobic stretch of 12 amino acid residues in the middle of alpha-synuclein is essential for filament assembly. *J Biol Chem, 276*(4), 2380-2386.

Giehm, L., Lorenzen, N., & Otzen, D. E. (2011). Assays for alpha-synuclein aggregation. *Methods, 53*(3), 295-305.

Giovannini, P., Piccolo, I., Genitrini, S., Soliveri, P., Girotti, F., Geminiani, G., . . . Caraceni, T. (1991). Early-onset Parkinson's disease. *Mov Disord, 6*(1), 36-42.

Glenner, G. G., & Wong, C. W. (1984). Alzheimer's disease: initial report of the purification and characterization of a novel cerebrovascular amyloid protein. *Biochem Biophys Res Commun, 120*(3), 885-890.

Goetz, C. G. (2011). The history of Parkinson's disease: early clinical descriptions and neurological therapies. *Cold Spring Harb Perspect Med, 1*(1), a008862.

Goldman, J., & Fahn, S. (2020). Chapter 2 - Parkinson disease and related disorders. In R. N. Rosenberg & J. M. Pascual (Eds.), *Rosenberg's Molecular and Genetic Basis of Neurological and Psychiatric Disease (Sixth Edition)* (pp. 19-30): Academic Press.

González-Lizárraga, F., Socías, S. B., Ávila, C. L., Torres-Bugeau, C. M., Barbosa, L. R. S., Binolfi, A., . . . Chehín, R. N. (2017). Repurposing doxycycline for synucleinopathies: remodelling of α-synuclein oligomers towards non-toxic parallel beta-sheet structured species. *Scientific Reports, 7*(1), 41755.

Gras, S. L., Tickler, A. K., Squires, A. M., Devlin, G. L., Horton, M. A., Dobson, C. M., & MacPhee, C. E. (2008). Functionalised amyloid fibrils for roles in cell adhesion. *Biomaterials, 29*(11), 1553-1562.

Guerrero-Ferreira, R., Taylor, N. M., Arteni, A. A., Kumari, P., Mona, D., Ringler, P., . . . Stahlberg, H. (2019). Two new polymorphic structures of human full-length alpha-synuclein fibrils solved by cryo-electron microscopy. *Elife, 8*.

Gupta, Y., Singla, G., & Singla, R. (2015). Insulin-derived amyloidosis. *Indian J Endocrinol Metab, 19*(1), 174-177.

Hashimoto, M., Hsu, L. J., Rockenstein, E., Takenouchi, T., Mallory, M., & Masliah, E. (2002). alpha-Synuclein protects against oxidative stress via inactivation of the c-Jun N-terminal kinase stress-signaling pathway in neuronal cells. *J Biol Chem, 277*(13), 11465-11472.

He, C. (2019). Special Issue on Regulating the Central Dogma. *Biochemistry, 58*(5), 295-296.

He, S., Zhong, S., Liu, G., & Yang, J. (2020). Alpha-Synuclein: The Interplay of Pathology, Neuroinflammation, and Environmental Factors in Parkinson's Disease. *Neurodegener Dis, 20*(2-3), 55-64.

Heise, H., Celej, M. S., Becker, S., Riedel, D., Pelah, A., Kumar, A., . . . Baldus, M. (2008). Solid-state NMR reveals structural differences between fibrils of wild-type and disease-related A53T mutant alpha-synuclein. *J Mol Biol, 380*(3), 444-450.

Heise, H., Hoyer, W., Becker, S., Andronesi, O. C., Riedel, D., & Baldus, M. (2005). Molecular-level secondary structure, polymorphism, and dynamics of full-length alpha-synuclein fibrils studied by solid-state NMR. *Proc Natl Acad Sci U S A, 102*(44), 15871-15876.

Hogen, T., Levin, J., Schmidt, F., Caruana, M., Vassallo, N., Kretzschmar, H., . . . Giese, A. (2012). Two different binding modes of alpha-synuclein to lipid vesicles depending on its aggregation state. *Biophys J, 102*(7), 1646-1655.

Horcas, I., Fernandez, R., Gomez-Rodriguez, J. M., Colchero, J., Gomez-Herrero, J., & Baro, A. M. (2007). WSXM: a software for scanning probe microscopy and a tool for nanotechnology. *Rev Sci Instrum, 78*(1), 013705.

Hoskin, J. O., Kiloh, L. G., & Cawte, J. E. (1969). Epilepsy and guria: The shaking syndromes of New Guinea. *Social Science & Medicine (1967), 3*(1), 39-48.

Hoyer, W., Antony, T., Cherny, D., Heim, G., Jovin, T. M., & Subramaniam, V. (2002). Dependence of alpha-synuclein aggregate morphology on solution conditions. *J Mol Biol, 322*(2), 383-393.

Huang, C., Ren, G., Zhou, H., & Wang, C. C. (2005). A new method for purification of recombinant human alpha-synuclein in Escherichia coli. *Protein Expr Purif, 42*(1), 173-177.

Jain, M. K., Singh, P., Roy, S., & Bhat, R. (2018). Comparative Analysis of the Conformation, Aggregation, Interaction, and Fibril Morphologies of Human alpha-, beta-, and gamma-Synuclein Proteins. *Biochemistry, 57*(26), 3830-3848.

Jao, C. C., Der-Sarkissian, A., Chen, J., & Langen, R. (2004). Structure of membrane-bound alpha-synuclein studied by site-directed spin labeling. *Proc Natl Acad Sci U S A, 101*(22), 8331-8336.

Jao, C. C., Hegde, B. G., Chen, J., Haworth, I. S., & Langen, R. (2008). Structure of membrane-bound alpha-synuclein from site-directed spin labeling and computational refinement. *Proc Natl Acad Sci U S A, 105*(50), 19666-19671.

Jensen, M. B., Bhatia, V. K., Jao, C. C., Rasmussen, J. E., Pedersen, S. L., Jensen, K. J., . . . Stamou, D. (2011). Membrane curvature sensing by amphipathic helices: a single liposome study using alpha-synuclein and annexin B12. *J Biol Chem, 286*(49), 42603-42614.

Jo, E., McLaurin, J., Yip, C. M., St George-Hyslop, P., & Fraser, P. E. (2000). alpha-Synuclein membrane interactions and lipid specificity. *J Biol Chem, 275*(44), 34328-34334.

Johnson, M., Coulton, A. T., Geeves, M. A., & Mulvihill, D. P. (2010). Targeted amino-terminal acetylation of recombinant proteins in E. coli. *PLoS One, 5*(12), e15801.

Killinger, B. A., Melki, R., Brundin, P., & Kordower, J. H. (2019). Endogenous alpha-synuclein monomers, oligomers and resulting pathology: let's talk about the lipids in the room. *NPJ Parkinsons Dis, 5*, 23.

Kiuru, S. (1998). Gelsolin-related familial amyloidosis, Finnish type (FAF), and its variants found worldwide. *Amyloid, 5*(1), 55-66.

Kjaer, L., Giehm, L., Heimburg, T., & Otzen, D. (2009). The influence of vesicle size and composition on alpha-synuclein structure and stability. *Biophys J, 96*(7), 2857-2870.

Knowles, T. P., Oppenheim, T. W., Buell, A. K., Chirgadze, D. Y., & Welland, M. E. (2010). Nanostructured films from hierarchical self-assembly of amyloidogenic proteins. *Nat Nanotechnol, 5*(3), 204-207.

Knowles, T. P., Vendruscolo, M., & Dobson, C. M. (2014). The amyloid state and its association with protein misfolding diseases. *Nat Rev Mol Cell Biol, 15*(6), 384-396.

Koonin, E. V. (2012). Does the central dogma still stand? *Biol Direct, 7*, 27.

Kosik, K. S., Joachim, C. L., & Selkoe, D. J. (1986). Microtubule-associated protein tau (tau) is a major antigenic component of paired helical filaments in Alzheimer disease. *Proc Natl Acad Sci U S A, 83*(11), 4044-4048.

Kruger, R., Kuhn, W., Muller, T., Woitalla, D., Graeber, M., Kosel, S., . . . Riess, O. (1998). Ala30Pro mutation in the gene encoding alpha-synuclein in Parkinson's disease. *Nat Genet, 18*(2), 106-108.

Kulikova, A. A., Makarov, A. A., & Kozin, S. A. (2015). Roles of zinc ions and structural polymorphism of β-amyloid in the development of Alzheimer's disease. *Molecular Biology, 49*(2), 217-230.

Kumar, N., Singh, Y., Yadav, G., Mathur, S. K., & Bhadani, U. K. (2018). Role of neomycin polymyxin sulfate solution bladder wash for prevention of catheter associated urinary tract infection in traumatic brain injury patient admitted to Intensive Care Unit: A prospective randomized study. *International journal of critical illness and injury science, 8*(1), 17-21.

Kurniawan, J., Ventrici de Souza, J. F., Dang, A. T., Liu, G. Y., & Kuhl, T. L. (2018). Preparation and Characterization of Solid-Supported Lipid Bilayers Formed by Langmuir-Blodgett Deposition: A Tutorial. *Langmuir, 34*(51), 15622-15639.

Kwa, A., Kasiakou, S. K., Tam, V. H., & Falagas, M. E. (2007). Polymyxin B: similarities to and differences from colistin (polymyxin E). *Expert Review of Anti-infective Therapy, 5*(5), 811-821.

Landman, D., Georgescu, C., Martin, D. A., & Quale, J. (2008). Polymyxins Revisited. *Clinical Microbiology Reviews, 21*(3), 449.

Larsen, K. E., Schmitz, Y., Troyer, M. D., Mosharov, E., Dietrich, P., Quazi, A. Z., . . . Sulzer, D. (2006). Alpha-synuclein overexpression in PC12 and chromaffin cells impairs catecholamine release by interfering with a late step in exocytosis. *J Neurosci, 26*(46), 11915-11922.

Lawrence, S., Alpar, H., McAllister, S., & Brown, M. (1993). Liposomal (MLV) Polymyxin B: Physicochemical Characterization and Effect of Surface Charge on Drug Association. *J. Drug. Target., 1*(4), 303-310.

Lee, C.-H., Kim, H. J., Lee, J.-H., Cho, H.-J., Kim, J., Chung, K. C., . . . Paik, S. R. (2006). Dequalinium-induced Protofibril Formation of α-Synuclein. *Journal of Biological Chemistry, 281*(6), 3463-3472.

Lee, H.-J., Choi, C., & Lee, S.-J. (2002). Membrane-bound α-Synuclein Has a High Aggregation Propensity and the Ability to Seed the Aggregation of the Cytosolic Form. *Journal of Biological Chemistry, 277*(1), 671-678.

Lee, J., Kim, S. Y., Hwang, K. J., Ju, Y. R., & Woo, H. J. (2013). Prion diseases as transmissible zoonotic diseases. *Osong Public Health Res Perspect, 4*(1), 57-66.

Lei, Z., Cao, G., & Wei, G. (2019). A30P mutant alpha-synuclein impairs autophagic flux by inactivating JNK signaling to enhance ZKSCAN3 activity in midbrain dopaminergic neurons. *Cell Death Dis, 10*(2), 133.

Lesage, S., Anheim, M., Letournel, F., Bousset, L., Honore, A., Rozas, N., . . . French Parkinson's Disease Genetics Study, G. (2013). G51D alpha-synuclein mutation causes a novel parkinsonian-pyramidal syndrome. *Ann Neurol, 73*(4), 459-471.

Li, B., Ge, P., Murray, K. A., Sheth, P., Zhang, M., Nair, G., . . . Jiang, L. (2018). Cryo-EM of full-length alpha-synuclein reveals fibril polymorphs with a common structural kernel. *Nat Commun, 9*(1), 3609.

Li, D., Jones, E. M., Sawaya, M. R., Furukawa, H., Luo, F., Ivanova, M., . . . Eisenberg, D. S. (2014). Structure-based design of functional amyloid materials. *J Am Chem Soc, 136*(52), 18044-18051.

Li, H. T., Du, H. N., Tang, L., Hu, J., & Hu, H. Y. (2002). Structural transformation and aggregation of human alpha-synuclein in trifluoroethanol: non-amyloid component sequence is essential and beta-sheet formation is prerequisite to aggregation. *Biopolymers, 64*(4), 221-226.

Li, J., Zhu, M., Rajamani, S., Uversky, V. N., & Fink, A. L. (2004). Rifampicin Inhibits α-Synuclein Fibrillation and Disaggregates Fibrils. *Chemistry & Biology, 11*(11), 1513-1521.

Li, Y., Zhao, C., Luo, F., Liu, Z., Gui, X., Luo, Z., . . . Li, X. (2018). Amyloid fibril structure of alpha-synuclein determined by cryo-electron microscopy. *Cell Res, 28*(9), 897-903.

Lima, M. M., Andersen, M. L., Reksidler, A. B., Vital, M. A., & Tufik, S. (2007). The role of the substantia nigra pars compacta in regulating sleep patterns in rats. *PLoS One, 2*(6), e513.

Liu, C., Zhao, Y., Xi, H., Jiang, J., Yu, Y., & Dong, W. (2021). The Membrane Interaction of Alpha-Synuclein. *Front Cell Neurosci, 15*, 633727.

Liu, H., & Naismith, J. H. (2008). An efficient one-step site-directed deletion, insertion, single and multiple-site plasmid mutagenesis protocol. *BMC Biotechnol, 8*, 91.

Llorens, F., Kruse, N., Schmitz, M., Shafiq, M., da Cunha, J. E., Gotzman, N., . . . Zerr, I. (2015). Quantification of CSF biomarkers using an electrochemiluminescence-based detection system in the differential diagnosis of AD and sCJD. *J Neurol, 262*(10), 2305-2311.

Lokappa, S. B., & Ulmer, T. S. (2011). Alpha-synuclein populates both elongated and broken helix states on small unilamellar vesicles. *J Biol Chem, 286*(24), 21450-21457.

Lorenzen, N., Lemminger, L., Pedersen, J. N., Nielsen, S. B., & Otzen, D. E. (2014). The N-terminus of alpha-synuclein is essential for both monomeric and oligomeric interactions with membranes. *FEBS Lett, 588*(3), 497-502.

Lucas, H. R., & Fernandez, R. D. (2020). Navigating the dynamic landscape of alpha-synuclein morphology: a review of the physiologically relevant tetrameric conformation. *Neural Regen Res, 15*(3), 407-415.

Macritchie, F. (1978). Proteins at interfaces. *Adv Protein Chem, 32*, 283-326.

Mahapatra, A., Sarkar, S., Biswas, S. C., & Chattopadhyay, K. (2019). An aminoglycoside antibiotic inhibits both lipid-induced and solution-phase fibrillation of α-synuclein in vitro. *Chemical Communications, 55*(74), 11052-11055.

Mahul-Mellier, A. L., Burtscher, J., Maharjan, N., Weerens, L., Croisier, M., Kuttler, F., . . . Lashuel, H. A. (2020). The process of Lewy body formation, rather than simply alpha-synuclein fibrillization, is one of the major drivers of neurodegeneration. *Proc Natl Acad Sci U S A, 117*(9), 4971-4982.

Majcher, M. J., & Hoare, T. (2019). Applications of Hydrogels. In M. A. Jafar Mazumder, H. Sheardown, & A. Al-Ahmed (Eds.), *Functional Biopolymers* (pp. 453-490). Cham: Springer International Publishing.

Maji, S. K., Schubert, D., Rivier, C., Lee, S., Rivier, J. E., & Riek, R. (2008). Amyloid as a depot for the formulation of long-acting drugs. *PLoS Biol, 6*(2), e17.

Maltsev, A. S., Ying, J., & Bax, A. (2012). Impact of N-terminal acetylation of alpha-synuclein on its random coil and lipid binding properties. *Biochemistry, 51*(25), 5004-5013.

Manyam, B. V. (1990). Paralysis agitans and levodopa in "Ayurveda": ancient Indian medical treatise. *Mov Disord, 5*(1), 47-48.

Maroteaux, L., Campanelli, J. T., & Scheller, R. H. (1988). Synuclein: a neuron-specific protein localized to the nucleus and presynaptic nerve terminal. *J Neurosci, 8*(8), 2804-2815.

Marsden, C. A. (2006). Dopamine: the rewarding years. *Br J Pharmacol, 147 Suppl 1*, S136-144.

Martinez, Z., Zhu, M., Han, S., & Fink, A. L. (2007). GM1 specifically interacts with alpha-synuclein and inhibits fibrillation. *Biochemistry, 46*(7), 1868-1877.

Masliah, E., Rockenstein, E., Veinbergs, I., Mallory, M., Hashimoto, M., Takeda, A., . . . Mucke, L. (2000). Dopaminergic loss and inclusion body formation in alpha-synuclein mice: implications for neurodegenerative disorders. *Science, 287*(5456), 1265-1269.

McClendon, S., Rospigliosi, C. C., & Eliezer, D. (2009). Charge neutralization and collapse of the C-terminal tail of alpha-synuclein at low pH. *Protein Sci, 18*(7), 1531-1540.

Menger, F. M., Galloway, A. L., & Chlebowski, M. E. (2005). Surface tension of aqueous amphiphiles. *Langmuir, 21*(20), 9010-9012.

Michaelson, D. M., Barkai, G., & Barenholz, Y. (1983). Asymmetry of lipid organization in cholinergic synaptic vesicle membranes. *Biochem J, 211*(1), 155-162.

Middleton, E. R., & Rhoades, E. (2010). Effects of curvature and composition on alpha-synuclein binding to lipid vesicles. *Biophys J, 99*(7), 2279-2288.

Miller, D. W., Hague, S. M., Clarimon, J., Baptista, M., Gwinn-Hardy, K., Cookson, M. R., & Singleton, A. B. (2004). Alpha-synuclein in blood and brain from familial Parkinson disease with SNCA locus triplication. *Neurology, 62*(10), 1835-1838.

Mingeot-Leclercq, M. P., Tulkens, P. M., Denamur, S., Vaara, T., & Vaara, M. (2012). Novel polymyxin derivatives are less cytotoxic than polymyxin B to renal proximal tubular cells. *Peptides, 35*(2), 248-252.

Modi, P., Mohamad, A., Phom, L., Koza, Z., Das, A., Chaurasia, R., . . . Yenisetti, S. C. (2016). Understanding Pathophysiology of Sporadic Parkinson's Disease in Drosophila Model: Potential Opportunities and Notable Limitations. In J. D. a. W. Kozubski (Ed.), *Challenges in Parkinson's Disease* (pp. 217-244). Rijeka: IntechOpen.

Mohapatra, A., & Chaudhary, N. (2021). N-terminal acetylation does not alter alpha-synuclein's interfacial properties. *Int J Biol Macromol, 174*, 69-76.

Mohite, G. M., Navalkar, A., Kumar, R., Mehra, S., Das, S., Gadhe, L. G., . . . Maji, S. K. (2018). The Familial alpha-Synuclein A53E Mutation Enhances Cell Death in Response to Environmental Toxins Due to a Larger Population of Oligomers. *Biochemistry, 57*(33), 5014-5028.

Mor, D. E., Ugras, S. E., Daniels, M. J., & Ischiropoulos, H. (2016). Dynamic structural flexibility of alpha-synuclein. *Neurobiol Dis, 88*, 66-74.

Moriarty, G. M., Janowska, M. K., Kang, L., & Baum, J. (2013). Exploring the accessible conformations of N-terminal acetylated alpha-synuclein. *FEBS Lett, 587*(8), 1128-1138.

Murphy, D. D., Rueter, S. M., Trojanowski, J. Q., & Lee, V. M. (2000). Synucleins are developmentally expressed, and alpha-synuclein regulates the size of the presynaptic vesicular pool in primary hippocampal neurons. *J Neurosci, 20*(9), 3214-3220.

Nasr, S. H., Dasari, S., Mills, J. R., Theis, J. D., Zimmermann, M. T., Fonseca, R., . . . Kurtin, P. J. (2017). Hereditary Lysozyme Amyloidosis Variant p.Leu102Ser Associates with Unique Phenotype. *J Am Soc Nephrol, 28*(2), 431-438.

Nemani, V. M., Lu, W., Berge, V., Nakamura, K., Onoa, B., Lee, M. K., . . . Edwards, R. H. (2010). Increased expression of alpha-synuclein reduces neurotransmitter release by inhibiting synaptic vesicle reclustering after endocytosis. *Neuron, 65*(1), 66-79.

Neumann, M., Sampathu, D. M., Kwong, L. K., Truax, A. C., Micsenyi, M. C., Chou, T. T., . . . Lee, V. M. (2006). Ubiquitinated TDP-43 in frontotemporal lobar degeneration and amyotrophic lateral sclerosis. *Science, 314*(5796), 130-133.

Nienhuis, H. L., Bijzet, J., & Hazenberg, B. P. (2016). The Prevalence and Management of Systemic Amyloidosis in Western Countries. *Kidney Dis (Basel), 2*(1), 10-19.

Ninkina, N., Peters, O., Millership, S., Salem, H., van der Putten, H., & Buchman, V. L. (2009). Gamma-synucleinopathy: neurodegeneration associated with overexpression of the mouse protein. *Hum Mol Genet, 18*(10), 1779-1794.

Nussbaum, R. L., & Ellis, C. E. (2003). Alzheimer's disease and Parkinson's disease. *N Engl J Med, 348*(14), 1356-1364.

O'Brien, J. S., & Sampson, E. L. (1965). Lipid composition of the normal human brain: gray matter, white matter, and myelin. *Journal of Lipid Research, 6*(4), 537-544.

Oeckl, P., Metzger, F., Nagl, M., von Arnim, C. A., Halbgebauer, S., Steinacker, P., . . . Otto, M. (2016). Alpha-, Beta-, and Gamma-synuclein Quantification in Cerebrospinal Fluid by Multiple Reaction Monitoring Reveals Increased Concentrations in Alzheimer's and Creutzfeldt-Jakob Disease but No Alteration in Synucleinopathies. *Mol Cell Proteomics, 15*(10), 3126-3138.

Orwa, J. A., Govaerts, C., Busson, R., Roets, E., Van Schepdael, A., & Hoogmartens, J. (2001). Isolation and structural characterization of polymyxin B components. *Journal of Chromatography A, 912*(2), 369-373.

Ouberai, M. M., Wang, J., Swann, M. J., Galvagnion, C., Guilliams, T., Dobson, C. M., & Welland, M. E. (2013). alpha-Synuclein senses lipid packing defects and induces lateral expansion of lipids leading to membrane remodeling. *J Biol Chem, 288*(29), 20883-20895.

Ovallath, S., & Sulthana, B. (2018). Gut and Parkinson's disease. *Ann. Mov. Disord., 1*(1), 20-29.

Pan, S., Huang, X., Wang, Y., Li, L., Zhao, C., Yao, Z., . . . Zhang, G. (2018). Efficacy of intravenous plus intrathecal/intracerebral ventricle injection of polymyxin B for post-neurosurgical intracranial infections due to MDR/XDR Acinectobacter baumannii: a retrospective cohort study. *Antimicrob. Resist. Infect. Control., 7*, 8-8.

Panja, A. S., Maiti, S., & Bandyopadhyay, B. (2020). Protein stability governed by its structural plasticity is inferred by physicochemical factors and salt bridges. *Sci Rep, 10*(1), 1822.

Park, S. M., Jung, H. Y., Kim, T. D., Park, J. H., Yang, C. H., & Kim, J. (2002). Distinct roles of the N-terminal-binding domain and the C-terminal-solubilizing domain of alpha-synuclein, a molecular chaperone. *J Biol Chem, 277*(32), 28512-28520.

Pasanen, P., Myllykangas, L., Siitonen, M., Raunio, A., Kaakkola, S., Lyytinen, J., . . . Paetau, A. (2014). Novel alpha-synuclein mutation A53E associated with atypical multiple system atrophy and Parkinson's disease-type pathology. *Neurobiol Aging, 35*(9), 2180 e2181-2185.

Pattison, J. (1998). The emergence of bovine spongiform encephalopathy and related diseases. *Emerg Infect Dis, 4*(3), 390-394.

Peng, C., Trojanowski, J. Q., & Lee, V. M. (2020). Protein transmission in neurodegenerative disease. *Nat Rev Neurol, 16*(4), 199-212.

Perandones, C., Giugni, J. C., Calvo, D. S., Raina, G. B., De Jorge Lopez, L., Volpini, V., . . . Micheli, F. E. (2014). Mosaicism of alpha-synuclein gene rearrangements: report of two unrelated cases of early-onset parkinsonism. *Parkinsonism Relat Disord, 20*(5), 558-561.

Perrin, R. J., Woods, W. S., Clayton, D. F., & George, J. M. (2000). Interaction of human alpha-Synuclein and Parkinson's disease variants with phospholipids. Structural analysis using site-directed mutagenesis. *J Biol Chem, 275*(44), 34393-34398.

Perrin, R. J., Woods, W. S., Clayton, D. F., & George, J. M. (2001). Exposure to long chain polyunsaturated fatty acids triggers rapid multimerization of synucleins. *J Biol Chem, 276*(45), 41958-41962.

Pfefferkorn, C. M., Jiang, Z., & Lee, J. C. (2012). Biophysics of alpha-synuclein membrane interactions. *Biochim Biophys Acta, 1818*(2), 162-171.

Pfefferkorn, C. M., & Lee, J. C. (2010). Tryptophan probes at the alpha-synuclein and membrane interface. *J Phys Chem B, 114*(13), 4615-4622.

Pinheiro, F., & Ventura, S. (2019). Inducing alpha-synuclein compaction: a new strategy for inhibiting alpha-synuclein aggregation? *Neural Regen Res, 14*(11), 1897-1898.

Pinney, J. H., Whelan, C. J., Petrie, A., Dungu, J., Banypersad, S. M., Sattianayagam, P., . . . Lachmann, H. J. (2013). Senile systemic amyloidosis: clinical features at presentation and outcome. *J Am Heart Assoc, 2*(2), e000098.

Pirc, K., & Ulrih, N. P. (2015). alpha-Synuclein interactions with phospholipid model membranes: Key roles for electrostatic interactions and lipid-bilayer structure. *Biochim Biophys Acta, 1848*(10 Pt A), 2002-2012.

Pirri, G., Giuliani, A., Nicoletto, S. F., Pizzuto, L., & Rinaldi, A. C. (2009). Lipopeptides as anti-infectives: a practical perspective. *Central European Journal of Biology, 4*(3), 258-273.

Poirel, L., Jayol, A., & Nordmann, P. (2017). Polymyxins: Antibacterial Activity, Susceptibility Testing, and Resistance Mechanisms Encoded by Plasmids or Chromosomes. *Clinical Microbiology Reviews, 30*(2), 557.

Polymeropoulos, M. H., Lavedan, C., Leroy, E., Ide, S. E., Dehejia, A., Dutra, A., . . . Nussbaum, R. L. (1997). Mutation in the alpha-synuclein gene identified in families with Parkinson's disease. *Science, 276*(5321), 2045-2047.

Powell-Jackson, J., Weller, R. O., Kennedy, P., Preece, M. A., Whitcombe, E. M., & Newsom-Davis, J. (1985). Creutzfeldt-Jakob disease after administration of human growth hormone. *Lancet, 2*(8449), 244-246.

Pozo Devoto, V. M., & Falzone, T. L. (2017). Mitochondrial dynamics in Parkinson's disease: a role for α-synuclein? *Dis. Model. Mech., 10*(9), 1075.

Prager, R., Ludvik, B., & Hartter, E. (1991). [Role of amylin in the pathogenesis of type II diabetes mellitus]. *Acta Med Austriaca, 18*(3), 61-62.

Proukakis, C., Dudzik, C. G., Brier, T., MacKay, D. S., Cooper, J. M., Millhauser, G. L., . . . Schapira, A. H. (2013). A novel alpha-synuclein missense mutation in Parkinson disease. *Neurology, 80*(11), 1062-1064.

Raghuraman, H., & Chattopadhyay, A. (2007). Melittin: a membrane-active peptide with diverse functions. *Biosci Rep, 27*(4-5), 189-223.

Rathinakumar, R., Walkenhorst, W. F., & Wimley, W. C. (2009). Broad-spectrum antimicrobial peptides by rational combinatorial design and high-throughput screening: the importance of interfacial activity. *J Am Chem Soc, 131*(22), 7609-7617.

Rhinn, H., Qiang, L., Yamashita, T., Rhee, D., Zolin, A., Vanti, W., & Abeliovich, A. (2012). Alternative α-synuclein transcript usage as a convergent mechanism in Parkinson's disease pathology. *Nature Communications, 3*, 1084-1084.

Rhoades, E., Ramlall, T. F., Webb, W. W., & Eliezer, D. (2006). Quantification of alpha-synuclein binding to lipid vesicles using fluorescence correlation spectroscopy. *Biophys J, 90*(12), 4692-4700.

Rodger, A. Circular Dichroism and Linear Dichroism. In *Encyclopedia of Analytical Chemistry* (pp. 1-34).

Rovere, M., Powers, A. E., Jiang, H., Pitino, J. C., Fonseca-Ornelas, L., Patel, D. S., . . . Bartels, T. (2019). E46K-like alpha-synuclein mutants increase lipid interactions and disrupt membrane selectivity. *J Biol Chem, 294*(25), 9799-9812.

Ruggeri, F. S., Benedetti, F., Knowles, T. P. J., Lashuel, H. A., Sekatskii, S., & Dietler, G. (2018). Identification and nanomechanical characterization of the fundamental single-strand protofilaments of amyloid alpha-synuclein fibrils. *Proc Natl Acad Sci U S A, 115*(28), 7230-7235.

Rui, Q., Ni, H., Li, D., Gao, R., & Chen, G. (2018). The Role of LRRK2 in Neurodegeneration of Parkinson Disease. *Curr Neuropharmacol, 16*(9), 1348-1357.

Runfola, M., De Simone, A., Vendruscolo, M., Dobson, C. M., & Fusco, G. (2020). The N-terminal Acetylation of alpha-Synuclein Changes the Affinity for Lipid Membranes but not the Structural Properties of the Bound State. *Sci Rep, 10*(1), 204.

Runwal, G., & Edwards, R. H. (2021). The Membrane Interactions of Synuclein: Physiology and Pathology. *Annu Rev Pathol, 16*, 465-485.

Rushworth, J. V., & Hooper, N. M. (2010). Lipid Rafts: Linking Alzheimer's Amyloid-beta Production, Aggregation, and Toxicity at Neuronal Membranes. *Int J Alzheimers Dis, 2011*, 603052.

Sambrook, J., Fritsch, E. F., & Maniatis, T. (1989). *Molecular cloning: a laboratory manual*: Cold spring harbor laboratory press.

Sandri, A. M., Landersdorfer, C. B., Jacob, J., Boniatti, M. M., Dalarosa, M. G., Falci, D. R., . . . Zavascki, A. P. (2013). Population Pharmacokinetics of Intravenous Polymyxin B in Critically Ill Patients: Implications for Selection of Dosage Regimens. *Clinical Infectious Diseases, 57*(4), 524-531.

Satlin, M. J., & Jenkins, S. G. (2017). 151 - Polymyxins. In J. Cohen, W. G. Powderly, & S. M. Opal (Eds.), *Infectious Diseases (Fourth Edition)* (pp. 1285-1288.e1282): Elsevier.

Segal-Maurer, S., Mariano, N., Qavi, A., Urban, C., & Rahal, J. J., Jr. (1999). Successful treatment of ceftazidime-resistant Klebsiella pneumoniae ventriculitis with intravenous meropenem and intraventricular polymyxin B: case report and review. *Clin Infect Dis, 28*(5), 1134-1138.

Seu, K. J., Cambrea, L. R., Everly, R. M., & Hovis, J. S. (2006). Influence of lipid chemistry on membrane fluidity: tail and headgroup interactions. *Biophys J, 91*(10), 3727-3735.

Shulman, J. M., De Jager, P. L., & Feany, M. B. (2011). Parkinson's disease: genetics and pathogenesis. *Annu Rev Pathol, 6*, 193-222.

Shvadchak, V. V., Falomir-Lockhart, L. J., Yushchenko, D. A., & Jovin, T. M. (2011). Specificity and kinetics of alpha-synuclein binding to model membranes determined with fluorescent excited state intramolecular proton transfer (ESIPT) probe. *J Biol Chem, 286*(15), 13023-13032.

Singleton, A. B., Farrer, M., Johnson, J., Singleton, A., Hague, S., Kachergus, J., . . . Gwinn-Hardy, K. (2003). alpha-Synuclein locus triplication causes Parkinson's disease. *Science, 302*(5646), 841.

Snead, D., & Eliezer, D. (2014). Alpha-synuclein function and dysfunction on cellular membranes. *Exp Neurobiol, 23*(4), 292-313.

Sode, K., Ochiai, S., Kobayashi, N., & Usuzaka, E. (2006). Effect of reparation of repeat sequences in the human alpha-synuclein on fibrillation ability. *Int J Biol Sci, 3*(1), 1-7.

Spillantini, M. G., Crowther, R. A., Jakes, R., Hasegawa, M., & Goedert, M. (1998). alpha-Synuclein in filamentous inclusions of Lewy bodies from Parkinson's disease and dementia with lewy bodies. *Proc Natl Acad Sci U S A, 95*(11), 6469-6473.

Spillantini, M. G., Schmidt, M. L., Lee, V. M., Trojanowski, J. Q., Jakes, R., & Goedert, M. (1997). Alpha-synuclein in Lewy bodies. *Nature, 388*(6645), 839-840.

Stansly, P. G., & Schlosser, M. E. (1947). Studies on Polymyxin: Isolation and Identification of Bacillus polymyxa and Differentiation of Polymyxin from Certain Known Antibiotics. *Journal of bacteriology, 54*(5), 549-556.

Stefanovic, A. N., Stockl, M. T., Claessens, M. M., & Subramaniam, V. (2014). alpha-Synuclein oligomers distinctively permeabilize complex model membranes. *FEBS J, 281*(12), 2838-2850.

Stockl, M., Fischer, P., Wanker, E., & Herrmann, A. (2008). Alpha-synuclein selectively binds to anionic phospholipids embedded in liquid-disordered domains. *J Mol Biol, 375*(5), 1394-1404.

Tanford, C. (1997). How protein chemists learned about the hydrophobic factor. *Protein Sci, 6*(6), 1358-1366.

Tashkandi, H., Shameli, A., Harding, C. V., & Maitta, R. W. (2018). Ultrastructural changes in peripheral blood leukocytes in alpha-synuclein knockout mice. *Blood Cells Mol Dis, 73*, 33-37.

Török, N., Majláth, Z., Szalárdy, L., & Vécsei, L. (2016). Investigational α-synuclein aggregation inhibitors: hope for Parkinson's disease. *Expert Opin. Inv. Drug., 25*(11), 1281-1294.

Trimble, M. J., Mlynarcik, P., Kolar, M., & Hancock, R. E. (2016). Polymyxin: Alternative Mechanisms of Action and Resistance. *Cold Spring Harb Perspect Med, 6*(10).

Tsigelny, I. F., Bar-On, P., Sharikov, Y., Crews, L., Hashimoto, M., Miller, M. A., . . . Masliah, E. (2007). Dynamics of alpha-synuclein aggregation and inhibition of pore-like oligomer development by beta-synuclein. *FEBS J, 274*(7), 1862-1877.

Tuttle, M. D., Comellas, G., Nieuwkoop, A. J., Covell, D. J., Berthold, D. A., Kloepper, K. D., . . . Rienstra, C. M. (2016). Solid-state NMR structure of a pathogenic fibril of full-length human alpha-synuclein. *Nat Struct Mol Biol, 23*(5), 409-415.

Ueda, K., Fukushima, H., Masliah, E., Xia, Y., Iwai, A., Yoshimoto, M., . . . Saitoh, T. (1993). Molecular cloning of cDNA encoding an unrecognized component of amyloid in Alzheimer disease. *Proc Natl Acad Sci U S A, 90*(23), 11282-11286.

Ulmer, T. S., Bax, A., Cole, N. B., & Nussbaum, R. L. (2005). Structure and dynamics of micelle-bound human alpha-synuclein. *J Biol Chem, 280*(10), 9595-9603.

Uversky, V. N. (2003). A protein-chameleon: conformational plasticity of alpha-synuclein, a disordered protein involved in neurodegenerative disorders. *J Biomol Struct Dyn, 21*(2), 211-234.

Uversky, V. N. (2010). Mysterious oligomerization of the amyloidogenic proteins. *FEBS J, 277*(14), 2940-2953.

Uversky, V. N. (2013). A decade and a half of protein intrinsic disorder: biology still waits for physics. *Protein Sci, 22*(6), 693-724.
Uversky, V. N. (2019). Intrinsically Disordered Proteins and Their "Mysterious" (Meta)Physics. *7*(10).
Uversky, V. N., Li, J., & Fink, A. L. (2001). Evidence for a partially folded intermediate in alpha-synuclein fibril formation. *J Biol Chem, 276*(14), 10737-10744.
Vaara, M. (2009). New approaches in peptide antibiotics. *Curr Opin Pharmacol, 9*(5), 571-576.
Vaara, M. (2019a). Polymyxin Derivatives that Sensitize Gram-Negative Bacteria to Other Antibiotics. *Molecules, 24*(2).
Vaara, M. (2019b). Polymyxins and Their Potential Next Generation as Therapeutic Antibiotics. *Front Microbiol, 10*, 1689.
Vaara, M., Siikanen, O., Apajalahti, J., Frimodt-Moller, N., & Vaara, T. (2010). Susceptibility of carbapenemase-producing strains of Klebsiella pneumoniae and Escherichia coli to the direct antibacterial activity of NAB739 and to the synergistic activity of NAB7061 with rifampicin and clarithromycin. *J Antimicrob Chemother, 65*(5), 942-945.
Vaara, M., Vaara, T., & Vingsbo Lundberg, C. (2018). Polymyxin derivatives NAB739 and NAB815 are more effective than polymyxin B in murine Escherichia coli pyelonephritis. *J Antimicrob Chemother, 73*(2), 452-455.
Vaara, M., Viljanen, P., Vaara, T., & Makela, P. H. (1984). An outer membrane-disorganizing peptide PMBN sensitizes E. coli strains to serum bactericidal action. *J Immunol, 132*(5), 2582-2589.
van Meer, G., Voelker, D. R., & Feigenson, G. W. (2008). Membrane lipids: where they are and how they behave. *Nat Rev Mol Cell Biol, 9*(2), 112-124.
van Rooijen, B. D., Claessens, M. M., & Subramaniam, V. (2009). Lipid bilayer disruption by oligomeric alpha-synuclein depends on bilayer charge and accessibility of the hydrophobic core. *Biochim Biophys Acta, 1788*(6), 1271-1278.
Varkey, J., Isas, J. M., Mizuno, N., Jensen, M. B., Bhatia, V. K., Jao, C. C., . . . Langen, R. (2010). Membrane curvature induction and tubulation are common features of synucleins and apolipoproteins. *J Biol Chem, 285*(42), 32486-32493.
Vila, M., Vukosavic, S., Jackson-Lewis, V., Neystat, M., Jakowec, M., & Przedborski, S. (2000). α-Synuclein Up-Regulation in Substantia Nigra Dopaminergic Neurons Following Administration of the Parkinsonian Toxin MPTP. *Journal of Neurochemistry, 74*(2), 721-729.
Vilar, M., Chou, H. T., Luhrs, T., Maji, S. K., Riek-Loher, D., Verel, R., . . . Riek, R. (2008). The fold of alpha-synuclein fibrils. *Proc Natl Acad Sci U S A, 105*(25), 8637-8642.
Wallace, S. J., Li, J., Nation, R. L., Prankerd, R. J., Velkov, T., & Boyd, B. J. (2010). Self-Assembly Behavior of Colistin and Its Prodrug Colistin Methanesulfonate: Implications for Solution Stability and Solubilization. *J. Phys. Chem. B, 114*(14), 4836-4840.
Wang, C., Shah, N., Thakur, G., Zhou, F., & Leblanc, R. M. (2010). Alpha-synuclein in alpha-helical conformation at air-water interface: implication of conformation and orientation changes during its accumulation/aggregation. *Chem Commun (Camb), 46*(36), 6702-6704.
Wang, W., Perovic, I., Chittuluru, J., Kaganovich, A., Nguyen, L. T., Liao, J., . . . Hoang, Q. Q. (2011). A soluble alpha-synuclein construct forms a dynamic tetramer. *Proc Natl Acad Sci U S A, 108*(43), 17797-17802.
Wang, Y., Zhang, Y., Zhang, C., Hu, M., Yan, Q., Zhao, H., . . . Wu, Y. (2020). Cholesterol-Rich Lipid Rafts in the Cellular Membrane Play an Essential Role in Avian Reovirus Replication. *Front Microbiol, 11*, 597794.
Ward, K. E., Ropa, J. P., Adu-Gyamfi, E., & Stahelin, R. V. (2012). C2 domain membrane penetration by group IVA cytosolic phospholipase A(2) induces membrane curvature changes. *J Lipid Res, 53*(12), 2656-2666.
Waxman, E. A., Mazzulli, J. R., & Giasson, B. I. (2009). Characterization of hydrophobic residue requirements for alpha-synuclein fibrillization. *Biochemistry, 48*(40), 9427-9436.
Wells, G. A., Scott, A. C., Johnson, C. T., Gunning, R. F., Hancock, R. D., Jeffrey, M., . . . Bradley, R. (1987). A novel progressive spongiform encephalopathy in cattle. *Vet Rec, 121*(18), 419-420.

Westergard, L., Christensen, H. M., & Harris, D. A. (2007). The cellular prion protein (PrP(C)): its physiological function and role in disease. *Biochim Biophys Acta, 1772*(6), 629-644.

Williams, E. S., & Young, S. (1980). Chronic wasting disease of captive mule deer: a spongiform encephalopathy. *J Wildl Dis, 16*(1), 89-98.

Williams, E. S., & Young, S. (1982). Spongiform encephalopathy of Rocky Mountain elk. *J Wildl Dis, 18*(4), 465-471.

Yeagle, P. L. (2016). Chapter 10 - Membrane Proteins. In P. L. Yeagle (Ed.), *The Membranes of Cells (Third Edition)* (pp. 219-268). Boston: Academic Press.

Yeates, T. O. (2019). Protein assembles into Archimedean geometry. *Nature, 569*(7756), 340-342.

Zarranz, J. J., Alegre, J., Gomez-Esteban, J. C., Lezcano, E., Ros, R., Ampuero, I., . . . de Yebenes, J. G. (2004). The new mutation, E46K, of alpha-synuclein causes Parkinson and Lewy body dementia. *Ann Neurol, 55*(2), 164-173.

Zavascki, A. P., Goldani, L. Z., Li, J., & Nation, R. L. (2007). Polymyxin B for the treatment of multidrug-resistant pathogens: a critical review. *Journal of Antimicrobial Chemotherapy, 60*(6), 1206-1215.

Zhang, X. M., Anwar, S., Kim, Y., Brown, J., Comte, I., Cai, H., . . . Szele, F. G. (2019). The A30P alpha-synuclein mutation decreases subventricular zone proliferation. *Hum Mol Genet, 28*(14), 2283-2294.

Zheng, W., Sun, W., & Simeonov, A. (2018). Drug repurposing screens and synergistic drug-combinations for infectious diseases. *Br J Pharmacol, 175*(2), 181-191.

Zhu, M., & Fink, A. L. (2003). Lipid binding inhibits alpha-synuclein fibril formation. *J Biol Chem, 278*(19), 16873-16877.

Zhu, M., Qin, Z. J., Hu, D., Munishkina, L. A., & Fink, A. L. (2006). Alpha-synuclein can function as an antioxidant preventing oxidation of unsaturated lipid in vesicles. *Biochemistry, 45*(26), 8135-8142.